

Unified Total Synthesis of Lysolipin Natural Products

Methodology and Bioactivity behind Polycyclic Aromatic Compounds

Dissertation zur Erlangung des Doktorgrades (Dr. rer. nat.) der Mathematisch-Naturwissenschaftlichen Fakultät der Rheinischen Friedrich-Wilhelms-Universität Bonn

Vorgelegt von Jonas W. Meringdal

aus Aachen

Bonn, 2025

Angefertigt mit Genehm	igung der Mathematisch-Naturwissenschaftlichen Fakultät
der Rheinischen Friedric	h-Wilhelms-Universität Bonn
Gutachter/Betreuer:	Prof. Dirk Menche
Gutachter:	Prof. Sigurd Höger
	28. Oktober 2025
Tag der Promotion: Erscheinungsjahr:	2025
er serremangsjann.	

Acknowledgments

Prosperous collaborations and in-depth support sorted by major topic have been instrumental to the success of this thesis – hopefully, everybody has been duly recognized.

Supervision Prof. Dirk Menche. Scientific Committee Prof. Sigurd Höger, Prof. Thomas Bredow, Prof. Gerd Bendas. HPLC Andreas J. Schneider. NMR Dr. Senada Nozinovic, Ulrike Weynand, Dr. Karin Prochnicki, Hanelore Spitz. HRMS Dr. Marianne Engeser, Anette Reiner, Karin Peters-Pflaumenbaum, Florian Schäfer. GC-MS Lilly Hofmann, EA Dr. Sabine Rings, Nevena Petrova. Organization Dr. Gabriele Richardt, Britta Görlich, Isabel Scholz, Monika Klein. General Guidance Maximilian Hohlweck, Dr. Larissa von Krbek. Art Direction Sarah Jurytko, Lena W. Meringdal. Editing Wingkee Christine Li. Scientific Discussion Prof. Masauyki Inoue, Maximilian Heinemann, Maximilian Guhlke, Maximilian Notheis, Max Schönenbroicher, Lidón Pruñosa Lara, Niklas Gaida. Extreme Patience Sabine Meringdal, Friedhelm Wuppermann. Master's Thesis Vivienne Prangenberg, Leon C. Honsdorf, Tim Treiber, Wing-Si Li. **Bachelor's Thesis** Nguyen Thuy Duong Vu, Thomas Treu. **Long-Term Internship** Leo Stapper. WP13 Internships Kristina Heuser, Andreas Zalfen, Christian Köhler, Vigan Sahiti, Clemens Hermann, Jonas Brode. **Bachelor Internships** Johannes Volk, Lea Haake, Damla Aydemir, Leon-Gabriel Schlaug, Michelle Dittrich, Andreas Hamm, Niklas Felix Schmidt.

Abstract

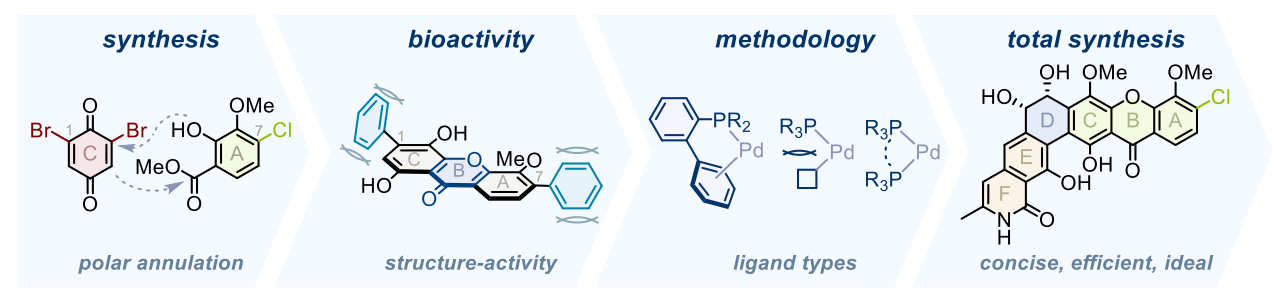


Table of Contents. Holistic total synthesis.

Lysolipin natural products are a family of bacterial polycyclic xanthones, renowned for their antibiotic potency and structural diversity. Yet, their complex architectures have long eluded synthetic access, and their antimicrobial prowess is offset by pronounced cytotoxicity. This thesis presents a modular total synthesis of the lysolipin family, integrating synthetic innovation, methodological development, and structure-activity exploration.

We began by reengineering Brassard's polar annulation sequence to accommodate halogenated, sterically congested xanthones resembling the lysolipin subunit. Detailed studies identified bromoquinones as superior coupling partners, optimized base-solvent systems for yield and scalability, and fine-tuned the acidity of the cyclization medium for selectivity. These improvements enabled efficient access not only to lysolipin fragments, but also to a broader class of densely functionalized polyhalogenated xanthones — substantially expanding the attainable chemical space.

These halogenated scaffolds proved potent lead structures and identified the xanthone unit as source for cytotoxicity in lysolipin natural products. In detail, chemoselective cross-coupling yielded a diversified set of xanthones with potent antiproliferative activity – comparable to the clinical benchmark doxorubicin – yet likely operating through a distinct mode of action. Moreover, potent xanthones resembled the lysolipin family, revealing the natural chloride as a tunable pharmacophore: cross-coupling leads to anticancer scaffolds, whereas dehalogenation reduces off-target toxicity in antibiotic design.

To streamline bond formation in complex target synthesis, recent mechanistic insights in Suzuki-Miyaura cross-couplings were condensed into rational selection guides that replace trial-and-error optimization. Crucially, ligand geometry emerged as the key determinant of reaction outcome, leading to the definition of four universal ligand types to simplify reaction planning.

This mechanistic framework enabled the total synthesis of lysolipin members CBS72, CBS87 and CBS100. Guided by ligand types, a very demanding aromatic keto-arylation merged sensitive xanthone and isocoumarin fragments into a synthetically versatile desoxybenzoin. Complementary advances – including base-catalyzed asymmetric Davis oxidation and late-stage aminolysis – addressed substrate lability and catalyst poisoning while minimizing protective group chemistry. These innovations culminated in concise, high-yielding total syntheses, with two out of three reactions forming a lysolipinic bond – a remarkable two- to threefold improvement over prior strategies.

Together, this work demonstrates how mechanistically guided synthesis can unlock inaccessible chemical space, translating rational design into architectural complexity and pharmacological potency, and reaffirms total synthesis as a powerful driver of scientific discovery.

Abbreviations

ac	acetone	MOM	methoxymethyl
AIBN	azobisisobutyronitrile	MOTCE	2,2,2-trichloroethoxymethyl
вом	benzyloxymethyl	MRSA	methycilin-resistant
CAN	ceric ammonium nitrate		Staphylococcus aureus
DABCO	1,4-diazabicyclo[2.2.2]octane	NBS	<i>N</i> -bromosuccinimide
DCDMH	1,3-dichloro-5,5-dimethyl-	NCS	<i>N</i> -chlorosuccinimide
	hydantoin	NMO	N-methylmorpholine oxide
DCM	dichloromethane	PIDA	phenyliodine(III)-diacetate
DDQ	2,3-dichloro-5,6-dicyano-	ру	pyridine
	1,4-benzoquinone	ROS	reactive oxygen species
DEAD	diethyl azodicarboxylate	TBAF	tetrabutylammoniumfluorid
DMAP	4-dimethylaminopyridine	TBD	triazabicyclodecene
DMF	dimethylformamide	TBS	tert-butyldimethylsilyl
DMP	Dess-Martin periodinane	TCCA	trichloroisocyanuric acid
DMS	dimethylsulfate	TEMPO	2,2,6,6-tetramethylpiperidinyloxy
diox	dioxane	TFA	trifluoroacetic acid
dr	diastereomeric ratio	TIPS	triisopropylsilyl
ee	enantiomeric excess	TMEDA	tetramethylethylenediamine
Glc	glucoside	TMS	trimethylsilyl
HFIP	hexafluoro-2-propanol	SAR	structure-activity relationship
HPLC	high-pressure liquid	SEM	2-(trimethylsilyl)ethoxymethyl
	chromatography	SMC	Suzuki-Miyaura cross-coupling
HMDS	hexamethyldisilazane	tol	toluene
IBX	2-iodoxybenzoic acid	VRE	vancomycin-resistant
IPr	1,3-bis(2,6-diisopropylphenyl)		Enterococcus faecalis
	imidazole-2-ylidene	WHO	World Health Organization
LLS	longest linear sequence		

Table of Contents

ΑŁ	stract		. vii	
Αŀ	brevia	tions	ix	
1	From	Nature to Humanity	1	
2	Lysoli	oin Natural Products	3	
3	Histor	ic Total Syntheses	5	
	3.1	Classical Works	5	
	3.2	The Modern Age	.11	
	3.3	Post-Modern Synthesis	.21	
	3.4	Present Insights from the Past	. 24	
4	Appro	ach to Lysolipin Family	. 27	
5	Systematic Exploration of Polycyclic Xanthones2			
	5.1	Modular Synthesis of Halogenated Xanthones	. 29	
	5.2	Bioactive Agents from Polyhalogenated Xanthones	.33	
	5.3	Suzuki-Miyaura (Hetero-)Aryl Cross-Coupling	.43	
	5.4	Total Synthesis of Lysolipin Natural Products	.51	
6	From	Synthesis to Pharmacology	.61	
	6.1	Methodical Total Synthesis	.61	
	6.2	Towards Uncharted Lysolipins	.65	
	6.3	Promising Drug Leads	.66	
	6.4	Personal Conclusion	.67	
7	Refere	ences	.69	
0	Dublic	ations	0.1	

1 From Nature to Humanity

The global rise of antimicrobial resistance has prompted the World Health Organization (WHO) to urgently call for the discovery of novel antibiotics. In response, the pharmaceutical industry has invested heavily in large-scale, automated high-throughput facilities to mine the existing chemical space for bioactive compounds. While these technologies have improved the efficiency of compound discovery, progress has been constrained by overreliance on established synthetic methods, resulting in repeated exploration of familiar molecular scaffolds. As a result, the hit-to-lead process has failed to deliver new antibiotic classes, and novel core structures remain critically lacking.

Natural products continue to surpass this bottleneck.¹¹ In contrast to synthetic libraries, they offer exceptional structural diversity, complexity and rigidity that have been evolutionarily optimized for biological activity.¹² These features contribute to their remarkable clinical prevalence: one out of every ten approved drug and, impressively, half of all antibiotics can be traced back to a natural origin.¹³

Expanding the chemical space towards these privileged architectures requires methodological advances, including non-traditional bond disconnections, selective late-stage functionalization and asymmetric synthesis. ¹⁴ Ideally, these strategies result in direct and selective bond formation, minimizing circuitous functional group interconversions and protective group chemistry. ^{15,16} However, emergence – the phenomenon where unique properties arise upon combination of ordinary fragments – causes unexpected behavior of complex scaffolds, impeding the straightforward application of modern synthetic strategies. ¹⁷

By overcoming these challenges, natural product synthesis drives synthetic innovation, expands chemical space, and ultimately bridges rational design with nature's finest architectures, making total synthesis an indispensable art for humanity.

2 Lysolipin Natural Products

Bacterial polycyclic xanthones are a privileged class of highly oxygenated hexacyclic natural products, renowned for their antimicrobial and antiproliferative activities.¹⁸ Lysolipins, isolated from several *Streptomyces*, emerged as the most potent antibiotics in this class (Figure 1).^{19–24}

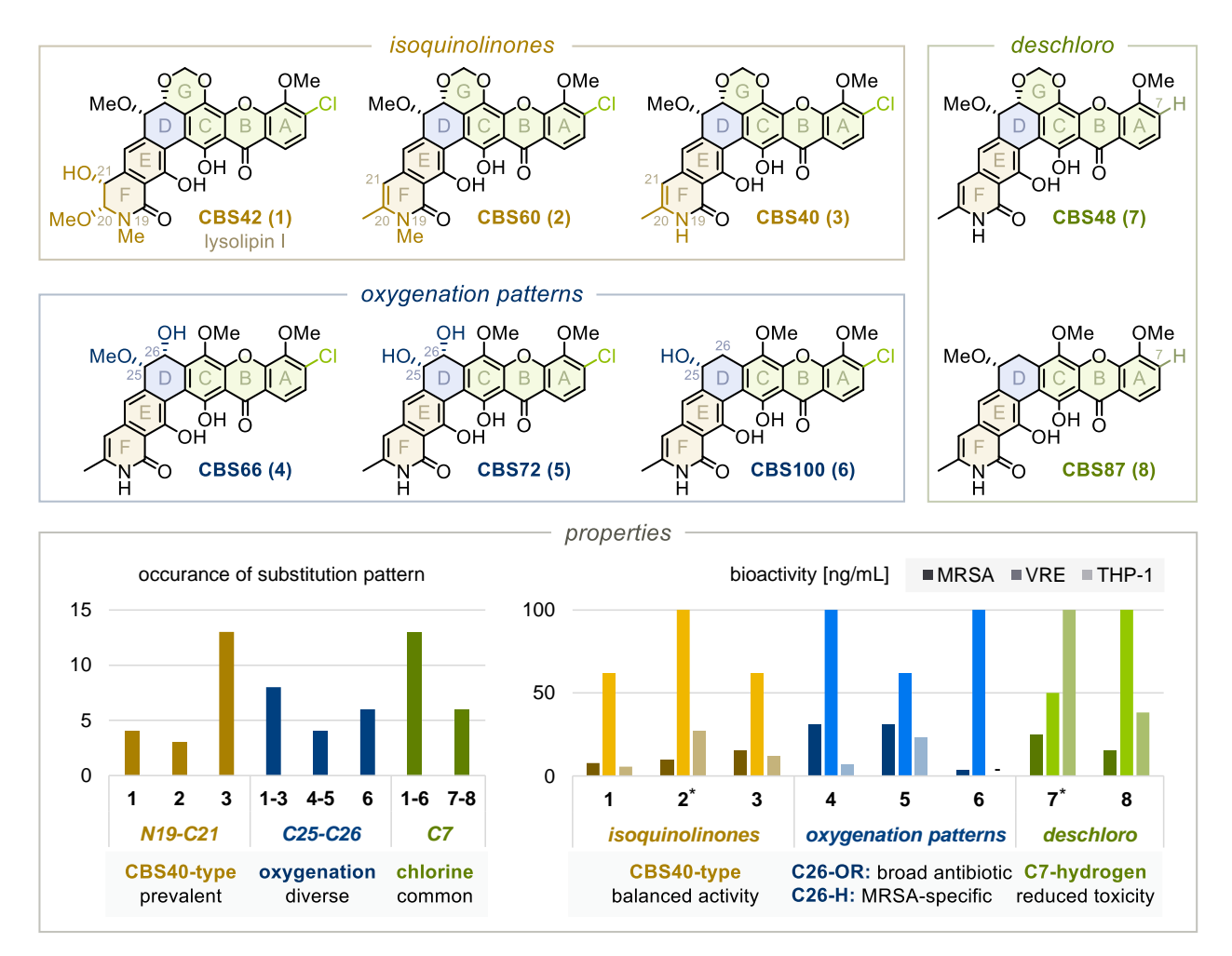


Figure 1. The lysolipin family in a nutshell: prevalent are CBS40-type lactam and C7-chlorine; D-ring determines antimicrobial activity, A-ring cytotoxicity. Bioactivity chart capped at 100 ng/mL. MRSA: methycilin-resistant *Staphylococcus aureus*, VRE: vancomycin-resistant *Enterococcus faecalis*. MRSA and VRE: minimal inhibitory concentrations, THP-1: half maximal inhibitory concentration. "-" cytotoxicity not determined, * minimal inhibitory concentrations approximated via complementary assay.²⁰

The structural diversity of the twenty lysolipins is remarkable.^{19,20,24} Unique features include three distinct isoquinolinone motives (orange), various *cis*-configured oxygenation patterns (blue) and an optional chlorine atom (green). Out of these, a CBS40-type F-ring (**3-6**) and C7-chlorine (**1-6**) prevail (orange and green), but D-ring patterns (blue) occur in equal proportions (left chart).

Lysolipin natural products are extremely active against drug-resistant bacteria, including MRSA – a WHO high-priority target¹ – and VRE, but cytotoxicity (THP-1) offsets this potency, limiting therapeutic potential (right chart).²⁰ In comparison, CBS40-type lactams (e.g. 3) and deschloro variants (7-8) exhibit reduced cytotoxicity, making them attractive synthetic target (orange and green). Furthermore, C25-C26-glycols (1-5 and 7) display broad-spectrum potency, whereas C25-mono-oxygenated members (6 and 8) selectively target MRSA in class-leading efficacy, stimulating a modular synthetic approach.

The mode of action of lysolipin natural products has yet to be fully elucidated. Early investigations indicate that lysolipin I (1) targets the bacterial membrane, 21,22 likely by binding to C55-lipid bactoprenol, a murein carrier for cell wall synthesis. The shared bioactivity and conformation among *cis*-glycol members suggest that a rigid, lipophilic shell (9) facilitates carrier interaction, resulting in broad-spectrum potency (Figure 2). 19,20,24 This is further supported by the markedly reduced activity of *trans*-glycol congeners, 26 which would disrupt this alignment by orienting perpendicular to the aromatic surface (10). 27

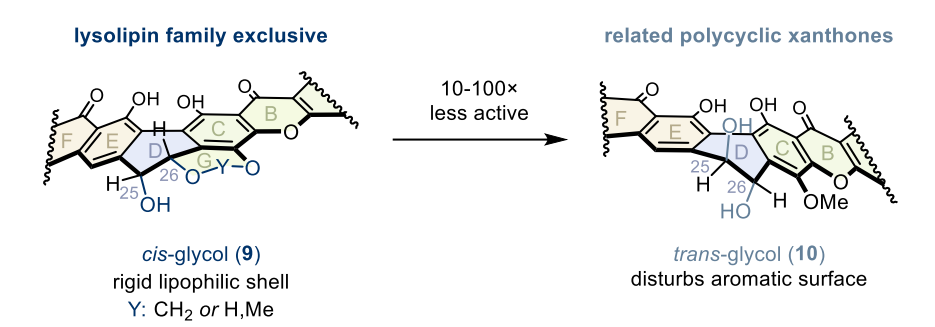


Figure 2. Glycol conformation determines antimicrobial activity of polycyclic xanthones.

The source of cytotoxicity remains unknown. While DNA intercalation similar to anthracyclines has been proposed, ¹⁸ this appears unlikely, as many polycyclic xanthones lack the sugar moiety essential for minor groove binding, yet surpass anthracyclines in potency (not shown). ²⁸ In conclusion, exquisite antimicrobial activities of lysolipins warrant a total synthesis. Synthetic efforts should prioritize the prevalent CBS40-lactam, while exploring diverse oxygenation patterns that drive target-specific potency. Tailored antiproliferative studies could reveal the source of cytotoxicity, guiding the development of safer analogs and anticancer drugs.

3 Historic Total Syntheses

Even though the remarkable bioactivity of lysolipin I (1) has been known for fifty years, a total synthesis for any of the twenty members has yet to be reported. $^{20-22}$ In a singular instance, Duthaler underwent extensive efforts to synthesize 11, but elaboration to 1 is neither reported nor apparent. $^{29-31}$

Figure 3. Failed center-to-edges total synthesis of lysolipin I.

To identify promising strategies, we will review historic polycyclic xanthone syntheses, noting that successful approaches dissected the central D-ring, thus constructing the xanthone (A-C) and heterocycle (E-F) beforehand. Guided by synthetic relevance (Chapter 1), the focus lies on overarching strategies to access uncharted scaffolds, 9,10 with emphasis on innovative approaches and emergent properties, 14,17 whereas protective group chemistry and functional group interconversion are discussed only when critical to the outcome. 15,16

3.1 Classical Works

Early reports focused on establishing fragment synthesis and coupling, targeting structurally less complex, mostly planar natural products.

Cervinomycin A₂ (1989)

In 1989, Kelly and co-workers reported the first polycyclic xanthone total synthesis, synthesizing cervinomycin A_2 (12) (Figure 4).³² They had to find solutions for the densely oxygenated xanthone unit (green), which also translates into a congested biaryl bond (blue). Furthermore, isocoumarin (E-F) is jointed with an oxazilidine (G), resulting in a quaternary hemiacetal at C20 (orange).

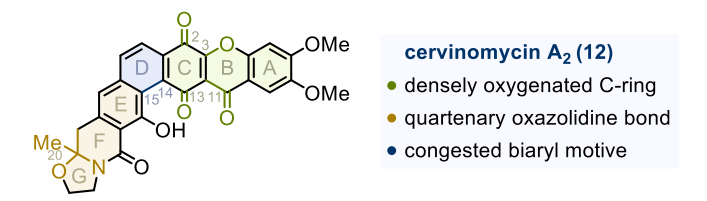


Figure 4. Challenging subunits in cervinomycin A₂.

Formal transposition of the methyl group from the C5-phenol to the C10-acid provided **14** (73%), initiating xanthone fragment synthesis (Figure 5). Interestingly, the authors forewent an operatively simple Fischer-Speier esterification in favor of a reactive but very dangerous diazomethane methylation.^{33,34} This suggests that the C10-acid lacks in reactivity, potentially due to an intramolecular hydrogen bond with the neighboring phenol (grey).

In the next step, they expanded Brassard's polar C-ring annulation strategy to include diiodo-benzoquinone **15** (48%). However, polar addition onto an electron deficient quinone seems to compromise the yield of **16**, since electron rich benzoquinones typically perform one and a half times better (over 80%),³⁵ highlighting a severe weakness of this valuable annulation sequence. Nevertheless, C-ring annulation efficiently provided xanthone **17** (69%) in a total of 6 steps and 24% yield.

Figure 5. Polar C-ring annulation provides xanthone fragments. MOM: methoxymethyl.

The authors opted for a directed *ortho*-metalation strategy to introduce the isoquinolinone ring on **18** (Figure 6).³⁶ First, steric hindrance from a distal silyl ether directs lithiation towards C17-amide **19** (87%). Then, the C17-amide favors metalation at C22, introducing an acetone unit in two steps (72%).

Despite being present in the natural product, the C17-amide was only used as a strong directing group, presumably due to a lack of suitable G-ring synthons. Thus, nitrosamide contraction (21) furnished C18-*tert*-butanolate 22,^{37,38} acidic deprotection thereof triggered F-ring cyclization and dehydration furnished C25-styrene 23 for later coupling (56%).

Finally, aminolysis installed the open G-ring in **25** (80%) and Mitsunobu cyclization closed the hemiaminal (99%), providing oxazolidine **26** in 9 steps and 28% yield. The usage of Mitsunobu conditions at this point is surprising, because (1) **25** should be unable to protonate the betaine

for turnover,^{39,40} and (2) **25** should readily cyclize to thermodynamically favored **26** without further additives (see below). Since the publication lacks any synthetic procedures, the stability of **25** remains speculative.

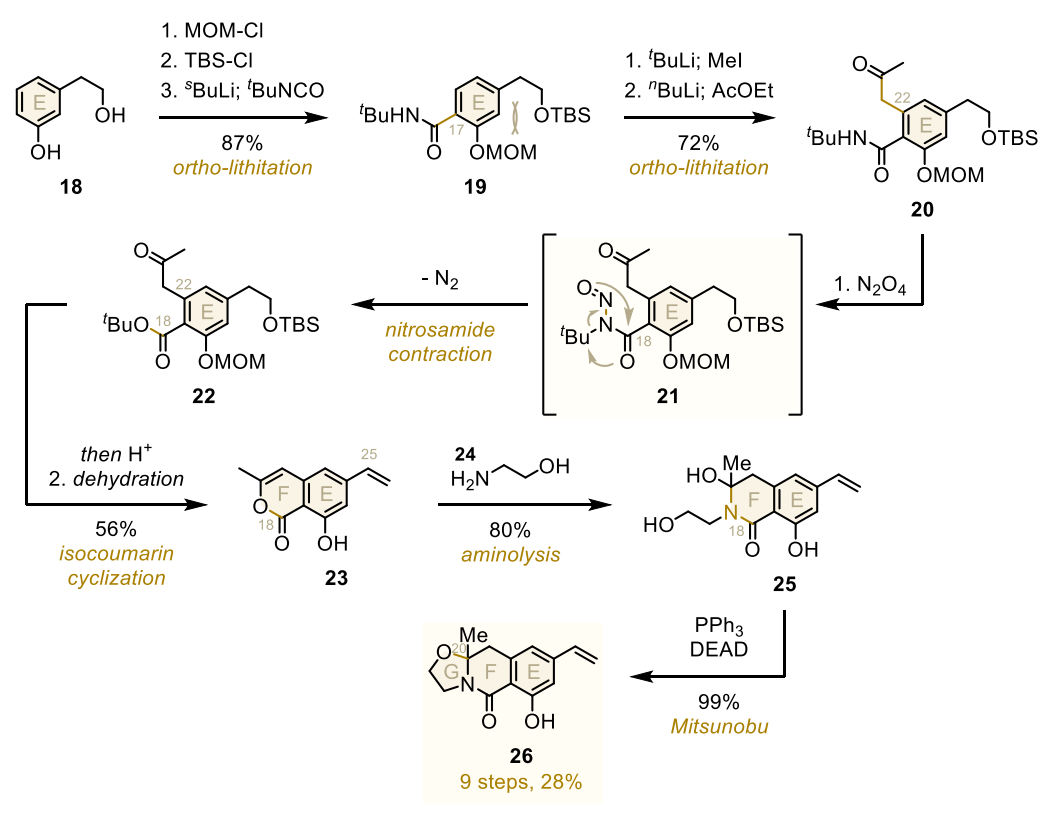


Figure 6. Sequential, directed metalations introduce the open F-ring of the isoquinolinone fragment. TBS: *tert*-butyldimethylsilyl, DEAD: diethyl azodicarboxylate.

As one of the earliest applications, Heck coupling jointed the fragments, efficiently providing stilbene **27** (65%). 41,42 Photochemical oxidation closed the D-ring and provided the natural benzoquinone C-ring (36%), yielding cervinomycin A_2 in an impressive concise sequence of 11 steps longest linear sequence (LLS) and 6% overall yield. Notably, even in absence of modern organic chemistry, every second reaction was a bond formation (50% ideality), meaning that strategic design kept protective group chemistry and functional group interconversions to a minimum. 15,16

Figure 7. Heck coupling and oxidative cyclization completed the first polycyclic xanthone total synthesis.

In particular, the C-ring annulation sequence stands out, requiring just three steps without additional protective groups. While a very concise transformation, photo-induced oxidative cyclization might need a reactive quinone C-ring, thereby restricted its application to **12**.

TMC-66 (2007)

While formally a polycyclic anthraquinone, the total synthesis of TMC-66 (**28**) by Hosokawa, Tatsuta and co-workers modernized polycyclic xanthone natural product synthesis (Figure 8).^{43,44} In particular, the authors developed elegant approaches to the chiral oxazolidine (orange) and ethyl-tethered bisphenol (blue).

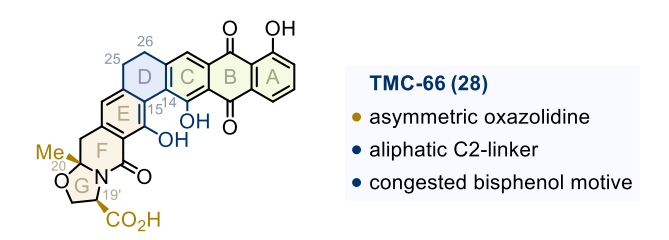


Figure 8. Elegantly solved, demanding structural features of TMC-66.

However, their anthraquinone fragment synthesis followed a classical route (Figure 9). First, air oxidation of the intermediate enolate provided benzoquinone **30** (47%). Then, Brassard's *endo*-Diels-Alder-elimination sequence (**33**) regioselectively furnished anthraquinone **34** (70%). Finally, triflation of the more acidic C1-phenol yielded **35** in five steps and 26% overall yield.^{45,46}

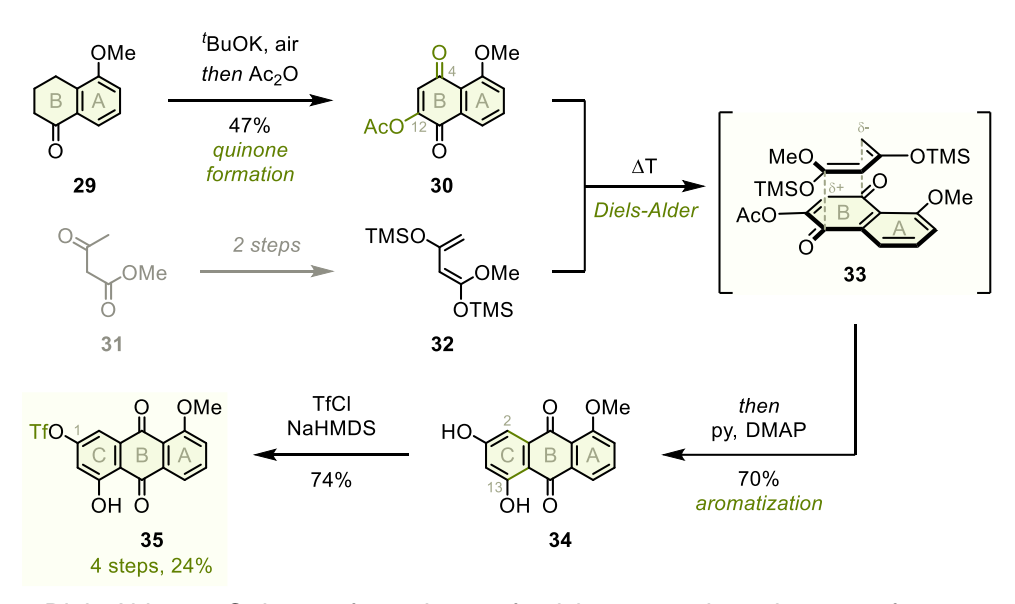


Figure 9. Diels-Alder C-ring formation furnishes anthraquinone fragment. DMAP: 4-dimethylaminopyridine, py: pyridine, HMDS: hexamethyldisilazane.

A significant advancement was their isocoumarin fragment synthesis, substituting the phenols in **36** to construct the full skeleton (Figure 10). First, triflation activated the phenols for cross-coupling. Then, site-selective Sonogashira coupling introduced the C_2 -linker at less hindered C24 (91%).⁴⁷ Next, Liu's modification of Migita's α -stannyl ketone coupling installed the open F-ring on **40** (83%).^{48,49} Finally, aminolysis with D-serine (**41**) diastereoselectively closed the lactam and oxazolidine ring through *Re*-face attack on intermediate C20-iminium ion **42** (60%), providing isoquinolinone **43** in just 5 steps and a remarkable 45% overall yield.⁴⁴

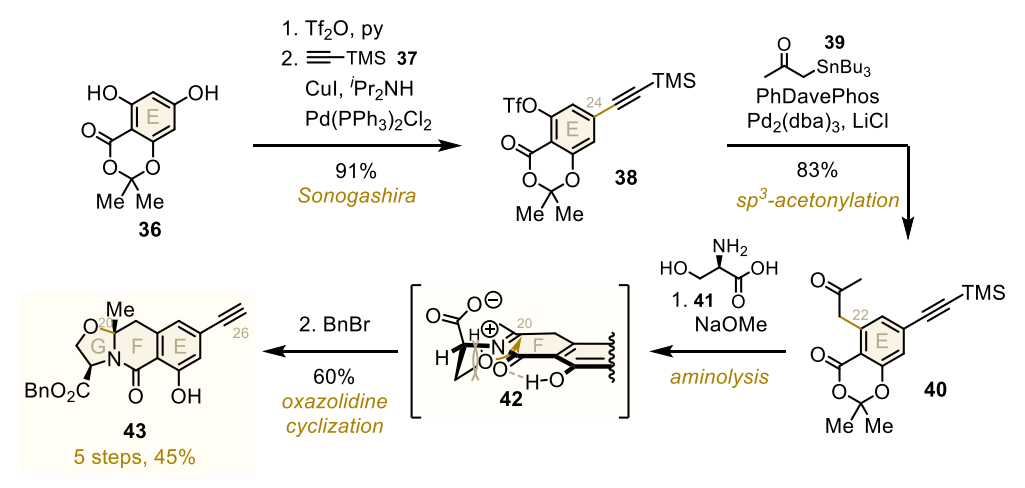


Figure 10. Cross-couplings enable concise isoquinolinone fragment synthesis. dba: dibenzylideneacetone, TMS: trimethylsilyl.

In the final steps, Sonogashira coupling jointed both fragments and Wilkinson reduction saturated C₂-linker **44** (63%) (Figure 11).^{47,50,51} Building on Koga's seminal work,^{52,53} optimized

copper(II)-complex **45** regioselectively closed the D-ring and upon deprotection (62%) TMC-66 (**28**) was obtained in just 9 steps LLS, 9% overall yield and 50% ideality.

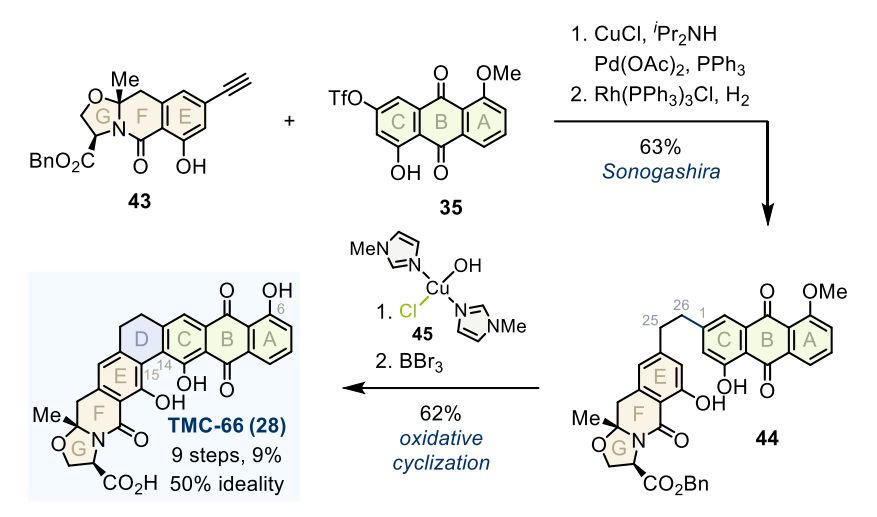


Figure 11. A unique copper oxidant closed the central D-ring.

In comparison, the isocoumarin strategy constitutes a two-fold improvement over elaborate lithiation chemistry (see above), highlighting the power of cross-couplings in fragment construction. Furthermore, copper oxidant **45** selectively couples both *ortho*-phenol position without prior activation – a regioselectivity that to this day is seldom reproduced.^{54,55}

3.2 The Modern Age

Modern work focused on extending the attainable structural space, putting a particular focus on asymmetric hydroxylated D-ring containing natural products.

FD-594 Aglycon (2009)

In 2009, Suzuki and co-workers heralded the modern era of polycyclic xanthone total synthesis (Figure 12), targeting FD-594 aglycon (46) containing a *trans*-dihydroxylated D-ring (blue).⁵⁶ Further challenges arise from the chiral isocoumarin unit (orange) and tetra-*ortho*-substituted benzophenone (green). Their work is an implicit compendium on challenges and solutions in asymmetric synthesis of these complex natural products.

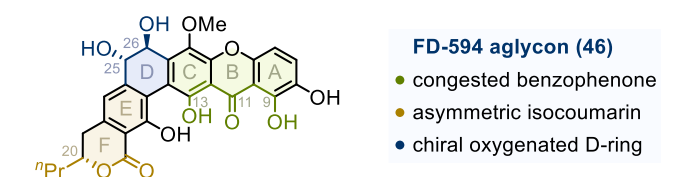


Figure 12. Unique motives in FD-594 aglycon.

Their xanthone fragment synthesis began with chloronium ion mediated aromatization of **47**,⁵⁷ followed by reductive desymmetrization, furnishing the C11-alcohol in **48** (Figure 13). Then, methylation gave the natural C2-anisole, and for A-ring annulation a C3-bromine was introduced as well as the C11-alcohol selectively oxidized to aldehyde **49** (59%). Nucleophilic addition of C10-lithiated **50** onto the C11-aldehyde **49** efficiently linked A- and C-ring together and the C11-alcohol was re-oxidized to C11-benzophenone **51** (85%). Finally, liberation of the C5-phenol set **52** up for B-ring closure (97%).

The early introduction of a C3-bromine indicates that the authors targeted an Ullman-coupling, since bromines are useful leaving groups in palladium and copper mediated cross-couplings. Yet, a nucleophilic aromatic substitution was reported instead, after substantial optimization to suppress dehydrative coupling of the C13-benzyl ether caused by the low electrophilicity of the C3-bromide (84%).⁵⁹ In comparison, steric hindrance strongly impedes both C-O and related C-N bond formation via cross-coupling, making nucleophilic substitution often the preferred option for *ortho*-substituted scaffolds.^{60–63} Based on these insights, later work used an electron withdrawing fluorine instead (Chapter 3.3). For subsequent fragment coupling, the C1-ester was hydrolyzed (99%), providing **54** in 13 steps and 41% yield.

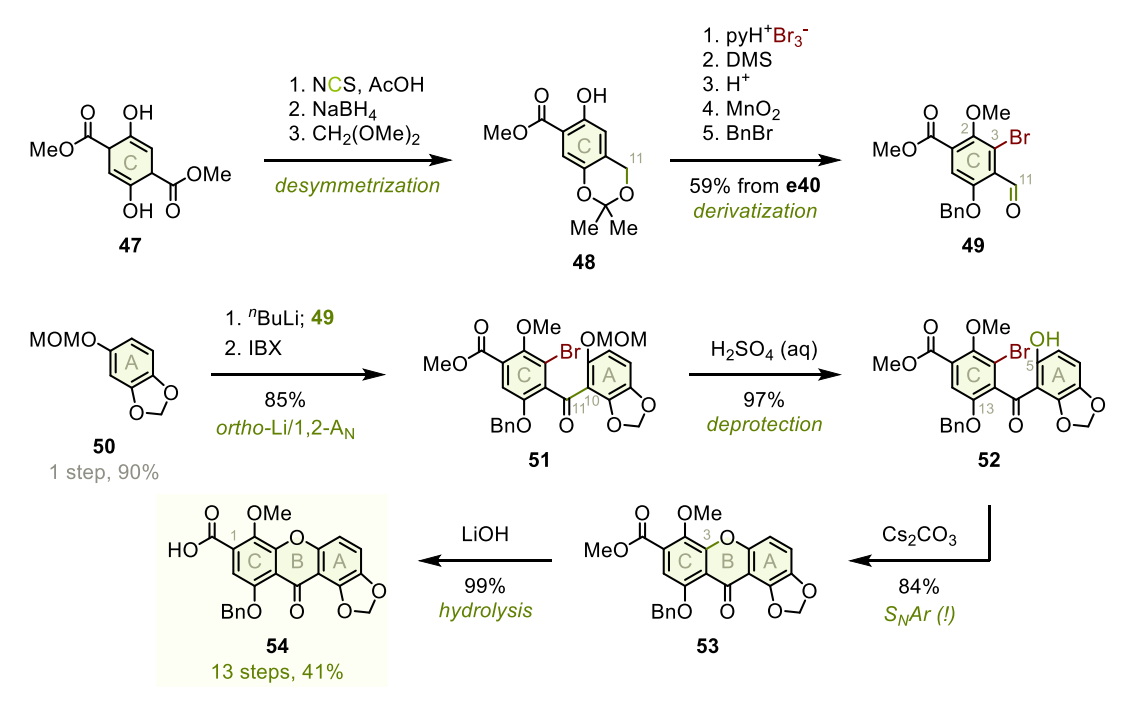


Figure 13. A surprising nucleophilic aromatic substitution furnishes the xanthone fragment. NCS: *N*-chlorosuccinimide, DMS: dimethylsulfate, IBX: 2-iodoxybenzoic acid.

Their isocoumarin fragment synthesis started with introduction of the C22-bromine for subsequent F-ring annulation (Figure 14), followed by protection of the remaining functional groups, providing **57** (88%). After lithium-halide exchange, nucleophilic ring-opening of epoxide **58** installed the open F-ring, and solvolysis of the MOM ether allowed the formation of the C17-triflate in **60** (51%).⁶⁴ Then, a very challenging alcohol cross-coupling with concomitant carbon monoxide incorporation closed the F-ring in **61** (91%). Arguably, both the C16-methoxy group and the C24-acetal set **61** up for double directed *ortho*-metalation to selectively introduce the C15-iodide.³⁶ However, the authors reported a rare phenol directed electrophilic aromatic substitution instead (**62**),⁶⁵ suggesting that the lactone was intolerant towards metalation reagents. Furthermore, while in principal only the C16-phenol had to be liberated for directivity, the C25-acetal was also deprotected and reduced, indicating that in this case both alcohols were required for selectivity.⁶⁶ In total, this detour would cost six steps: two protective group interconversions and one redox-cycle. Nevertheless, protection of the benzylic alcohol furnished **63** (83%) in 11 steps and 34% yield.

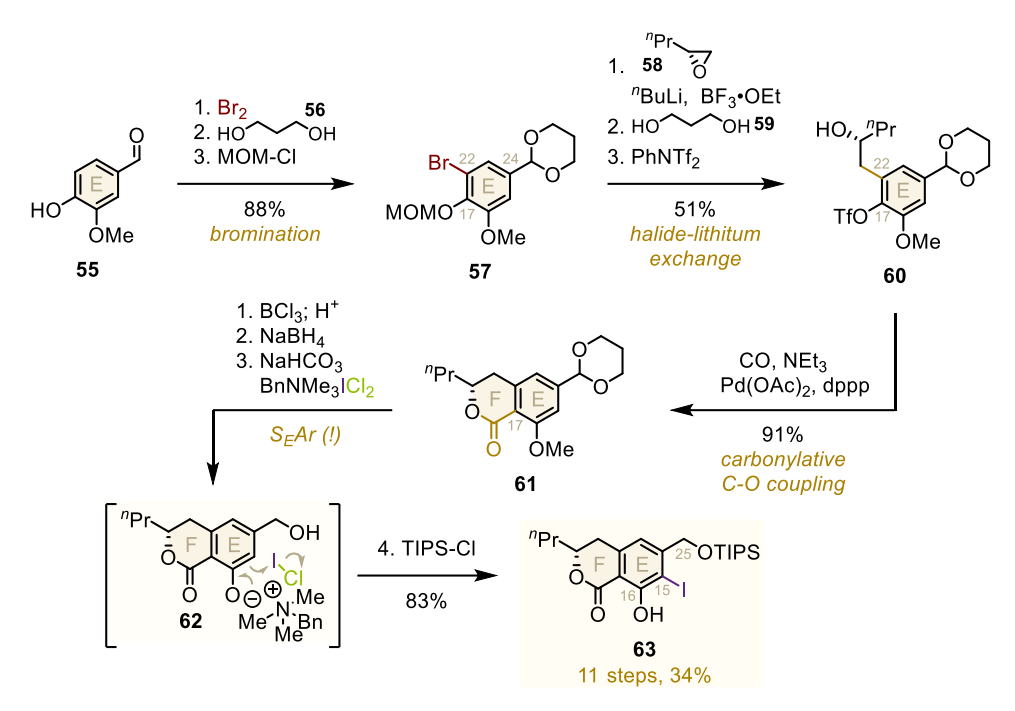


Figure 14. A demanding carbonylative cross-coupling and rare phenol directed iodination provided the isocoumarin fragment. TIPS: triisopropylsilyl.

In the end game (Figure 15), a temporary ester (quantitative) pre-organized **64** for biaryl bond formation to **65** and atroposelective lactone opening provided (*M*)-helical amide **67** (85%). Low selectivity from single step CBS reduction⁶⁷ caused the authors to develop this aminolysis strategy, which proceeded in good diastereoselectivity but required three additional steps to release C26-aldehyde **68** (63%).⁶⁸

Further troubles arose in transferring the chirality from axial to central, as the xanthone was intolerant to one electron pinacol coupling. Therefore, the C11-benzophenone had to be defunctionalized, such that after deprotection and oxidation to the C25-aldehyde xanthene **69** was obtained (81%).⁶⁹ Then, substrate-controlled pinacol coupling formed the *trans*-diol (**70**),⁷⁰ and C11-reoxidation furnished completed skeleton **71** (71%). Finally, a four step deprotection sequence (81%) furnished FD-594 aglycon (**46**) in lengthy 34 steps LLS but impressive 9% overall yield, suggesting thoroughly optimized protocols. Expectedly, the many functional group interconversions resulted in an ideality of just 18%.

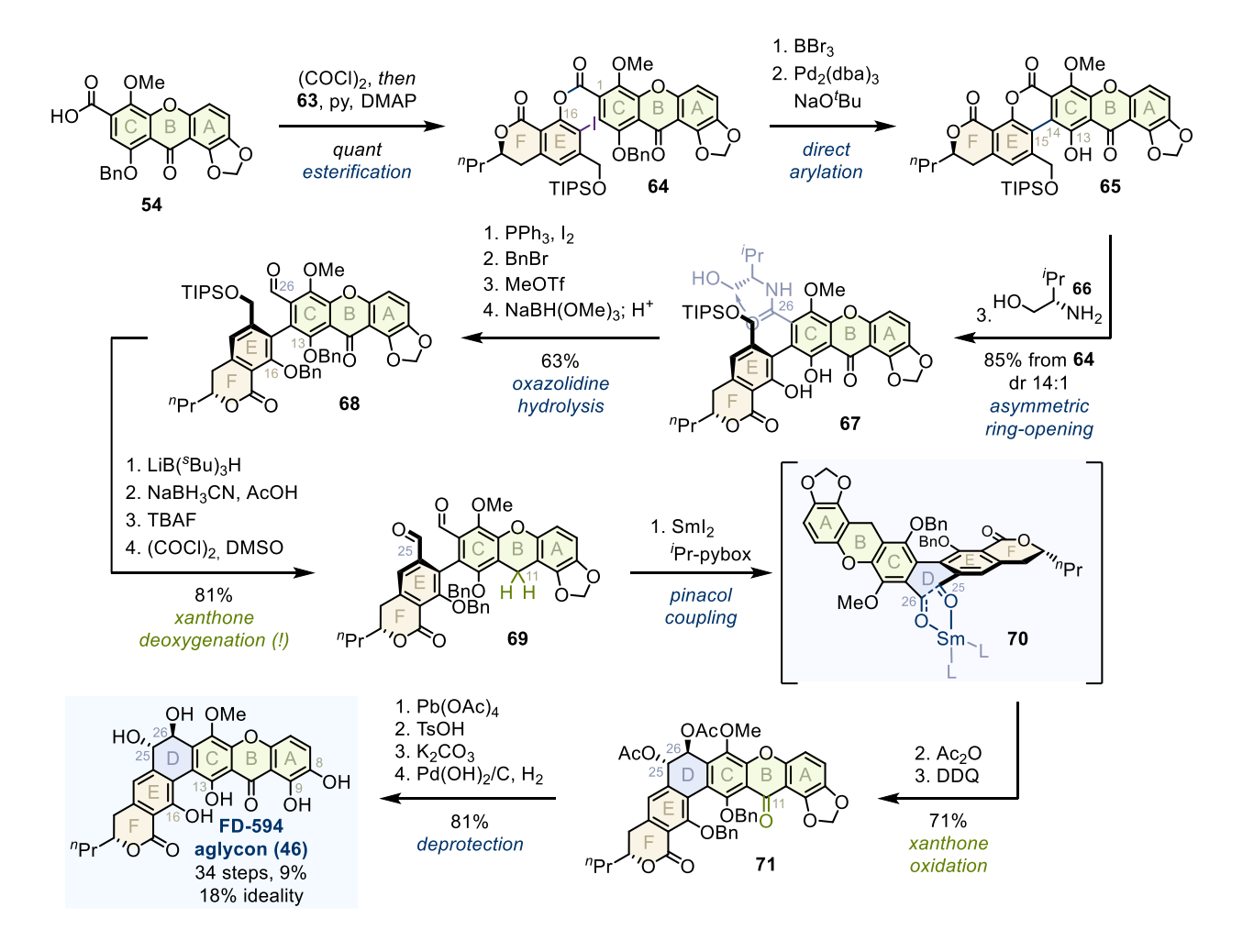


Figure 15. Translation of axial chirality to central chirality furnished the asymmetric D-ring. dr: diastereomeric ratio, TBAF: tetrabutylammoniumfluorid, DDQ: 2,3-dichloro-5,6-dicyano-1,4-benzoquinone.

An advantage over polar C-ring annulation (Chapter 3.1) is that Suzuki's lithiation strategy tolerates *ortho*-benzophenone substituents at all four positions. In fact, two of them direct the benzophenone bond formation (**51**). A downside is the requirement for pre-functionalized, fully protected substrates, resulting in over double the step length.

During the synthesis, polycyclic substrates exhibited a limited stability against one electron and metalation conditions. Possibly, multiple electrophilic centers complicate a selective reaction of these very reactive intermediates. By contrast, even challenging transition metal catalyzed bond formations such as direct arylation to **65** remain well-tolerated, making them the preferred method of choice.

While chirality transfer is a creative concept to construct the central *trans*-diol, the synthetic sequence may benefit from such a metal catalyzed approach, as currently nine late game steps are required to construct the D-ring (see also Chapter 3.3). With these insights in mind, a

streamlined synthesis could be possible, using considerably less than six different protection groups and sixteen protective group steps.

Simaomicin α (2013)

In 2013, Ready and co-workers were the first to synthesize an asymmetric mono-oxygenated D-ring (blue), targeting simaomicin α (72) (Figure 16).⁷¹ In addition, the C25-alcohol forms a mixed bridgehead acetal with the neighboring E-ring (orange), and the xanthone contains a chiral A-ring (green).

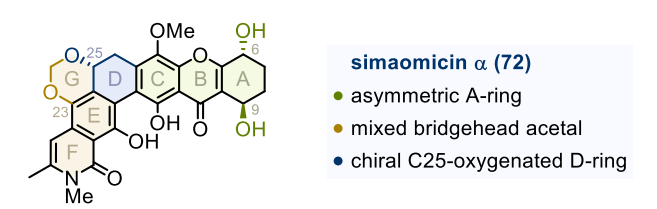


Figure 16. Chirality and a mixed acetal linker distinguish simaomicin α.

Overall, the authors adopted Suzuki's xanthone fragment synthesis, but refrained from disclosing synthetic procedures and yields for the first third of the synthesis (Figure 17), obstructing reproduction and translation to related natural products.^{71,72} After kinetic resolution, Baylis-Hilman conditions introduced the C10-iodine for later coupling,^{73,74} and Luche reduction provided **75** (67%).⁷⁵ In line with previous challenges during metalation chemistry, the authors forewent double directed *ortho*-metalation to C12 in favor of a two-step phenol directed formylation sequence, eventually arriving at elaborate **78** (77%).³⁶

After deprotonation of the C5-alcohol, lithium-halide exchange furnished the C10-nucleophile to link A- and C-ring together, resulting in **79** (80%). After oxidation of both alcohols (**80**),⁷⁶ acidic conditions liberated the C3-phenol for B-ring cyclization at C5, and tautomerization towards the thermodynamically favored, conjugated B-ring transposed the C5-alcohol to C9, completing xanthone skeleton **81** (73%). Because hydration of the intermediate carbocation proceeded unselectively, a redox cycle had to correct the C9-stereocenter (65%).^{76,77}

In the final steps, Stille-allylation introduced the masked C₂-linker at C1 (97%), and dihydroxylation of the terminal alkene followed by glycol cleavage unmasked the sensitive C25-aldehyde **85** for later coupling in a long 19 steps and unknown overall yield.

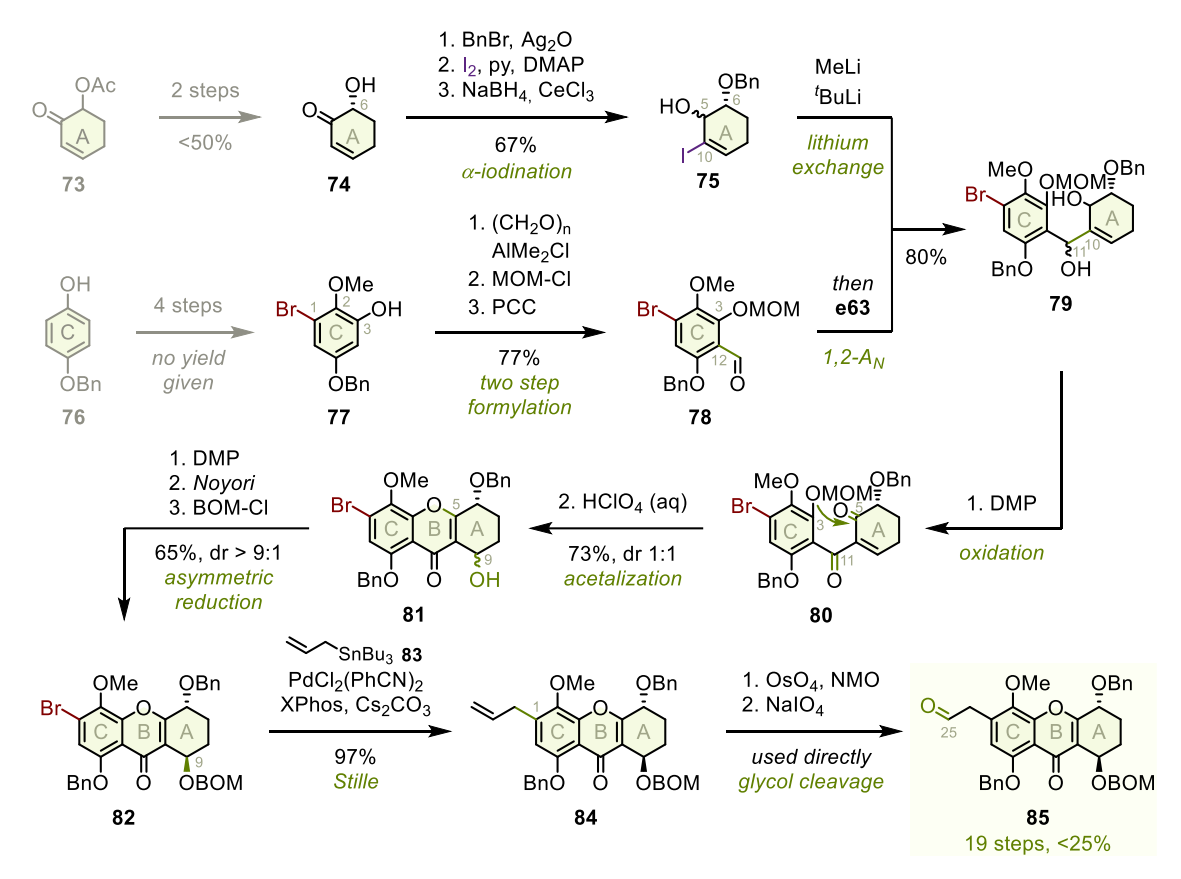


Figure 17. Transpositional B-ring cyclization and oxidative allyl-cleavage furnished the xanthone fragment. DMP: Dess-Martin periodinane, BOM: benzyloxymethyl, NMO: *N*-methylmorpholine oxide.

In contrast, their isocoumarin synthesis was exceptionally short (Figure 18). After oxidation of the aldehyde, Schotten-Baumann conditions furnished amide **88**. Then, the C21-alcohol was oxidized, cyclized and eliminated to close the F-ring, providing **89** in a remarkable 5 steps and 51% overall yield.

Figure 18. Concise isoquinolinone fragment synthesis. TEMPO: 2,2,6,6-tetramethylpiperidinyloxy.

The authors pursued a very demanding metalation strategy to join both fragments, since aldehyde **85** was readily deprotonated to the corresponding enolate (not shown) under various conditions (Figure 19). Eventually, lanthanoid salts – in particular lanthanum(III)-chloride with additional lithium chloride for solubility – were found to promote nucleophilic addition, arriving at jointed **90** (76%).⁷⁸ Again, a redox cycle had to correct the racemic C25-stereocenter in **91**

(92%). 76,77 After substantial optimization, the authors identified that only a methylene with leaving groups of different strength could prevent polymerization by stepwise reaction (92), furnishing mixed bridgehead acetal 93 (65%). In the final steps, the G-ring facilitated oxidative D-ring cyclization through pre-organization, such that after deprotection (74%) the enantiomer of simaomicin α (72) was obtained in a lengthy 27 steps LLS, unknown overall yield and 28% ideality.

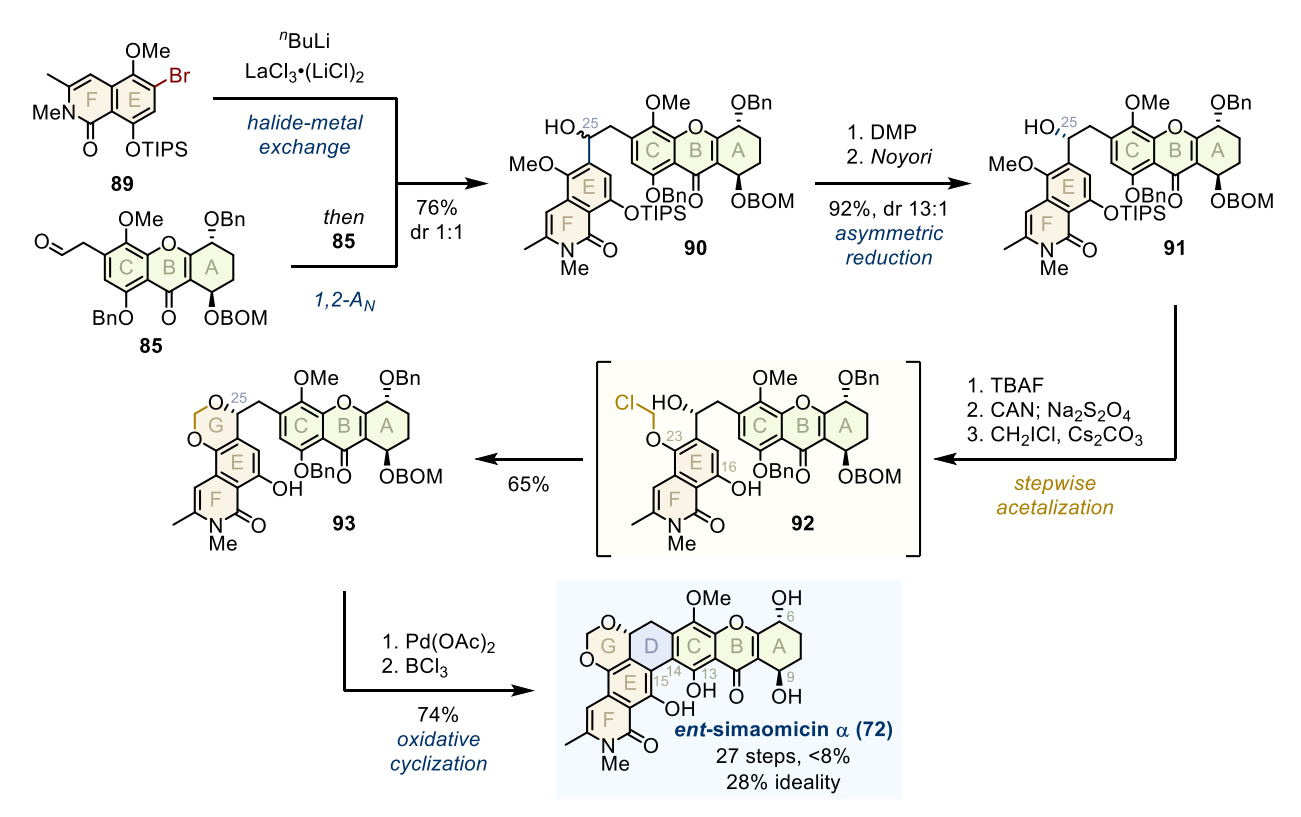


Figure 19. A lanthanum salt jointed both fragments and stepwise acetal formation pre-organized the skeleton for ultimate D-ring cyclization. CAN: ceric ammonium nitrate.

Overall, asymmetric bond formation remains an unsolved challenge, as all stereocenters had to be corrected in separate redox cycles. In conjunction with a lack of suitable synthons, this results in six steps needed to form the outer D-ring — a three-fold extension over non-hydroxylated D-rings (Chapter 3.1). In contrast, the planar isoquinolinone fragment was efficiently accessed. Finally, stepwise G-ring acetalization represents an insightful solution to the disparate nucleophilicity of aromatic and aliphatic alcohols.

Kigamicin Aglycon (2019)

In 2019, Ready tried to translate established sequences to kigamicin aglycon (94) (Figure 20), containing a C26-ether (blue).⁷⁹ While at first glance almost identical to simaomicin α (72) and

TMC-66 (28), the authors encountered severe difficulties in forming the regioisomeric bridgehead acetal (green) and decarboxylated oxazolidine (orange).

Figure 20. Superficially identical to previous natural products but in reality unique: the kigamicin family.

The authors revamped their A-ring synthesis (Figure 21), presumably to circumvent late correction of the C9-stereocenter (see above). In detail, **96**^{80,81} was protected under neutral conditions, see such that after iodination a substrate controlled Luche reduction furnished desired C9-alcohol **97** (54%). The remaining sequence to **98** largely follows paths taken (69%). New was a mismatched C5-specific Riley oxidation (**99**) to initiate dehydrative B-ring cyclization (70%), section (70%), providing **100** in 14 steps and rather low 10% yield.

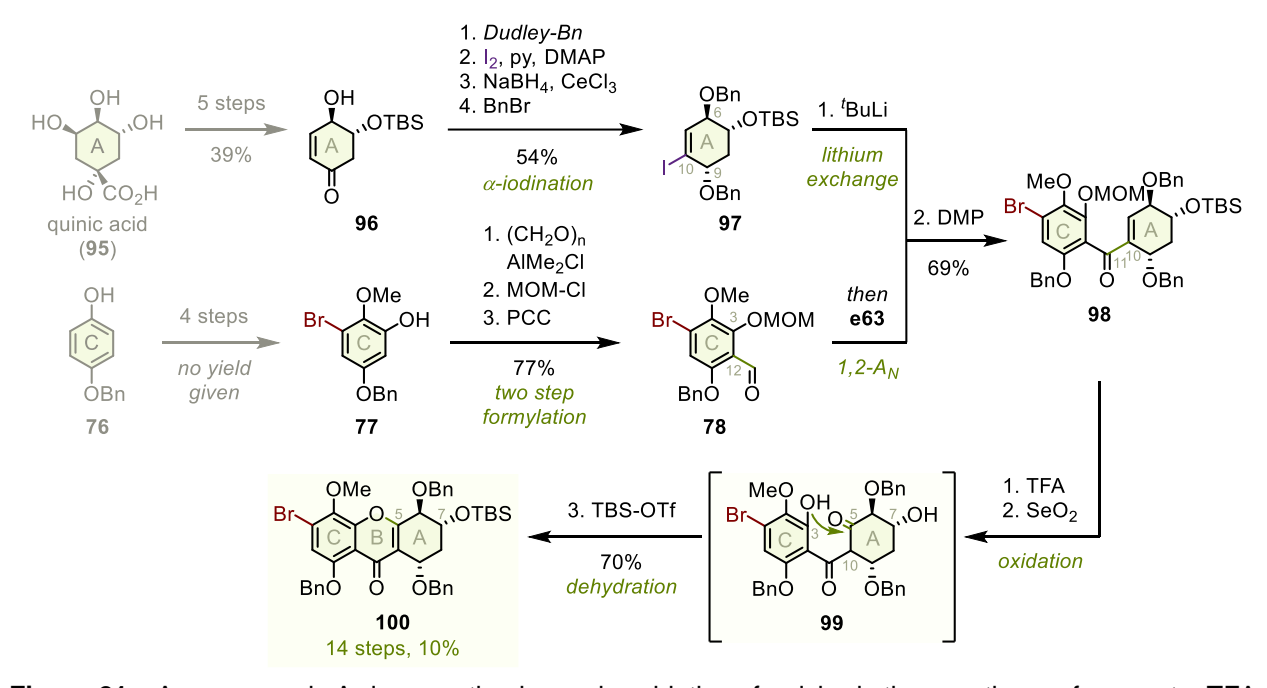


Figure 21. A revamped A-ring synthesis and oxidation furnished the xanthone fragment. TFA: trifluoroacetic acid.

For the isocoumarin fragment, they inverted Hosokawa's and Tatsuta's coupling strategy (Chapter 3.1) to allow for in-between decarboxylation (Figure 22). Thus, acetonylation of C24-protected **101**⁸⁵ installed the open F-ring at C22 (80%),^{48,49} and aminolysis with concomitant oxazolidine cyclization provided the isoquinolinone skeleton **103** (80%).^{43,44} After controlling *Re*-face addition on C20, the C19'-acid was removed via decarboxylation of the intermediate

selenoester, furnishing **104** (56%).⁸⁶ Upon deprotection and triflation of the more reactive unhindered C24-phenol (90%), Sonogashira coupling introduced the C₂-linker for subsequent fragment coupling (77%),⁴⁷ providing **106** in 12 steps and 22% overall yield.

Figure 22. An inverted cross-coupling order enabled intermediate decarboxylation to the final isoquinolinone fragment. AIBN: azobisisobutyronitrile.

The combination of Merck's base⁸⁷ and Fu's catalyst⁸⁸ efficiently furnished congested C1-alkyne **107** (70%). However, exceptionally poor scalability and mediocre regioselectivity (3:1 not shown) limited hydration of the internal alkyne to C26-ketone **108** (57%).⁸⁹ The ketone was enantioselectively reduced (60%),⁷⁷ and Hosokawa's and Tatsuta's copper oxidant **45** selectively closed the central D-ring under optimized conditions, yielding **110** (61%).^{43,44} Alas, severe sensitivity of the A-ring prohibited further elaboration to C26-acetal **111**, prematurely ending the total synthesis of kigamicin aglycon (**94**).

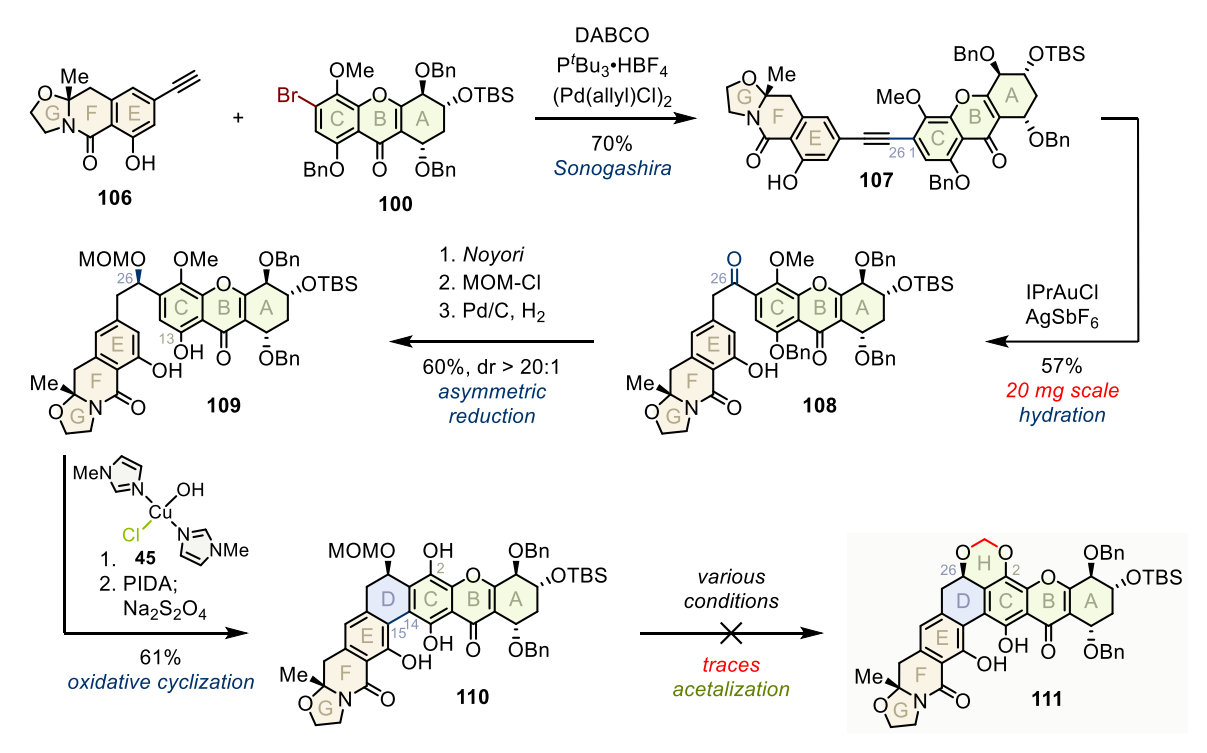


Figure 23. Limited scalability and severe sensitivity of the tetrahydroxanthone precluded a successful endgame. DABCO: 1,4-diazabicyclo[2.2.2]octane, IPr: 1,3-bis(2,6-diisopropylphenyl)imidazole-2-ylidene, PIDA: phenyliodine(III)-diacetate.

Taken together, this total synthesis underlines the limitation of traditional bond formation in delivering functionalized intermediates. Specifically, while established coupling methods delivered carbon skeletons 103 and 107 in good yield (80% and 70%), subsequent remodeling to correct oxygenation patterns towards 104 and 108 represent the two lowest yielding transformations of the total synthesis (56% and 57%). Furthermore, both transformations required several reactions, either due to the need for pre-activation (104) or because of scale limitation (108). These findings illustrate a broader and persistent challenge in synthetic chemistry: the selective late-stage functionalization of complex scaffolds (Chapter 1). Therefore, an initial bond forming reaction that concomitantly installs the desired functional groups has the potential to be more selective and concise.

Importantly, the authors extended copper oxidant **45** to xanthone containing natural products. Finally, comparison to their successful total synthesis of simaomicin α (**72**) suggests that the mixed bridgehead acetal (**111**) must be introduced before D-ring cyclization, possibly because ring strain prohibits further derivatization.

3.3 Post-Modern Synthesis

Recent work aims for a concise asymmetric total synthesis, replacing traditional elongated sequences with challenging direct bond formations.

FD-594 (2020)

In 2020, Gao rejuvenated the synthesis of the central D-ring (blue) of FD-594 aglycon (**46**) while also accessing its glycosylated counterpart **112** (green, not discussed) (Figure 24).⁹⁰

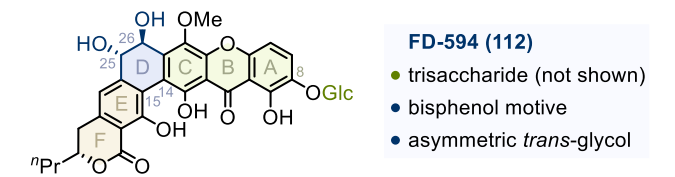


Figure 24. New approaches to the challenges of FD-594 rejuvenate its synthetic impact. Glc: glucoside.²⁷

For xanthone fragment synthesis (Figure 25), the authors adopted Suzuki's lithiation strategy to fluorine-bearing **114** (86%). Like Ready, they synthesized SEM protected **115** without disclosing synthetic procedures and yields for six out of seven steps, meaning that over 40% of their fragment synthesis remains undocumented.^{72,90} Then, the fluorine group directed lithiation towards C10,³⁶ and nucleophilic addition onto the C11-aldehyde furnished **116** (77%). Oxidation provided the C11-benzophenone,⁷⁶ and deprotection liberated C3-phenol **117** for subsequent cyclization. With the C5-fluorine as enhanced leaving group, nucleophilic substitution proceeded under common conditions,⁵⁹ such that after protective group interconversion (61%) **118** was obtained in **13** steps and unknown yield.

Figure 25. Xanthone synthesis inspired by Suzuki and Ready. SEM: 2-(trimethylsilyl)ethoxymethyl, MOTCE: 2,2,2-trichloroethoxymethyl.

For the isocoumarin fragment (Figure 26), Morken's alkyl cross-coupling followed by oxidative cleavage installed the open F-ring and released C20-alcohol **121** (70%). Formylation at C17 closed the F-ring (**123**), presumably after orthoester formation with the C20-alcohol (not shown). Jones oxidation corrected the C18-oxidation state, and after deprotection the less hindered C24-alcohol was selectively triflated for further elaboration, providing **124** (73%). Sonogashira coupling introduced the C_2 -linker at C24 (80%), and copper catalyzed hydroboration thereof surprisingly furnished (*E*)-boronic ester **126** (87%) in a total of 8 steps and 36%.

Figure 26. Isocoumarin synthesis starts with a demanding Suzuki-Miyuara-alkylation and ends with a boronic ester for kindred fragment coupling. ee: enantiomeric excess.

In a concise endgame (Figure 27), Suzuki-Miyaura cross-coupling forged both fragments to stilbene **127** (92%).⁹⁴ Stoichiometric Sharpless dihydroxylation introduced the central

trans-diol,⁹⁵ and protective group chemistry liberated the C13 and C16-phenols in **128** as anchor points for subsequent cyclization (90%). Improved copper oxidant **129** enabled bisphenol coupling, such that after deprotection (71%) FD-594 aglycon (**46**) was isolated in 21 steps LLS, unknown overall yield and decent ideality of 34%. Despite being essential for the total synthesis, a synthetic procedure for **129** was not provided in the experimental part of the manuscript.^{72,90}

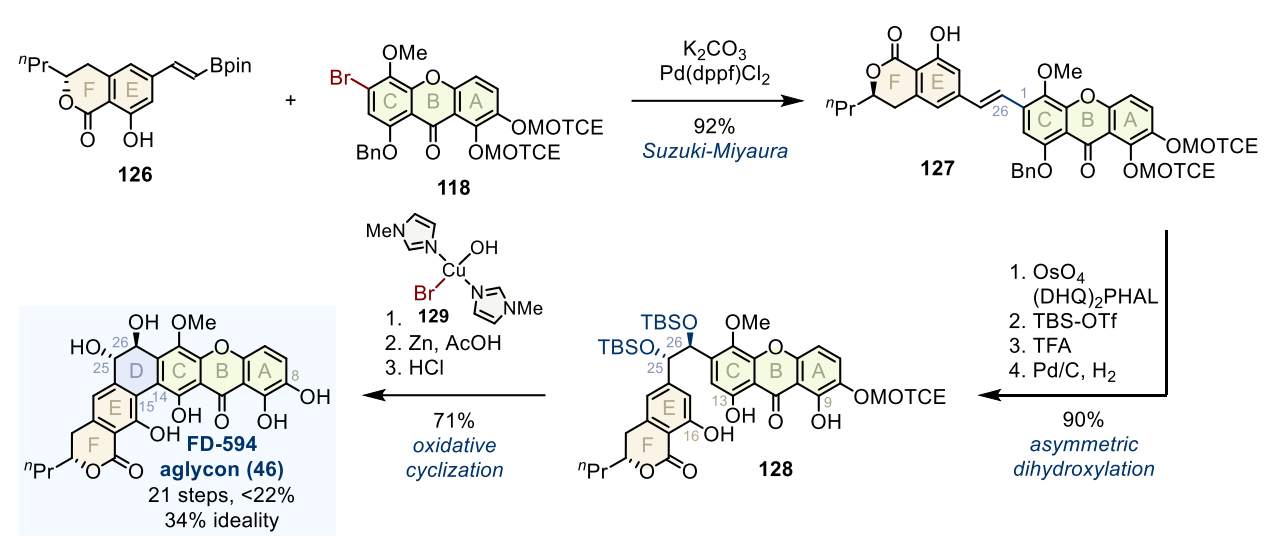


Figure 27. Stoichiometric dihydroxylation and copper oxidized cyclization form the central D-ring.

The revised endgame – in particular the asymmetric dihydroxylation – constitutes a major advancement over an elaborate chirality transfer strategy (Chapter 3.2), improving step size and overall yield by a factor of two. Meanwhile copper(II)-imidazole oxidants emerge as preferred option for late stage D-ring closure, since they exploit the natural substitution pattern for regioselectivity instead of requiring pre-functionalized scaffolds. Finally, a demanding site-selective alkyl cross-coupling shortens isocoumarin fragment synthesis, while in principal requiring a less extensive protective group scheme.

In the light of these advancements, the current xanthone strategy appears circuitous. Altogether, four out of six unique protective groups stem from this sequence, yet the late game requires at most a single protected phenol at C8.

3.4 Present Insights from the Past

Projecting established total syntheses onto lysolipin natural products reveals two possible routes to xanthone fragment **133** (Figure 28). The more common approach involves nucleophilic addition of lithiated **131**, but it incorporates three major drawbacks (grey route). First, aldehyde precursor **130** must be laboriously formed over often undisclosed sequences, suggesting shallow overall yields. ^{71,72,90} Second, although a C9-anisole improves selectivity during the initial metalation step, it is absent from desired xanthone fragment **133**. ^{20,56} Third, harsh lithiation conditions impose extensive protective group chemistry on the whole sequence. ^{56,71,90} In contrast, polar addition enables coupling of readily and commercially available quinones **134** ^{72,96} without the need for a C9-substituent or protective group chemistry (black route). ^{32,35} However, its utility is currently limited by a narrow substrate scope – in particular the inability to accommodate C6-substituents and (poly)halogenated scaffolds such as **133**. ^{32,35}

Figure 28. Narrow substrate scope limits broad application of polar ring annulation in xanthone synthesis.

Three elegant routes have been developed for F-ring introduction (Figure 29). Among these, the acetonylation sequence by Hosokawa and Tatsuta is particularly attractive (black route), ^{48,49} as it would deliver the natural skeleton **137** after aminolysis with ammonia. ^{43,44} In contrast, alkyl cross-coupling with **120** would result in an aliphatic isocoumarin, ⁹⁰ and dehydrative cyclization of **86** most likely requires the C23-anisole for reactivity, ⁷¹ meaning that these sequences detour from target **137**.

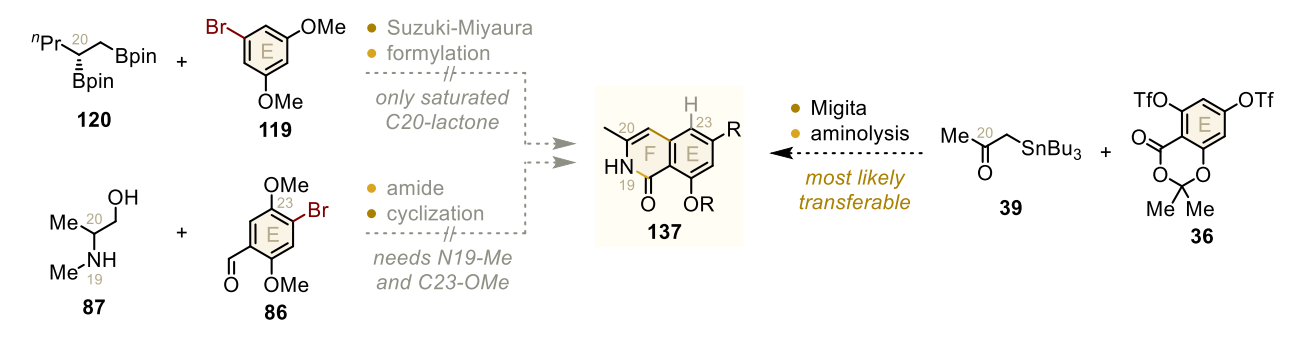


Figure 29. Conciseness and modularity makes Migita-acetonylation an attractive choice.

Substantial efforts have been directed to the construction of chiral, oxygenated D-ring containing natural products. Although selected creative solutions have emerged, these remain confined to the disclosed motives (Figure 30). In detail, Ready successfully hydrated internal alkyne 107, 79 but electronic effects limit oxygenation to C26, disfavoring desired C25-alcohol 138. Furthermore, Gao achieved enantioselective dihydroxylation of (*E*)-stilbene 127, 90 yet transferring this sequence to a hypothetic (*Z*)-stilbene would afford mostly racemic 139 due to a mirror plane in the central alkene. 95 In contrast, ultimate D-ring cyclization using copper(II)-oxidants such as 129 has been well-established. 43,44,79,90

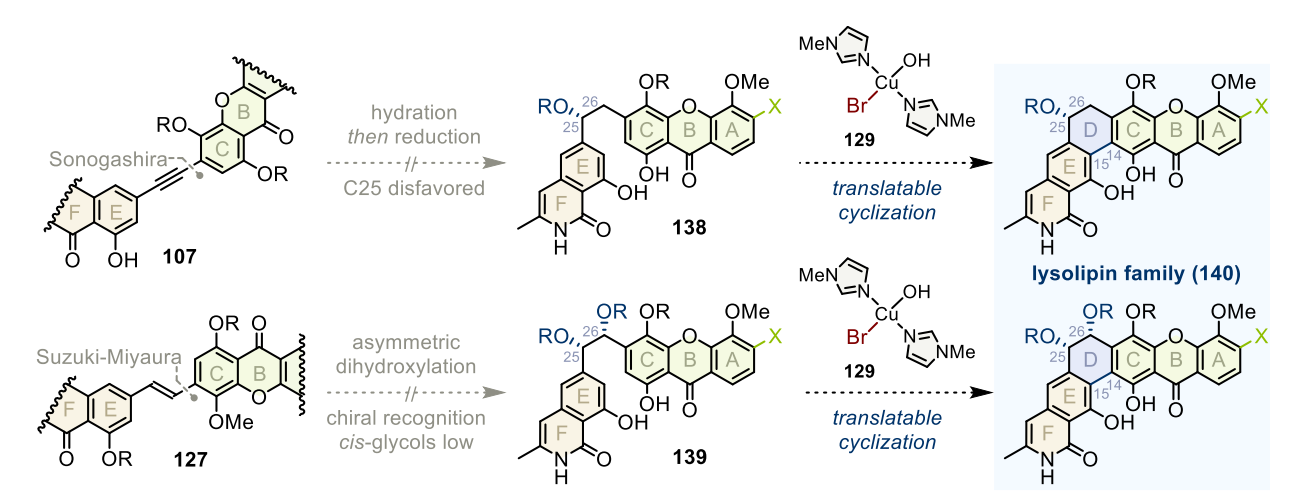


Figure 30. Unique oxygenation patterns are the central synthetic challenge of lysolipin natural products.

Thus, the unique oxygenation patterns of lysolipin natural products (**140**) emerge not only as focal point for bioactivity, but also as the central synthetic challenge. Access to these structures will likely involve hitherto unexplored sequences. ¹⁴ Moreover, expansion of Brassard's polar ring annulation strategy would improve fragment availability, thereby supporting systematic exploration of subsequent coupling strategies.

4 Approach to Lysolipin Family

The hybrid structure **140** serves as a general representation for potent lysolipin members (Figure 31). Key features include a sterically congested, optionally chlorinated A-ring (green), an unsubstituted lactam motif (orange) and synthetically challenging, diverse D-ring oxygenation patterns (blue). To investigate this chemotype, a four-part strategy is outlined. The initial stage establishes access to the natural xanthone core. This is followed by a systematic investigation of its structure-activity relationships to identify the origins of cytotoxicity. Next, modern cross-coupling chemistry is explored, focusing on application in complex target synthesis. In the final stage, these advances converge in a modular total synthesis of lysolipin natural products.

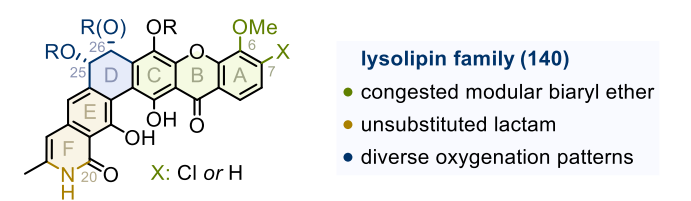


Figure 31. Unique, challenging and potent structural features of the lysolipin family.

5 Systematic Exploration of Polycyclic Xanthones

While the original publications present the results in full detail (Chapter 8), this section reflects on their role in progressively deepening our understanding of polycyclic aromatic compounds, with a particular emphasis on lysolipin natural products. We begin by placing the studies into the broader context, proceed to discuss central outcomes, and conclude with a critical summary and directions for follow-up research.

5.1 Modular Synthesis of Halogenated Xanthones

Bibliography

Title Modular Synthesis of Halogenated Xanthones by a Divergent Coupling Strategy

Authors Jonas W. Meringdal, Alexander Kilian, Wingkee C. Li, Maximilian J. B. Heinemann,

Marvin Rausch, Tanja Schneider and Dirk Menche*

Reference *J. Org. Chem.* **2022**, *87*, 9375.⁹⁷

Abstract A versatile strategy to halogenated xanthones was developed that relies on a

modular coupling of vanillin derivatives with a dibromoquinone. Depending on

the reaction conditions, either the 6- or the 7-bromo heterocycles may be

obtained in a divergent manner. These heterocycles may be readily further

elaborated by sequential Sonogashira couplings, and the sequence may be

successfully applied to substructures of the antibiotic lysolipin.

Contribution Jonas W. Meringdal and Alexander Kilian contributed equally. Jonas W. Meringdal

optimized the experimental results, resynthesized and characterized several

compounds, composed the Supporting Information section, and contributed to

writing of the manuscript. The other authors from our group prepared individual

compounds while the biological testing was done by Marvin Rausch and Tanja

Schneider.

29

Context and Concept

Inspired by recent polycyclic xanthone total syntheses (Chapter 3), lysolipin natural products (140) were retrosynthetically disconnected at C1 and C14, revealing xanthone fragment 141 as key intermediate (Figure 32). 141 was envisioned to arise from polar annulation between quinone 142a and phenols 143 or 144. While such annulations are established for several oxygenated xanthones, 32,35,98 analogous approaches for polyhalogenated and specifically 2-substituted scaffolds such as 141 remain underdeveloped, most likely due to phenols 143-144 lacking nucleophilicity and sterically obstructing C-O bond formation. 99 Nonetheless, xanthone 141 is central not only to the total synthesis of lysolipin natural products but also as a potential diversifiable lead structure for xanthone-based drugs, thus warranting further exploration of this promising annulation strategy.

Figure 32. Retrosynthetic disconnection identifies xanthone 141 as key intermediate.

Results and Realizations

The original report had decent success using iodobenzoquinone **15** (Chapter 3.1). However, in our hand **15** and products thereof proved very labile. Therefore, we focused on optimizing the polar addition between readily available⁹⁶ and more stable bromoquinone **142a** and phenol **143a** (Figure 35).

This decision proved fruitful, since the same conditions – potassium fluoride in warm DMF – improved the yield one and a half times (75%), suggesting that the lability from **15** was indeed detrimental to the reaction performance.³² After demonstrating the superiority of **142a**, we desired to improve scalability, focusing on bases of lesser toxicity. Recently employed potassium carbonate offered improved safety but lacked selectivity (34%).⁹⁸ Two unexplored bases emerged as particularly viable: sodium hydride in DMF and cesium carbonate in DCM, both affording **145a** in very high yields (>95%). Ultimately, cesium carbonate was adopted due to its superior safety profile.¹⁰⁰

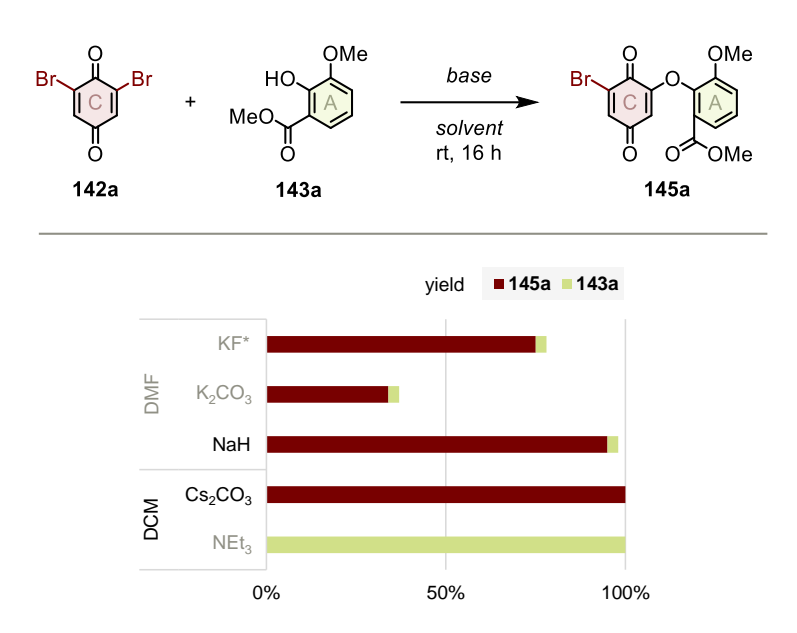


Figure 33. Optimization identifies two useful conditions for polar addition. * reaction at 75 °C.

These optimized conditions enabled access to both C1- and C14-brominated xanthones, utilizing established sequences (Figure 34).^{32,35,98} Non-chlorinated derivatives were obtained in good to high yields (38-62%, dark bars). However, the presence of C7-chlorine drastically reduced the overall yield, severely limiting the utility of this route (12-18%, light bars). Furthermore, low reactivity and side reactions prohibited late stage interconversion of **141a** to chlorine-bearing **141b** (not shown). Although Sonogashira coupling allowed further derivatization, the resulting structures were biologically inactive and dead ends for the total synthesis of **140** (Chapter 3.4).⁹⁷

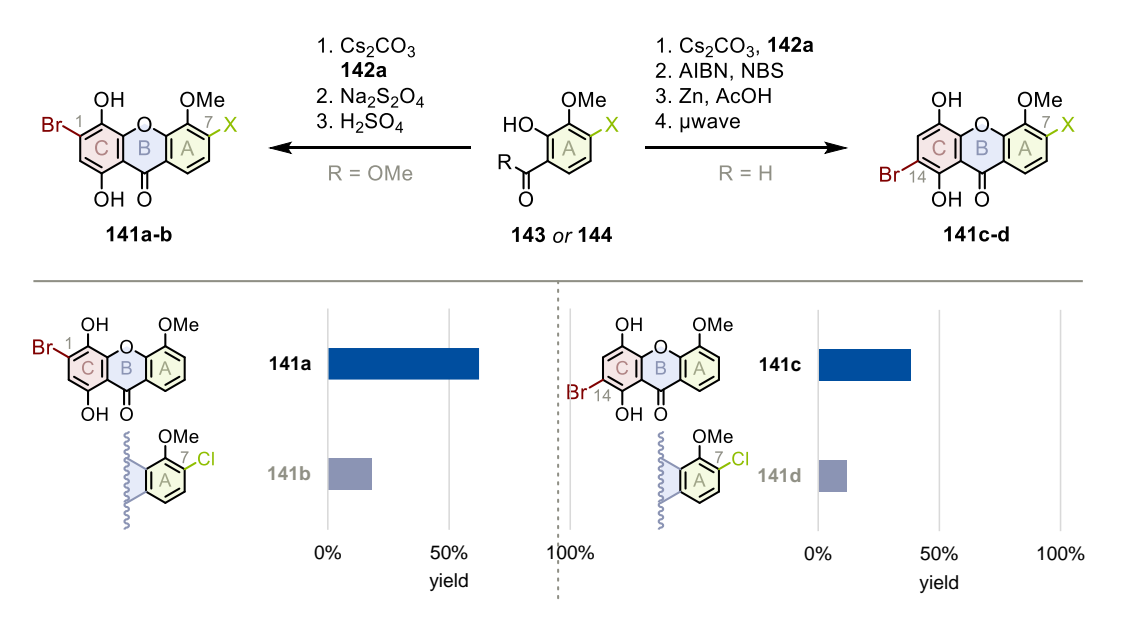


Figure 34. Poor tolerance of chlorine scaffolds limits synthetic applicability. NBS: *N*-bromosuccinimide.

Further limitations arose from the synthesis of chlorinated building blocks **143b** and **144b** (Figure 35). Particularly detrimental, benzaldehyde **147** was obtained in low yield (29%) and its

deprotection proved inconsistent, especially on larger scale. Moreover, it must be noted that many of the reported yields were based on impure products, leading to poor reproducibility (see also Chapter 5.2).^{97,101} In response, revised protocols, validated by multiple operators, were later established (Chapter 5.2 and 5.4).

$$\begin{array}{c} \text{1. } ^{S}\text{BuLi, C}_2\text{Cl}_6 \\ \text{2. } ^{S}\text{BuLi, TMEDA} \\ \text{DMF} \\ \text{146} \\ \end{array} \\ \begin{array}{c} \text{1. NaClO}_2 \\ \text{NaH}_2\text{PO}_4 \\ \text{2. MeOH} \\ \text{HOME} \\ \text{MeOME} \\ \text{Inconsistent} \\ \text{Inconsistent} \\ \text{OMe} \\ \text{Inconsistent} \\ \text$$

Figure 35. Inconsistency and impracticality plague A-ring synthesis. TMEDA: tetramethylethylenediamine. DMF: dimethylformamide.

Importance and Implications

This study demonstrates that polar annulation can, in principle, be extended to the synthesis of C6-substituted, polyhalogenated xanthones such as **141** (Figure 36). However, the current scope and efficiency are insufficient for further usage. Furthermore, an effective derivatization towards bioactive analogues remains to be identified. Moving forward, three main challenges must be addressed: (1) a selective and scalable route to chlorinated A-ring precursors, (2) a robust and high-yielding C-ring annulation strategy compatible with chlorine-bearing substrates, and (3) an effective derivatization method for xanthone-based bioactive agents. Solving these challenges will be essential for the total synthesis of lysolipin natural products and defining their pharmacophore.

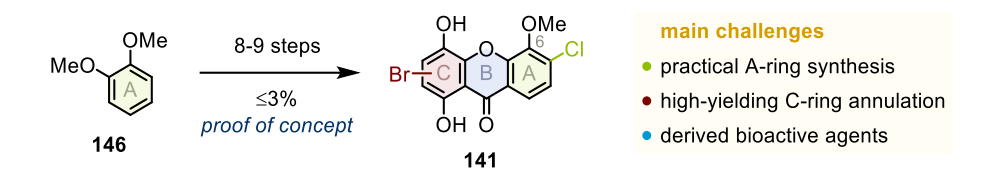


Figure 36. Summary and limitations of the synthetic route.

5.2 Bioactive Agents from Polyhalogenated Xanthones

Bibliography

Title Diversity Oriented Synthesis of Novel Xanthones Reveal Potent

Doxorubicin-Inspired Analogs

Authors Jonas W. Meringdal, Leon Bade, Prof. Gerd Bendas* and Prof. Dirk Menche*

Reference *ChemMedChem* **2024**, *19*, e202400055. ¹⁰²

Abstract Inspired by potent antiproliferative xanthone natural products and so far limited

examples of derived bioactive agents, a structure-activity study of architecturally

novel types of xanthones is reported. Their preparation was enabled in a short

and divergent manner by a modular chlorination in combination with optimized

protocols for a polar condensation and a hetero-cyclization. Application of these

procedures allowed for the synthesis of various polyhalogenated representatives

(including mixed bromo/chloro xanthones) that were obtained in up to fourfold

improved yields as compared to previous procedures. Subsequent Suzuki

coupling of either halide enabled access to phenyl- and chloro-bearing

xanthones, which may be functionalized at four out of five non-hydroxylated

positions. Antiproliferative assays against breast cancer cell lines revealed potent

activities of some of these simplified analogs that are in the range of

pharmaceutically used anticancer drug doxorubicin.

Contribution Jonas W. Meringdal conceptualized the project. He investigated, analyzed and

visualized the results, excluding bioactivity studies. He wrote the initial draft and

contributed to the revised manuscript.

Context and Concept

The structure-activity relationship (SAR) and mode of action of anthraquinones such as doxorubicin (148) are well understood,²⁸ leading to their widespread application in cancer therapy (Figure 37, left side).¹⁰³ However, a major drawback of anthraquinones is their cardiotoxicity. It is believed that the quinone B-ring (orange) plays a critical role in generating reactive oxygen species (ROS) via one-electron reduction, which in turn cause toxic effects on the heart.¹⁰⁴

In comparison, closely related xanthones have also demonstrated significant antitumor activity, with substantial evidence supporting their potential in cancer treatment (Figure 37, right side). Crucially, the pyranone B-ring of xanthones (blue) is considered to be redox innocent, suggesting a reduced propensity for ROS generation and, consequently, lower cardiotoxicity. However, unlike anthraquinones, the limited chemical diversity of accessible xanthones hampers the understanding of their SAR and mode of action, complicating their development as clinically viable alternatives. Consequently, ready synthetic access to a diversifiable xanthone core would facilitate the development of heart-safe cancer drugs.

Recognizing that lysolipin natural products (140) accommodate the same oxygenation pattern as doxorubicin (148), we hypothesized that their remarkable nanomolar activity could stem from the xanthone subunit (black). Intriguingly, the cytotoxicity of lysolipin natural products decreases with the presence of the C7-hydrogen (green), suggesting that substitution might increase activity (Chapter 2). Motivated by these observations and the need for safer chemotherapeutics, we set out to develop an efficient strategy for synthesizing a diverse set of doxorubicin inspired xanthones and evaluate their antiproliferative activity.

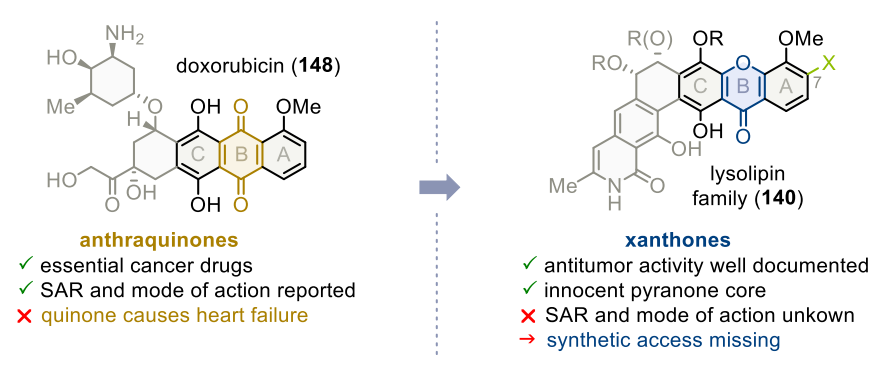


Figure 37. Limited methodology restricts application of xanthones as potential heart-safe cancer drugs.

Results and Realizations

Building on earlier work (Chapter 5.1), we envisioned a concise and divergent synthetic strategy (Figure 38, top part). First, modular chlorination of readily available phenol **149** replaces the capricious A-ring synthesis. ^{107–109} Then, C-ring annulation with a bromoquinone constructs the xanthone core. Finally, Suzuki-Miyaura phenylation gives the desired antiproliferative activity. ¹¹⁰ Each key step introduces a new molecular dimension, resulting in a SAR cube build around general structure **150** (bottom part). Drawing from design of experiment theory, these dimensions are assumed to be independent. ^{111,112} Thus, synthesizing three edges of the cube from a common structure should give the SAR of all structures of chemotype **150**, rapidly revealing an optimal substitution pattern.

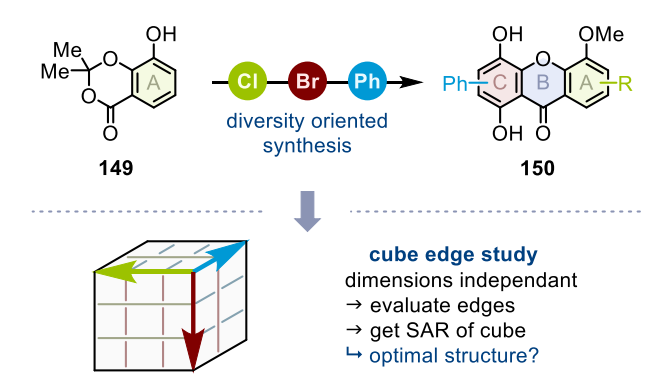


Figure 38. Diversity oriented cube edge study efficiently identifies the most active xanthone structure.

In contrast to previous reports, chlorination of **149** was nonselective under various conditions (Figure 39). ^{107,108} Furthermore, while ammonium salt catalysis was expected to selectively form C7-chlorinated **151a** via phenol coordination, C9-chlorinated **151b** was preferred. ¹⁰⁸ The increase in selectivity for **151b** at a lower temperature and with a weaker chlorinating agent (DCDMH) suggests that the C10-ester, rather than the C6-phenol, directs substitution (chart). This observation challenges the proposed mechanism, which postulated that the phenol donates a hydrogen bond to the catalyst's chloride ion, thereby forming an unusual, localized ion pair that directs regioselectivity toward **151a** (light green). ¹⁰⁸ Instead, these data suggest that the substrate acts as hydrogen bond acceptor to the chlorinated ammonium salt catalyst, resulting in a confined transition state (dark green). Because esters are stronger directing groups than phenols, ³⁶ this mechanism correctly predicts **151b** as favored product.

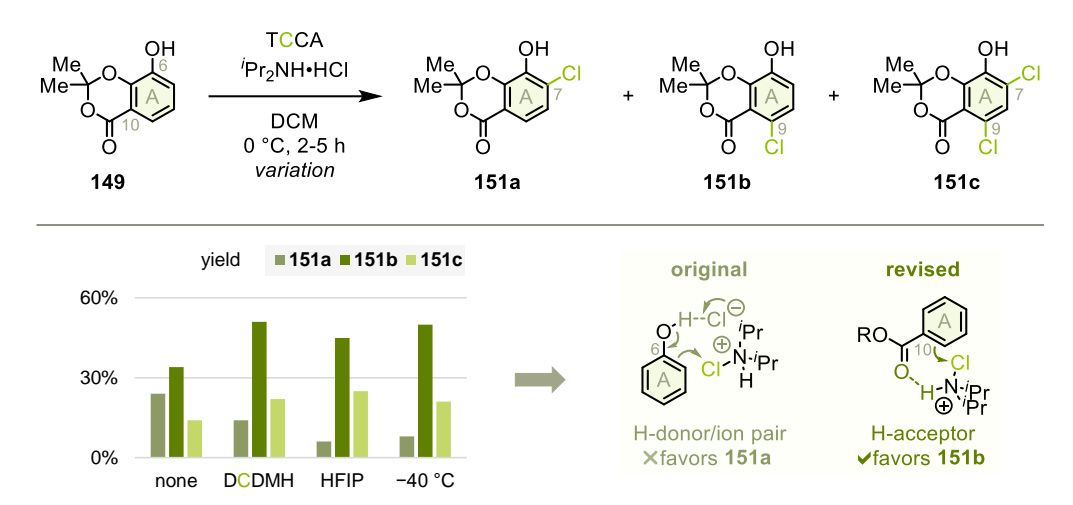


Figure 39. Investigation of ammonium salt catalyzed chlorination leads to a revised mechanism. TCCA: trichloroisocyanuric acid. DCDMH: 1,3-dichloro-5,5-dimethylhydantoin. HFIP: hexafluoro-2-propanol.

For isolation, a short reaction time with TCCA as chlorination agent yielded an appreciable ratio of the three desired chlorination patterns **151** (Figure 40, left chart).¹⁰⁸ Subsequent Williamson ether synthesis using a strong organic base, followed by lactone methanolysis completed the A-ring substitution pattern on **143** in a short and divergent manner (69-87%), thereby establishing the first structural dimension (right chart).¹⁰⁹

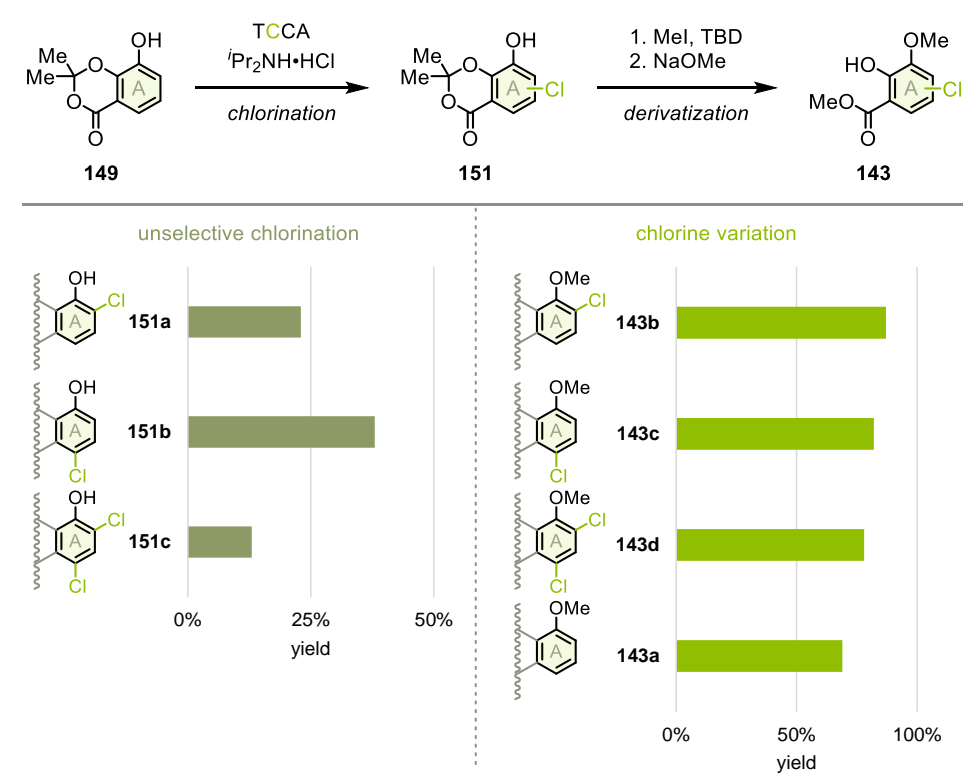


Figure 40. Halogenation valorization furnishes a divergent chlorination pattern. TBD: triazabicyclodecene.

With A-ring variants in hand, the next step was polar annulation of the C-ring. However, polar addition to **145b** proved irreproducible under previously reported conditions (Figure 41).⁹⁷

Preliminary optimization revealed that at least three equivalents of labile quinone **142a** were required, significantly more than the originally reported 1.7 equivalents, most likely to compensate for decomposition under basic conditions (not shown). While cesium carbonate was confirmed as the optimal base (82%), a significantly shorter reaction time of two hours – rather than two days – was essential to prevent degradation of intermediate **145b** (left chart). Similarly, shortening the reduction time from the reported two hours improved yields (right chart, red bars). While polar addition also tolerated acetone and dioxane as solvents (76-82%, grey bars), the subsequent reduction performed best in less polar DCM (77%, red bars), casting doubt on the reported high yields of **152b** with ethyl acetate as solvent.

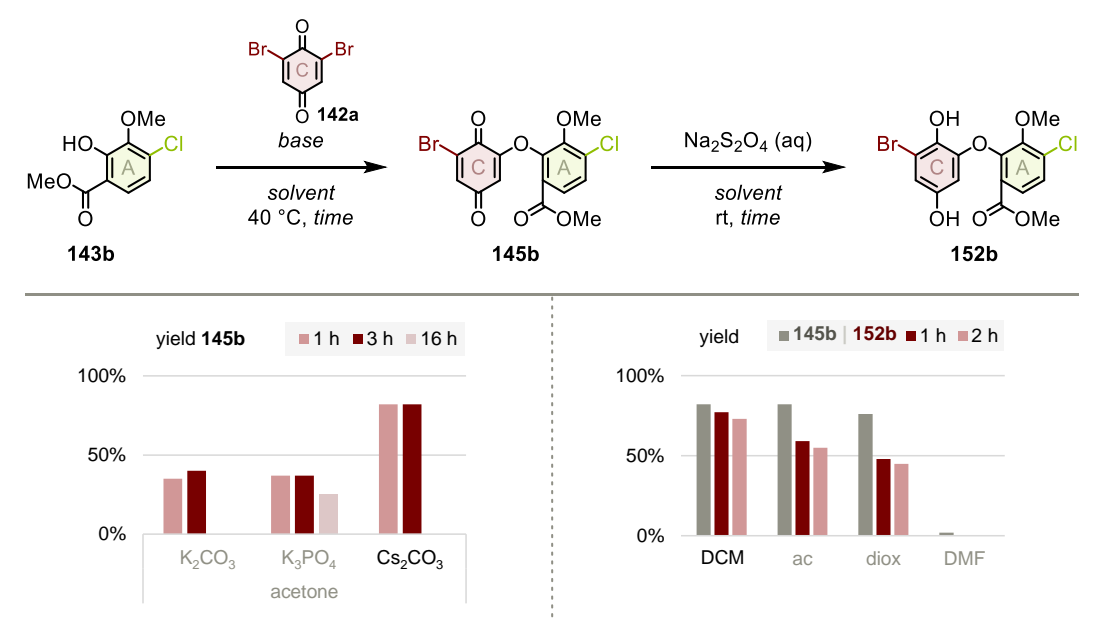


Figure 41. Optimization of polar addition highlights short reaction times as critical. ac: acetone. diox: dioxane. DCM: dichloromethane.

Sulfuric acid, originally reported for B-ring annulation,⁹⁷ caused undesired demethylation of the C6-anisole under various conditions, most likely because of its strong Brønsted acidity (Figure 42, grey). Switching to less acidic¹¹³ methanesulfonic acid enabled efficient ring closure without side reactions, providing 59% of desired **141d** as single product (blue). Notably, trifluoroacetic acid was inactive, confirming that strong acidity is required (not shown).

Figure 42. A weaker acid suppresses demethylation during B-ring annulation.

Despite the narrow reaction window, these optimized conditions proved to be remarkably robust (Figure 43). Thus, variation of quinone **142** introduced diverse C-ring patterns (left side). Likewise, the modular A-ring chlorination pattern could be selectively converted (right side). Overall, while C9-substituted members **141f-g** remain challenging (both 6%, light green bars), these protocols significantly expand the xanthone chemical space – particularly in the underexplored realm of polyhalogenated scaffolds (39-75%).⁹⁹

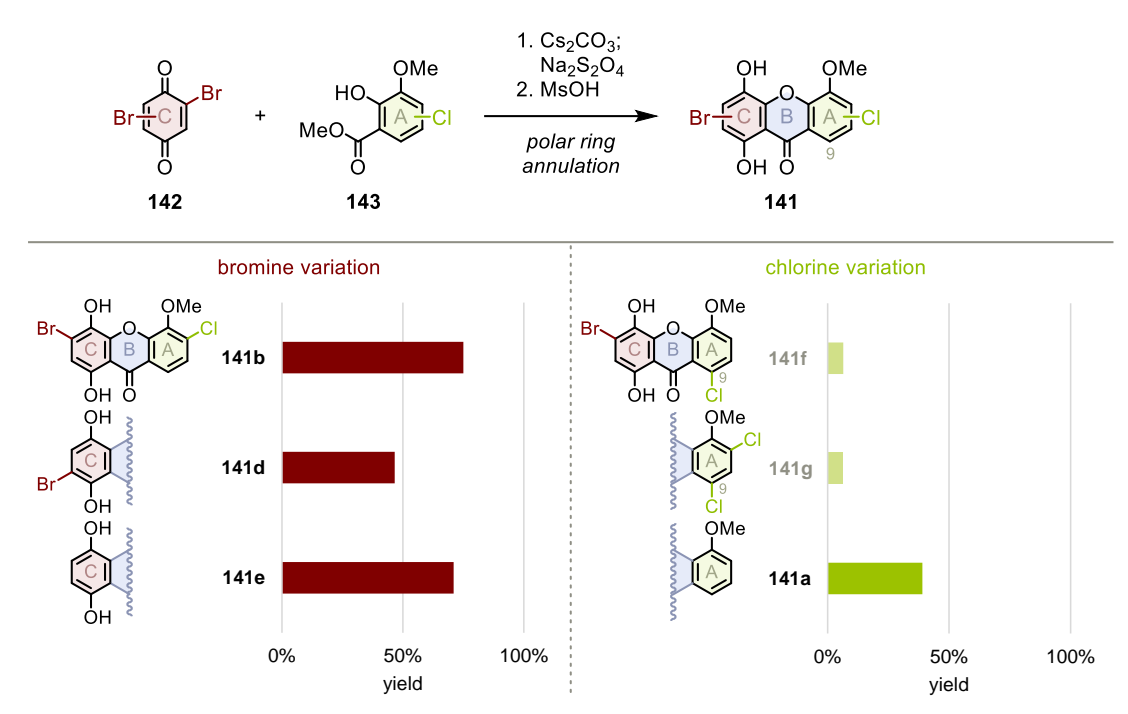


Figure 43. Polar ring annulation gives a diverse set of polyhalogenated xanthones.

Site-selective Suzuki-Miyaura coupling achieved the final diversification (Figure 44). Depending on the catalyst, the C7-chlorine is either retained (153) or replaced (154), granting access to the complete SAR cube centered on 154a (24% to quantitative). Coincidentally, 154a emerged as the most potent, broad-spectrum antiproliferative xanthone in our series (chart, red bars). Strikingly, its antiproliferative activity rivals that of commercially drug doxorubicin (148, orange bars) despite its reduced structural complexity, indicating a high potency of the xanthone core. Structurally related members were also effective, validating the cube edge study design (blue box). These active xanthones resemble the parent natural products 140, typically featuring a C7-substituent and a side chain at C1, suggesting that the xanthone subunit contributes significantly to the antiproliferative activity of 140.

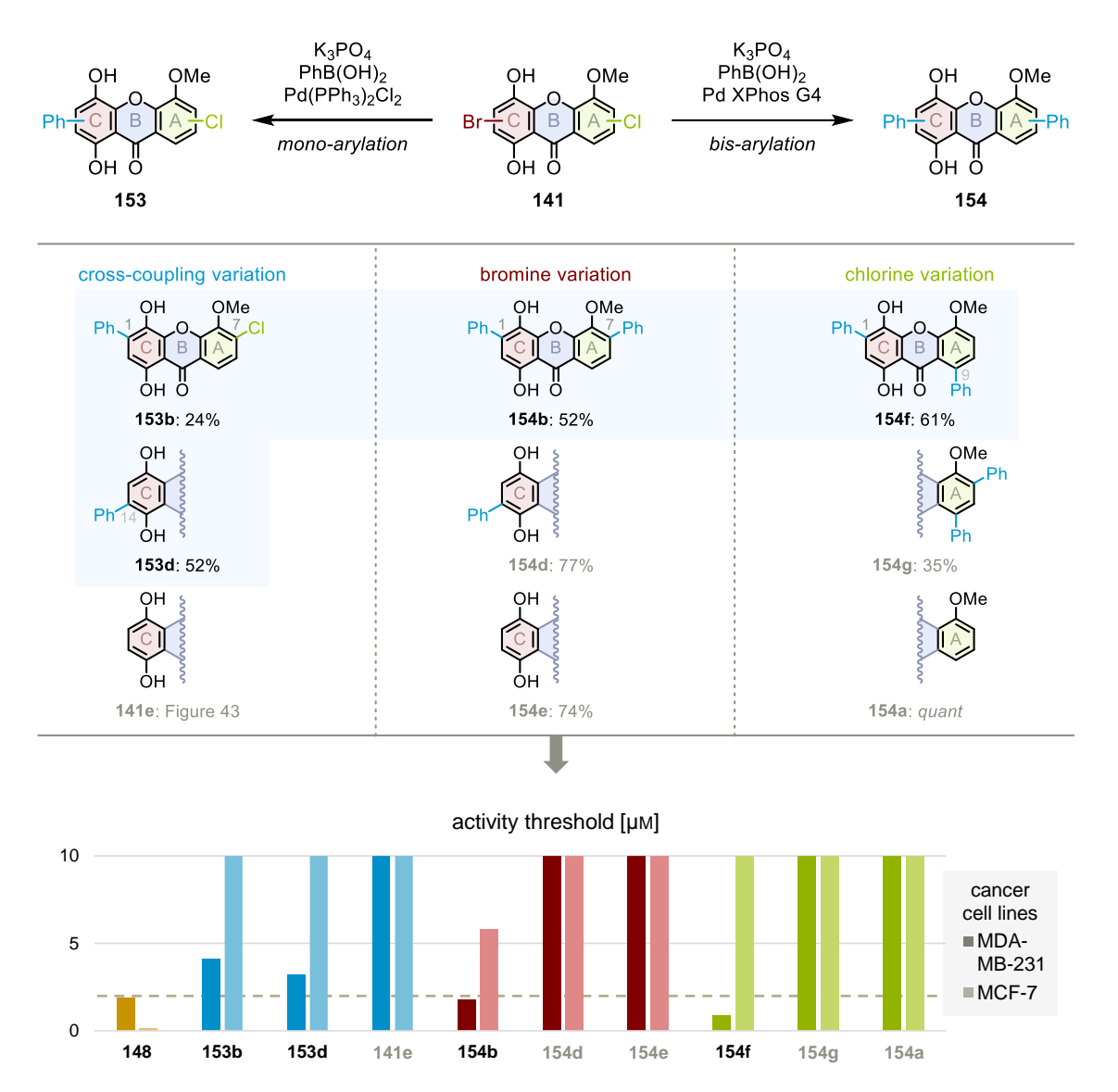


Figure 44. SAR cube completion identifies potent xanthone derivatives (blue box). Chart capped at 10 μM.

Importance and Implications

This study delivers a strategically designed, high-yielding synthetic route towards uncharted, densely functionalized xanthones (Figure 45). Central to the approach was polyhalogenated scaffold **141**, which was synthesized through a concise four-step sequence with overall yields that are typically reserved for a single transformation (27-62%).⁹⁹ Further strengths of the route lie in its robustness and modularity: C7-chlorines are now tolerated (green), a modular C-ring is readily introduced (red), and the final Suzuki-Miyaura cross-coupling proceeds site-selective without the need for phenol protection groups (turquoise and blue). Together, these features efficiently access chemotype **150**, strategically expanding the xanthone chemical space.

Yet, this methodology is not without its limitations. Regioselective installation of the A-ring substitution pattern remains to be solved (151). Furthermore, the polar annulation step now depends on an excess of quinone 142, complicating purification, interfering with xanthone cyclization and ultimately limiting scale-up of 141. Finally, inconsistent yields in the Suzuki-Miyaura cross-coupling signal a need for deeper mechanistic understanding, especially since lysolipin natural products (140) will require the cross-coupling of even more complex substrates. Resolving these issues will be vital for translating this synthetic route into a total synthesis of 140.

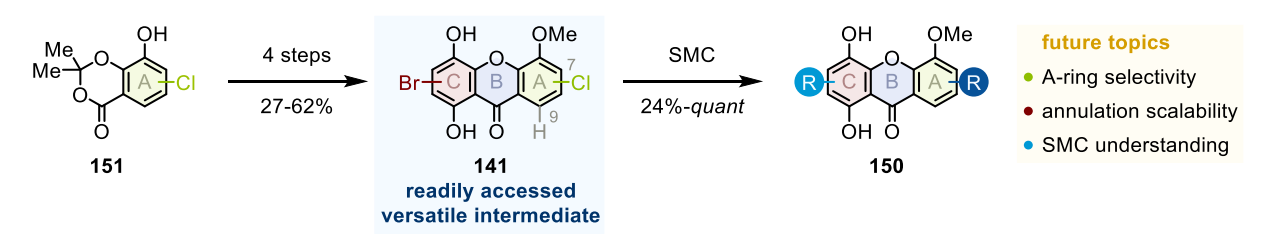


Figure 45. Highlights and limitations of the synthetic strategy. SMC: Suzuki-Miyaura cross-coupling.

From a medicinal standpoint, this strategy provided a significant discovery: xanthone **154b** emerged as very potent scaffold. Despite lacking the aminosugar (turquoise) essential for the potency of doxorubicin (**148**),²⁸ **154b** exhibits comparable antiproliferative activity, indicating that the xanthone core alone (blue) delivers substantial antiproliferative activity (Figure 46). Importantly, the improved potency of **154b** over its mono-phenyl analogs challenges a DNA intercalation mechanism (Chapter 2),¹⁸ as the perpendicular orientated phenyl substituents are larger than the intercalation pocket formed between two base pairs (turquoise).¹¹⁴ Collectively, these findings highlight the therapeutic potential of xanthones, not only as heart-safe alternatives to anthraquinones, but as potentially superior leads with a unique mode of action.

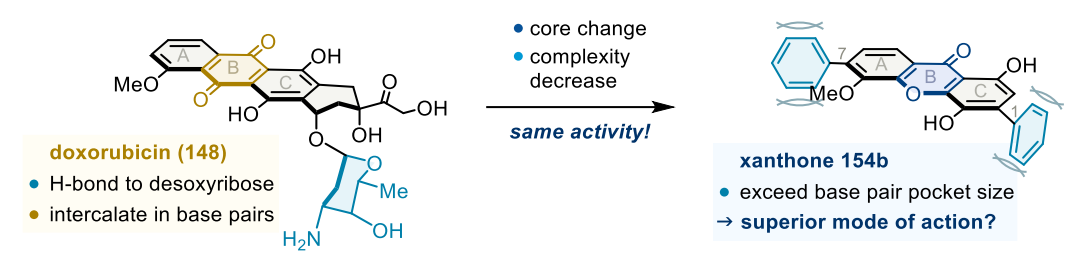


Figure 46. Structure-activity insights highlight xanthones as unique and potential superior leads.

From the perspective of the lysolipin family, C1-substituents are underlined as key modulators for bioactivity, stimulating a modular synthetic approach to the C2-linker of parent **140**. Moreover, the natural C7-chloride offers dual functional potential: selective cross-coupling could improve antiproliferative activity, whereas strategic dehalogenation could provide selectivity towards bacterial over mammalian targets.

5.3 Suzuki-Miyaura (Hetero-)Aryl Cross-Coupling

Bibliography

Title Suzuki-Miyaura (hetero-)aryl cross-coupling:

recent findings and recommendations

Authors Jonas W. Meringdal and Dirk Menche*

Reference *Chem. Soc. Rev.* **2025**, *54*, 5746. 115

Abstract The Suzuki-Miyaura cross-coupling is a powerful method for carbon-carbon bond

formation, widely applied with various substrates, catalysts, reagents and solvents. However, numerous reported protocols make finding optimal

conditions for a specific substrate time-consuming. This tutorial review provides a

comprehensive overview on recent developments in Suzuki-Miyaura reactions,

focusing on optimizing the most common application: palladium and nickel

phosphine catalyzed (hetero-)aryl bond formation. Key mechanistic insights into

ligand selection, base and boron reagent choice as well as potential additives,

and their effects on the reaction outcome are discussed in detail. Based on a

systematic analysis, these parameters will be grouped together. Recommended

conditions for each group will then be provided to accelerate the optimization

process and enhance the application of this pivotal bond forming reaction.

Contribution Jonas W. Meringdal conceptualized the project. He performed, curated,

evaluated and visualized the recent literature. He wrote the initial draft and

revised the manuscript.

Context and Concept

Today, every eighth reaction in drug discovery is a Suzuki-Miyaura cross-coupling and two out of three carbon-carbon bonds are formed this way, putting the Suzuki-Miyaura reaction at the forefront of synthetic organic chemistry (Figure 47).^{4,6,7} In particular, the environmentally benign, commercially available reagents and mild reaction conditions have sparked the development of numerous protocols, essentially allowing every reaction parameter to be fine-tuned.¹¹⁶ Over the years, major pharmaceutical companies have invested in large, automated high-throughput experimentation facilities to identify the best protocol.^{2,3} Nevertheless, even after exhaustive screening, the average reported yield remains modest, revealing the limitations of a brute force approach.^{4,6} More critically, in the absence of such infrastructure, most practitioners are left to rely on trial and error, hoping that by chance useful conditions are identified. In response, we propose a rational selection guide, informed by a critical analysis of seminal work from the past decade (see publication for a detailed breakdown).¹¹⁵



Figure 47. Suzuki-Miyaura cross-couplings are widely used in drug discovery, but the absence of a comprehensive overview makes reaction optimization a tedious and inefficient process.¹¹⁷

Results and Realizations

Recent experimental breakthroughs have fundamentally revised the catalytic cycle of Suzuki-Miyaura cross-couplings (Figure 48).^{118–120} At the core of this updated mechanism is the direct reaction between oxidative addition complex **157** and boronate **158**, forming a mono-ligated (ML₁) pre-transmetallation complex (**159**).¹¹⁹ In this intermediate, one coordination site is occupied by a distal Pd-O-B bond instead of a second phosphine ligand.¹¹⁸ Crucially, transmetallation of **159** is typically the rate-determining step, making the formation and stability of this ML₁ complex the key lever for reaction optimization.^{119–124}

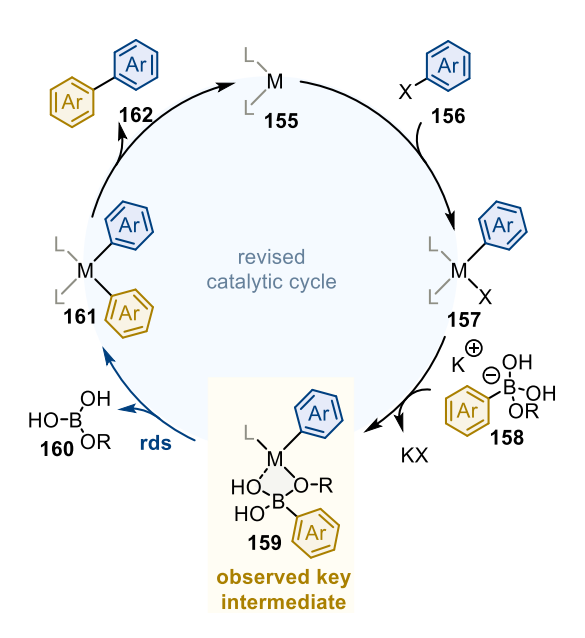


Figure 48. Transmetallation of mono-ligated 159, formed from boronate 158, is the rate-determining step.

Ligand Selection

Accounting for these factors, we developed a rational ligand selection guide structured around three concepts: ligand types, reaction groups and buried volume.

Based on their binding mode, ligands fall into four types (I-IV), with ligands of the same type exhibiting a similar reactivity and selectivity (Figure 49).¹²⁵ Type I and II ligands favor a ML₁ catalyst, which accelerates transmetallation and is ideal when side reactions are minimal and the boronate unreactive (orange box).¹²⁵ In contrast, type III and IV ligands stabilize bis-ligated (ML₂) complexes, which are more resistant to side reactions but inherently slower.¹²²

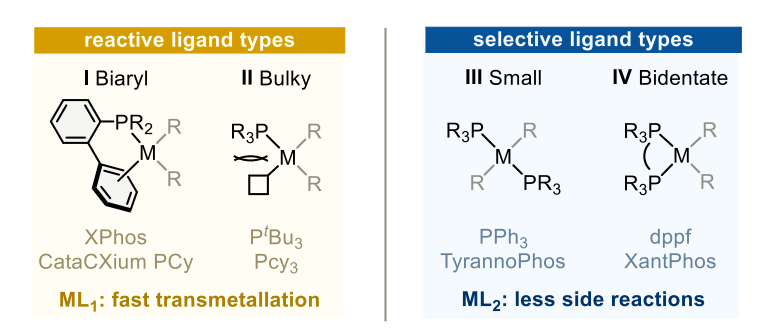


Figure 49. Binding mode dominates the reactivity and selectivity of ligand types (I-IV).

The choice of ligand is further refined by reaction groups (**A-C**), which reflect combined substrate and metal effects (Figure 50). Group **A** – palladium-halide couplings – benefits from ML₁-enforcing ligands for maximum turnover (orange box). Group **B**, including triflate substrates and nickel-catalyzed reactions, requires ligands capable of toggling between ML₁ and ML₂ states. Here, ML₁ supports turnover, while ML₂ promotes triflate oxidative addition and protects the sensitive nickel center (brown box). Group **C** covers the most demanding

systems, including sensitive substrates and catalyst poisons, where bis-ligation is essential to suppress side reactions. While palladium is only affected by donating poisons (dark blue), nickel is also vulnerable to acceptor functional groups (light blue). 127,128

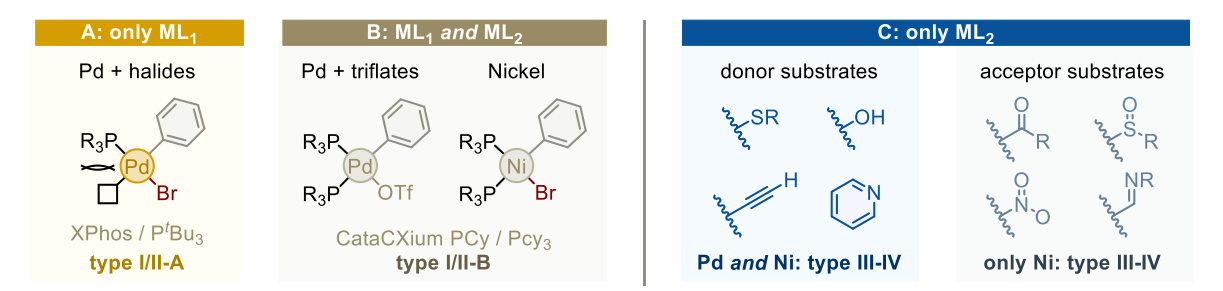


Figure 50. The combination of metal and substrate defines reaction groups (**A-C**), which together with ligand types (**I-IV**) determines the optimal ligand.

The final piece is the buried volume, a quantitative measure of a ligand's steric footprint within the metal's first coordination sphere (Figure 51). ^{129,130} The minimum buried volume predicts the smallest steric profile accessible to a ligand (type I-III). ¹²⁵ Values above 32% enforce mono-ligation (group **A**), 29-32% represents a balance where bis-ligation is disfavored but possible (group **B**), and below 29% ML₂ complexation dominates (group **C**). For biaryl ligands (type I), the Boltzmann buried volume, reflecting the conformational average, further refines predictions. ¹²⁶ If this value exceeds 52%, mono-ligation is enforced (group **A**), whereas below 52% bis-ligation becomes possible if the minimum buried volume is also under 32% (group **B**).

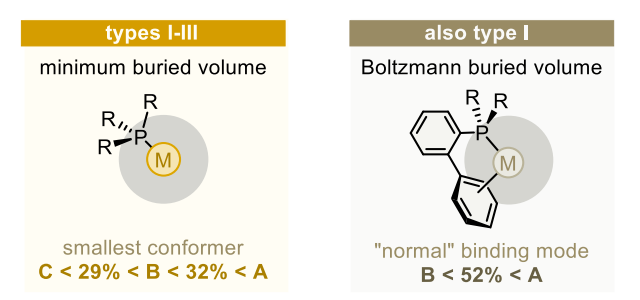


Figure 51. Buried volume thresholds quantitatively link ligand types (**I-III**) to reaction groups (**A-C**), guiding ligand selection.

In complex target synthesis, emergent properties often obscure the required reactivity and selectivity.¹⁷ A reliable strategy then involves testing one ligand of each type, guided by the reaction group, to efficiently identify the optimal ligand type (see Chapter 5.4 for application). Prevalent ligands for each type and group can be selected from Figure 49 and Figure 50 (grey). Subsequent optimization can draw from well-performing ligands summarized in the original publication (Fig. 26)¹¹⁵ or from the large scale screening by Doyle and Sigman (Supporting

Information).¹²⁵ Additionally, Gensch, Sigman and Aspuru-Guzik provide an online phosphine ligand database with computed descriptors, including absolute buried volumes (divide by 179.59 for percentage).¹³⁰

Boron Source and Activation

Once a suitable ligand is identified, matching the boron source to the substrate-dependent stability of the boronate^{131,132} becomes critical for maximizing turnover (Figure 52). Most substrates are sufficiently stable on the reaction timescale, making boronic acids and pinacol esters the preferred choice due to their high reactivity and commercial availability (orange box).^{133–135} Moderately sensitive substrates, such as electron-deficient arenes and several heterocycles, benefit from slow-release sources like BF₃K^{136,137} and MIDA¹³⁸ boranes (grey box). These boron sources minimize protodeboration by releasing small amounts of the reactive boronic acid over time, which is rapidly consumed in the cross-coupling. The most labile substrates – unsubstituted 2-pyridines or *ortho*-difluorinated arenes – require direct coupling of inert MIDA¹³⁹ and DAN^{140,141} boranes to bypass the unstable boronic acid entirely (blue box).

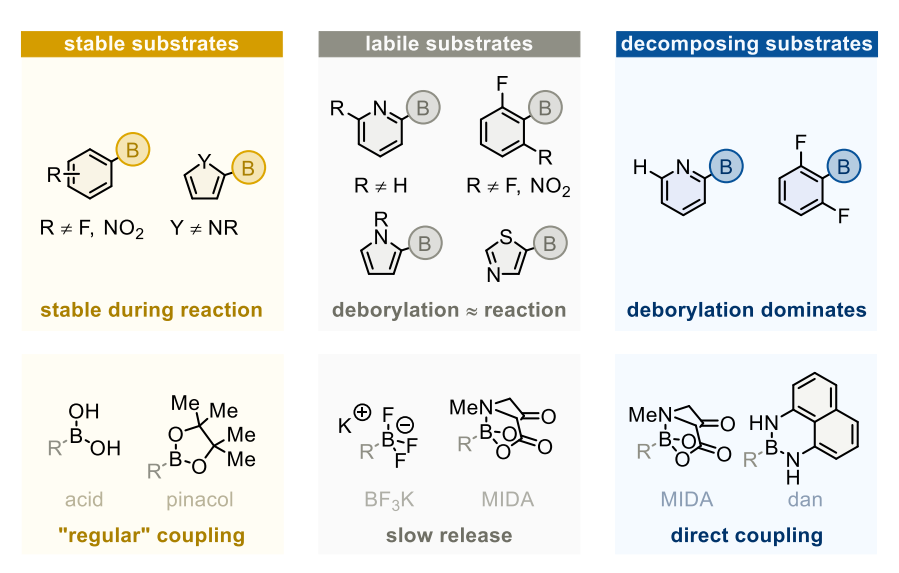


Figure 52. Boron sources matched to the substrate-dependent stability.

With the boron source matched, optimizing base, solvent, and additives becomes important. While slow-release and direct coupling strategies require narrowly defined conditions (see references above), reactions involving boronic acids and esters allow broader refinement of these parameters.

The base must be strong enough to generate the boronate required for transmetallation.¹¹⁹ This means that its basicity should match or exceeds the pK_a of the substrate's boronic acid, while also mitigating substrate-specific deborylation mechanisms (Figure 53).^{131,132} Highly sensitive

2-pyridine substrates benefit from the strongest possible bases (orange box). In contrast, 3,4-heterocycles require a base whose strength approximates this pK_a (grey box). Most other substrates are less sensitive to the exact base strength, provided it exceeds the pK_a by at least one unit to suppress autocatalytic protodeboration (blue box).

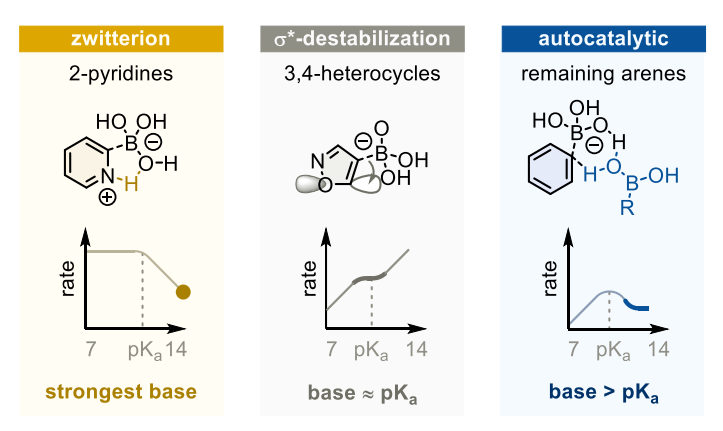


Figure 53. Base strength matched to the three key deborylation mechanisms.

Solvents and Additives

While Suzuki-Miyaura cross-couplings conventionally use aqueous solvents, inorganic bases and no additives, these conditions fail in demanding scenarios. Evaluating pre-transmetallation equilibria from the organic layer where the catalyst resides, addresses common issues (Figure 54). First, poor solubility of polar boronates can be resolved by phase-transfer cations and lipophilic bases (orange box). Second, iodide byproducts – highly soluble in organic solvents – drive the catalytic cycle backwards. Switching to biphasic systems with a non-polar solvent efficiently removes iodides into the aqueous layer (blue box). 102,143

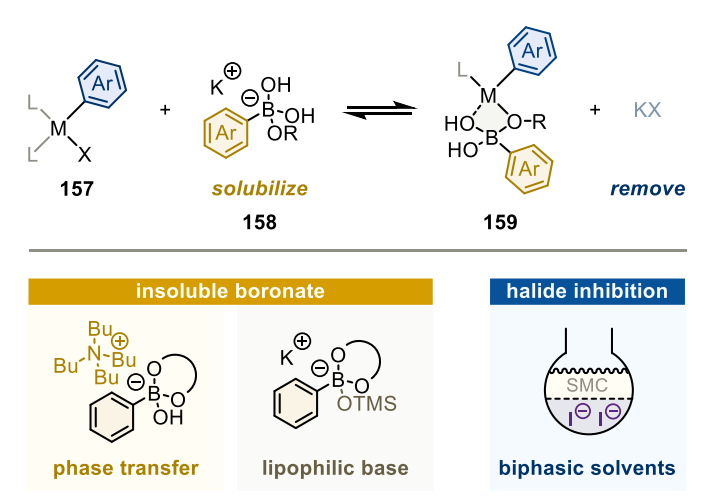


Figure 54. Managing boronate solubility and halide removal restores turnover.

Third, strongly coordinating groups form stable off-cycle complex **163** (Figure 55).¹²⁴ Here, Lewis acids sequester non-acidic poisons (orange box), whereas soluble halide salts re-activate the catalyst (blue box), facilitating type **I-II** ligands under challenging conditions.¹²⁴

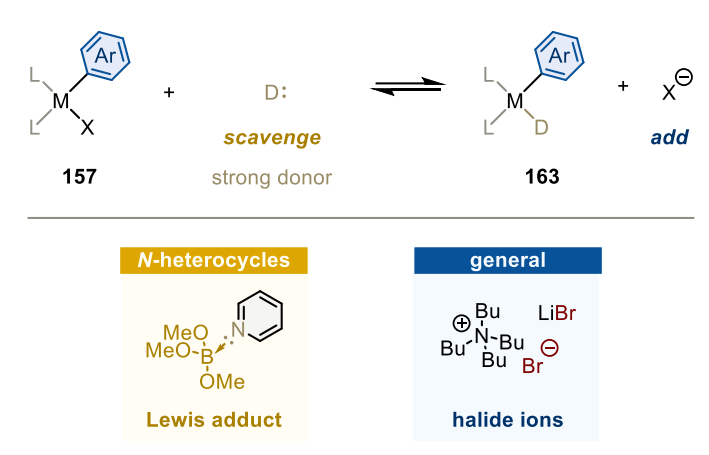


Figure 55. Lewis adduct and halide ions remedy catalyst poisoning.

Importance and Implications

This study reframes Suzuki-Miyaura cross-coupling reactions by connecting recent mechanistic breakthroughs with practical, predictive guidelines. It introduces selection guides from ligands to additives that replace empirical trial-and-error with rational design, already successfully applied in complex target synthesis. 147–150 The most important insight is that in most cases ligand geometry, rather than donor strength, determines the reaction outcome. In the final step, this underlying principle will be extended to advanced cross-coupling reactions, demonstrating its broad applicability.

5.4 Total Synthesis of Lysolipin Natural Products

Bibliography

Title Ligand Type Guided Keto-Arylation Enables Modular Total Synthesis of Polycyclic

CBS Xanthones

Authors Jonas W. Meringdal, Vivienne Prangenberg, Tim Treiber, Andreas J. Schneider,

Leon Honsdorf and Dirk Menche*

Reference Angew. Chem. Int. Ed. 2025, e202513532 (Selected as Hot Paper). 151

Abstract The first total synthesis of the potent polycyclic xanthone antibiotics CBS72,

CBS87 and CBS100 was accomplished by a modular strategy featuring a very

demanding intermolecular aromatic keto arylation. Central to the solution was a

recently-developed ligand type approach, rather than brute force screening,

demonstrating the usefulness of this novel concept in complex target synthesis.

Additional key features include an asymmetric Davis hydroxylation proceeding

with only catalytic amounts of base, thus enabling the conversion of a highly

sensitive, elaborate substrate. Furthermore, a late stage aminolysis completed

the polycyclic framework, circumventing laborious protective group chemistry.

Together, this strategy provides a concise, high yielding access, confirming the

full architecture of this most potent class of polyaromatic xanthones, and

establishes ligand types as a powerful design tool for sophisticated

cross-couplings.

Contribution Jonas W. Meringdal conceptualized the project and supervised the synthetic part.

He investigated, initially synthesized, optimized and characterized the majority of

compounds, excluding HPLC analysis and separation. He curated, analyzed and

visualized synthetic data. He wrote the initial draft and revised the manuscript.

Context and Concept

With a solid foundation established (Chapter 5.1-5.3), a modular synthetic strategy was devised to address the unique structural features of lysolipin natural products, targeting very potent members CBS72 (5), CBS87 (8) and CBS100 (6) (Figure 56). First, late-stage aminolysis circumvents catalyst poisoning, nucleophilic substitution and laborious protective group chemistry of the unsubstituted C18-lactam, a motif exclusive to lysolipin family (orange). Second, tailored oxygenations reduce the distinct D-ring substitution patterns to common intermediate 165 (blue). Third, a very demanding^{62,152} interaromatic keto-arylation fragments 165 into isocoumarin 166 and xanthone 167 (red). While site-selective, sequential cross-couplings could introduce the acetophenone and F-ring (brown),⁴³ Dakin oxidation and directed *ortho*-metalation could finally provide access to the natural A-ring (green).¹⁵³

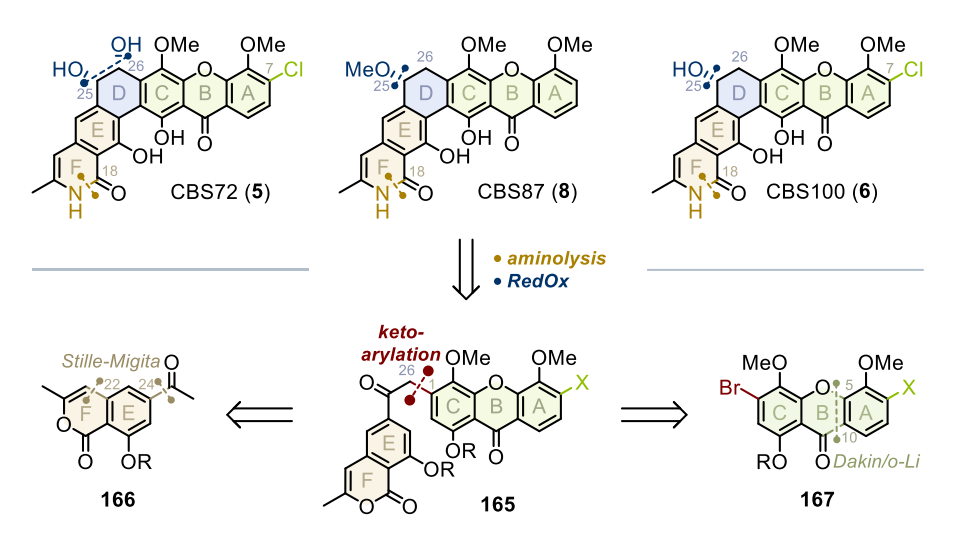


Figure 56. The exclusive structure of CBS natural products demand a unique synthetic strategy.

Results and Realizations

We began by synthesizing chloroxanthone **167b** (Figure 57). Since chlorine introduction had suffered from poor selectivity (Chapter 5.1-5.2), we started from 3-chlorosalicylaldehyde (**169**), using its aldehyde as handle to construct the complete xanthone skeleton. First, the C5-aldehyde served as a masked phenol, selectively affording the elusive C6-mono-methyl ether **171** after methylation and Dakin oxidation with **170** (99%).¹⁵³ Then, in the form of a strongly coordinating MOM ether, the unmasked C5-phenol directed *ortho*-lithiation to C10, furnishing methyl ester **143b** after mildly basic esterification (80%).^{36,154} Finally, the C5-phenol initiated polar C-ring annulation at C3, providing xanthone skeleton **141b** (56%).^{97,102}

Importantly, NMR data suggested that the C7-chlorine enforced a congested intramolecular hydrogen bond, which only a small and strong base would deprotonated (grey). Thus, using

sodium hydride – and no other base – the polar addition proceeded with only a small excess of **142a** (see publication for details), facilitating purification and thereby enhancing scalability (compare Chapter 5.2).

Following the same principle, methylation of the more acidic phenol introduced the natural C2-anisole, and SEM-protection provided much-needed solubility (89%), completing fragment **167b** in 9 steps and 40% overall yield. ¹⁵⁵

Figure 57. Dakin oxidation installs A-ring substituents and polar annulation provides xanthone fragment.

With xanthone **167b** in hand, our next target was isocoumarin **166** (Figure 58). Building on prior work (Chapter 3.1), we applied our ligand type concept (Chapter 5.3) to selectively introduce the acetophenone and F-ring on **36**. Exploiting first order kinetics (see Supporting Information), a selective small phosphine ligand (type **III**) introduced enol **172** solely at C24 (85%).¹⁵⁶ Next, a very reactive biaryl ligand (type **I**) promoted the challenging transmetallation of *sp*³-stananne **39**.^{43,48} Subsequent cyclization and SEM-protection (82%) completed fragment **166a** in 5 steps and 70% yield after a single pass, meaning that a single uninterrupted sequence instead of a product of best-case results from multiple attempts produced this yield. Moreover, interception of its enolate provided acetate **166b** and trimethylsilyl ether **166c** as alternative C26-nucleophiles (53% and quantitative).^{155,157} Notably, only very cold reaction temperatures and rapid cryogenic chromatography prevented ample decomposition of **166c**, foreshadowing downstream challenges.

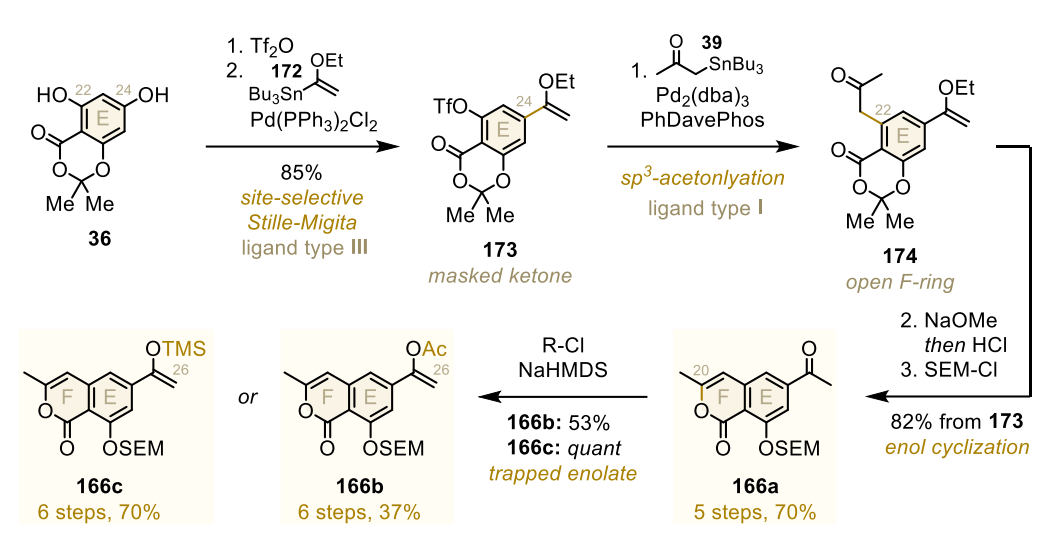


Figure 58. Site-selective, sequential Stille-Migita couplings forge isocoumarin skeleton.

With fragment synthesis complete, we turned our attention to the central keto-arylation (Figure 59). Since carbon nucleophiles lack in transmetallation strength, we focused on reactive ligand types (I-II), omitting type III ligands (blue).^{62,158} To activate ketone donor **166**, we evaluated both basic (**A-B**)^{159–161} and tin mediated (**C-D**)^{49,162} conditions (brown).

In line with our screening protocol for advanced intermediates (Chapter 5.3), reaction monitoring revealed that each condition required a vastly different ligand type (left chart). Among these, condition **D-II** not only provided the highest yield (36%) but also kept side products to a minimum (see publication). Therefore, we selected this conditions, focusing on increasing the transmetallation rate (middle chart). An equimolar catalyst (PdL₁), obtained from additional palladium, proved critical, and toluene emerged as the optimal solvent (56%). As anticipated for a halide substrate, ligands that solely form mono-ligated complexes (type **II-A**) were most effective (right chart). Notably, while QPhos (type **II**) delivered good conversion (50%), a type **I** ligand with identical steric and electronic profile was largely inactive (HandaPhos: 15%), underlining the critical role of ligand types in elaborate cross-coupling reactions. Finally, a marginal excess of ligand provided jointed **165b** in several hundred milligrams (62%).

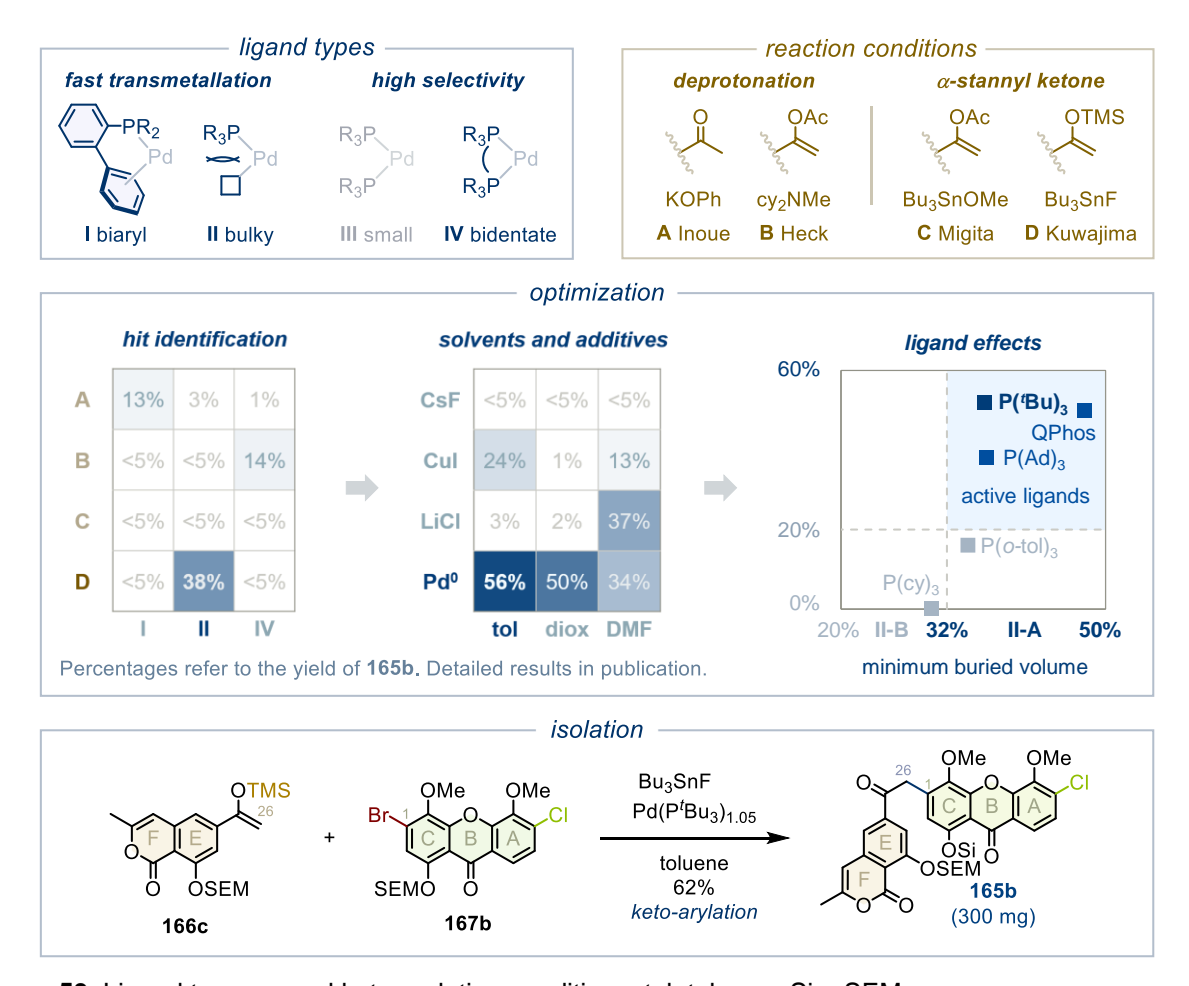


Figure 59. Ligand types reveal keto-arylation conditions. tol: toluene. Si = SEM.

With the keto-arylation accomplished, we proceeded to elaborate **165b**, targeting CBS100 (**6**) (Figure 60). First, Noyori transfer hydrogenation installed the C25-stereocenter in **177** (quantitative).⁷⁷ The high enantiopurity (90% ee) is likely due to a C-H- π interaction in transition state **176** (orange),¹⁶⁷ since sterically based asymmetric reductions proceeded less selectively (56-76% ee).¹⁶⁸ Next, forceful ammonia incorporation completed skeleton **178** as planned (66%).¹⁶⁹ Finally, copper(II)-oxidant **129**, obtained from an improved protocol (see publication), regioselectively closed the D-ring, such that after *in situ* deprotection of the C25-alcohol (58%) CBS100 (**6**) was isolated in 15 steps, 10% overall yield and 62% ideality.⁹⁰

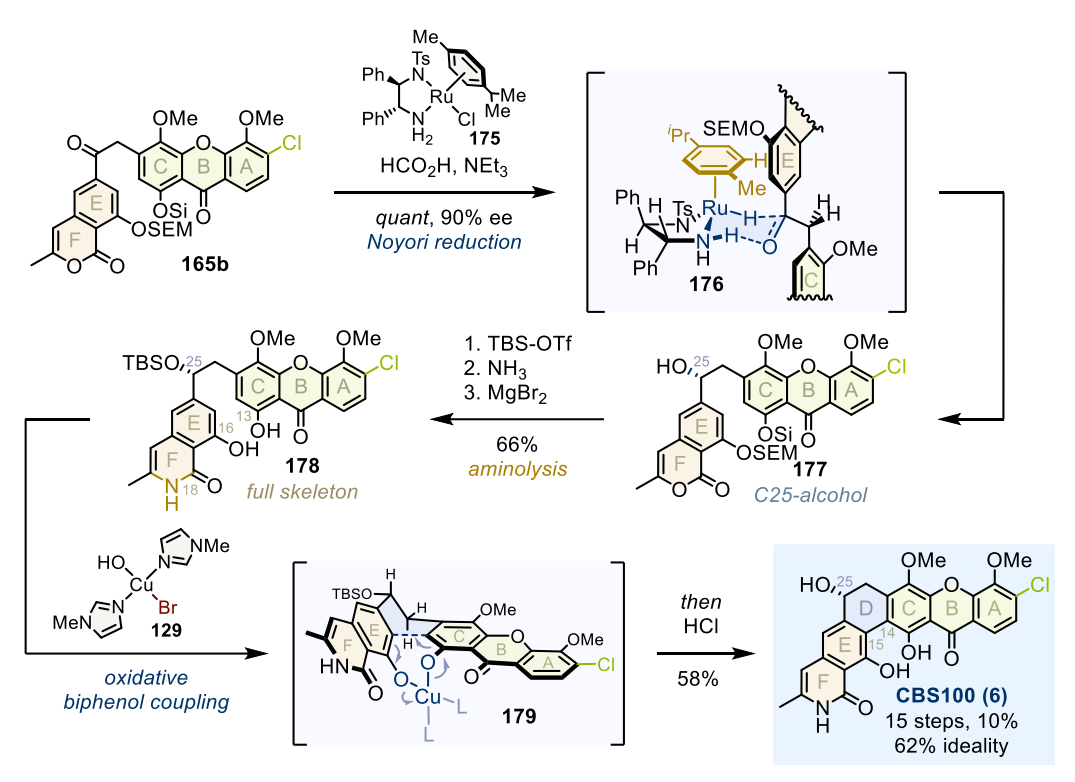


Figure 60. Late stage aminolysis finalizes CBS100 skeleton for ultimate cyclization.

After establishing access to a chlorinated member, we applied our protocols to hydrogen-bearing CBS87 (8), encountering a remarkable transferability (Figure 61). Under identical conditions, xanthone **167a** was obtained (28%)^{97,102,155} and coupled with isocoumarin **166c** (58%),⁴⁹ furnishing central intermediate **165a**. Noyori transfer hydrogenation afforded the C25-alcohol in identical enantiopurity (90% ee),⁷⁷ but Grob-fragmentation obstructed basic etherification thereof.¹⁷⁰ Instead cationic methylation with silver(I)-oxide provided C25-methyl ether **180** (61%).¹⁷¹ As before, late-stage aminolysis was well-tolerated (84%), and copper oxidation furnished CBS87 (8) (45%) in 12 steps, 4% overall yield and 69% ideality.^{90,169}

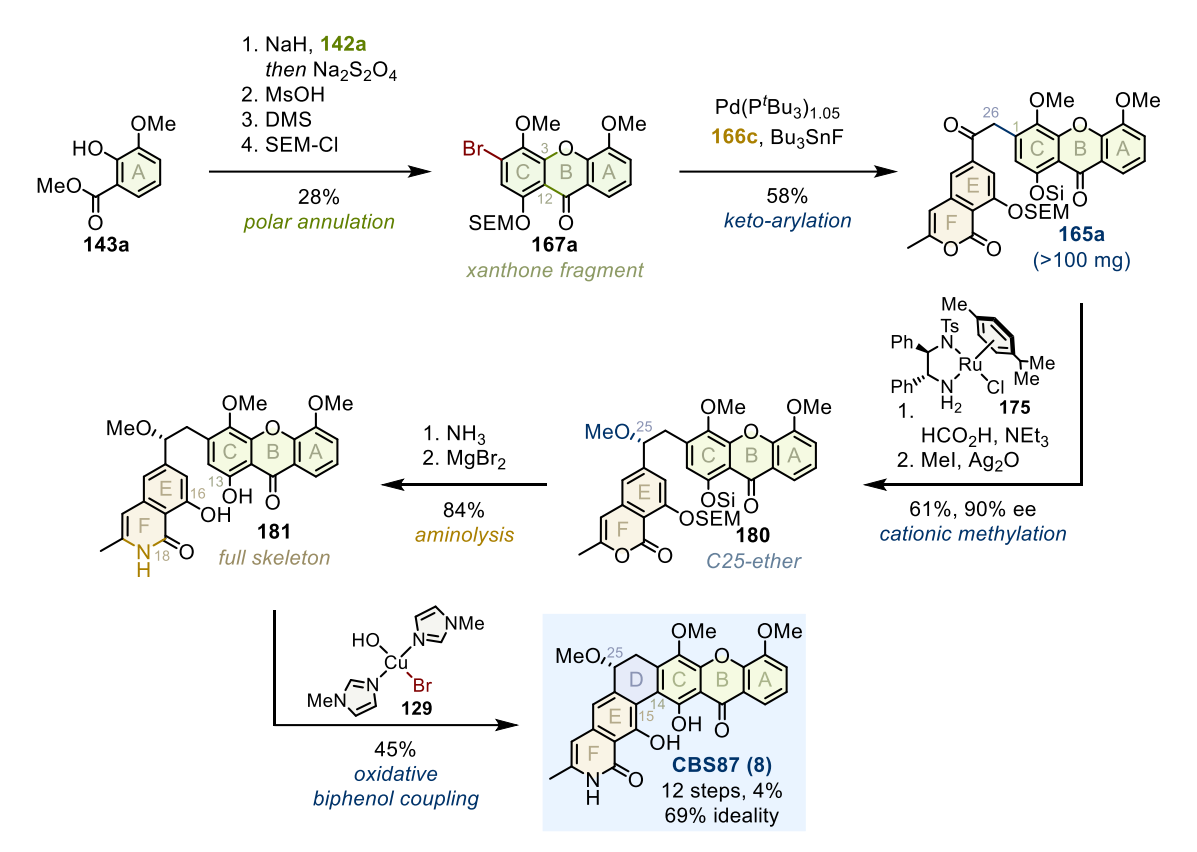


Figure 61. Robust protocols translate into a concise total synthesis of CBS87.

With fragment compatibility validated, we turned to the most challenging member, CBS72 (5), featuring an elusive *cis*-glycol (Figure 62). As before, the conjoint skeleton proved intolerant towards strong bases required for Davis α -hydroxylation. However, a serendipitous error – an order of magnitude more diluted NaHMDS-solution – revealed that this transformation also proceeds with catalytic quantities of base, thus expanding the scope towards base-labile **165b**. Presumably, hemiaminal **182** is both catalytically competent and kinetically trapped, allowing the selective formation of benzoin **183**. Although rapid air oxidation of the resulting C26-alcohol precluded isolation of **183**, immediate chelate-controlled reduction with zinc borohydride delivered the important *cis*-glycol **185** in a single step (91%, 84% ee, dr > 20:1). 174

Late stage aminolysis completed skeleton **186** (60%) and copper cyclization closed the D-ring. 90,169 Surprisingly, after deprotection CBS72 was isolated predominantly as lactim **187**, which gradually tautomerizes to reported²⁰ lactam **5** in solution (59%). This behavior is neither described in literature, nor had it occurred during the synthesis of CBS87 (**8**) and CBS100 (**6**). As evidenced by NMR, the only difference between these members is that the *cis*-dihydroxylated D-ring in CBS72 (**5**) forces a single rigid conformer, whereas mono-oxygenation permits several D-ring conformers in CBS87 (**8**) and CBS100 (**6**). Although a water-assisted tautomerization

mechanism seems plausible, the factors governing tautomeric preference and their relevance to biological activity remain to be identified. In the end, CBS72 (5) was isolated in 16 steps, 8% overall yield and 59% ideality.

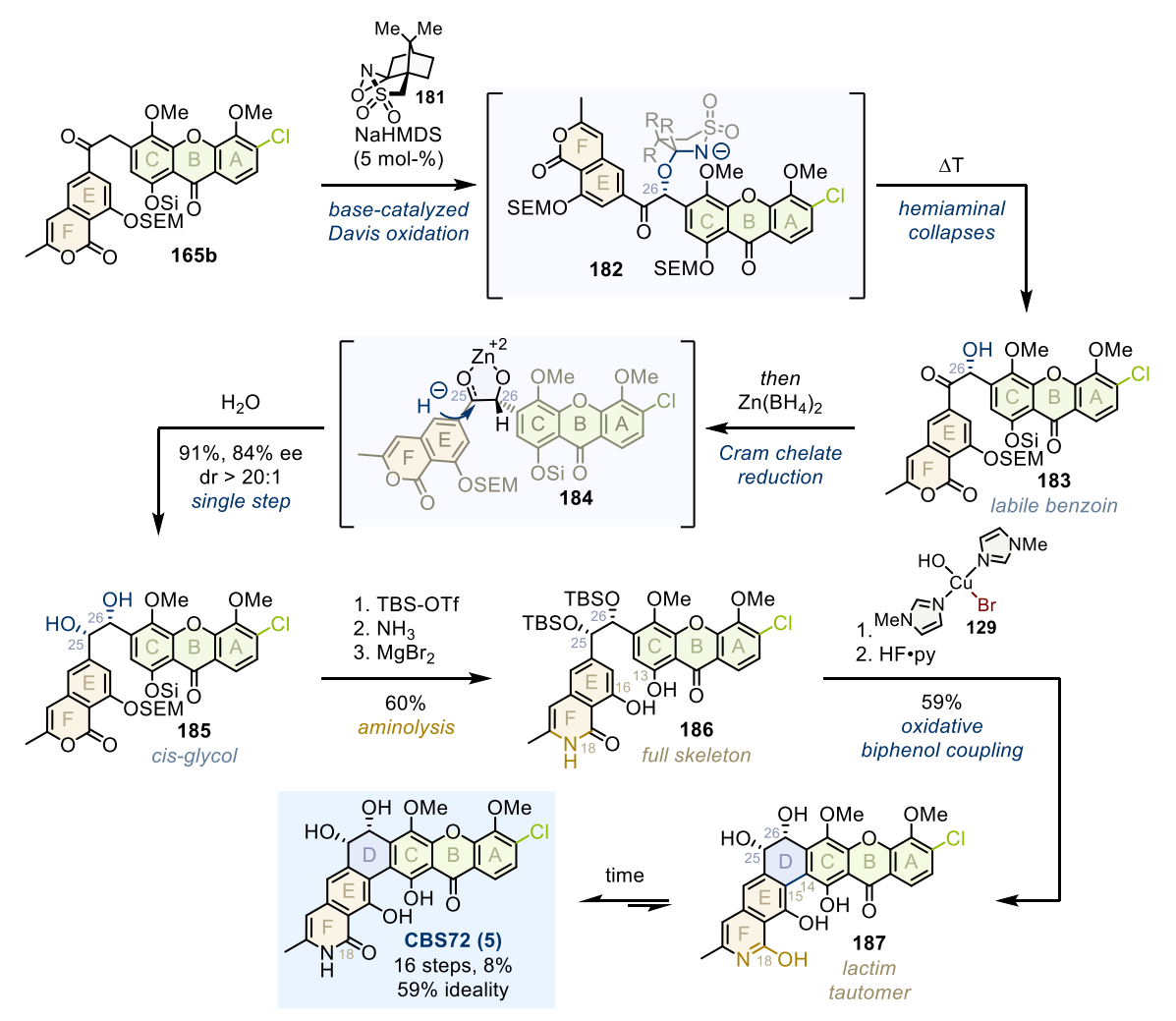


Figure 62. Unprecedented base-catalyzed Davis oxidation unlocks cis-glycol of CBS72.

Importance and Implications

This study establishes the first total synthesis of lysolipin natural products CBS72 (5), CBS87 (8), and CBS100 (6) through a concise, modular strategy (Figure 63). A revamped A-ring synthesis and optimized polar addition provided scalable access to xanthone 167 (28-40%). Site-selective, sequential cross-couplings afforded isocoumarin 166c in excellent yield (70%). Leveraging ligand types and ligation states, demanding interaromatic keto-arylation furnished а desoxybenzoin 165 as central, versatile intermediate (58-62%). Late stage aminolysis delivered CBS100 (6) and CBS87 (8) in good yield (25-40%). To accommodate base-labile 165, an innovative base-catalyzed Davis oxidation was developed, culminating in the selective synthesis of CBS72 (5) (34%). Throughout this work, mechanistic insights guided the design of highly selective, challenging transformations (see Supporting Information for details), replacing protective group chemistry and functional group interconversions with direct bond-forming reactions. As a result, the synthetic routes are short (12-16 steps LLS), exhibit remarkable idealities (59-69%) and proceed in good to excellent overall yields (4-10%).

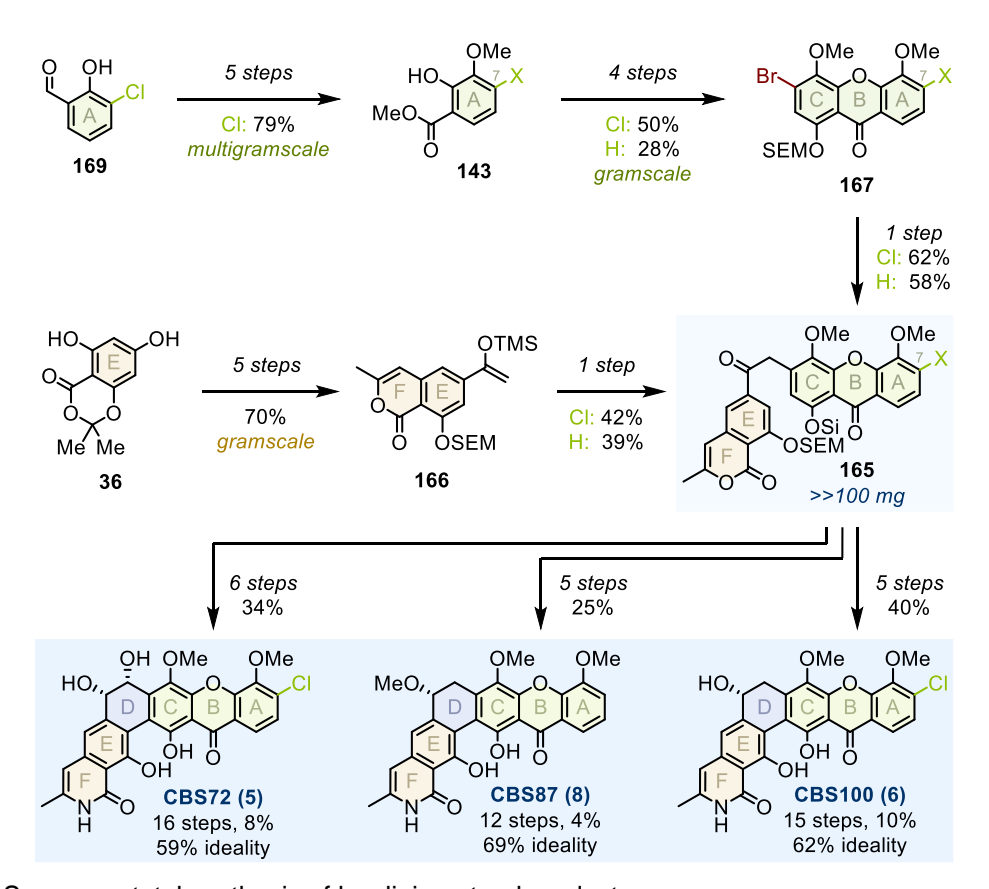


Figure 63. Summary: total synthesis of lysolipin natural products.

Yet, efforts to elaborate benzoin **182** into C25-methylated *cis*-glycols were obstructed by severe lability and steric hindrance (Figure 64). Amine bases racemized the C26-stereocenter and acidic

conditions led to decomposition. Low reactivity further narrowed possible conditions, resulting in TBS protected **188** as the only viable option (87%). As a consequence, Noyori transfer hydrogenation was sterically impeded even when using more reactive catalysts.^{77,175} Furthermore, CBS reduction favored unwanted *trans*-glycol **189** irrespective of the employed enantiomer, suggesting dominant substrate control following a polar Felkin-Anh mechanism. In the end, sodium borohydride favored *cis*-glycol **190** the most (20%), but steric encumbrance and severe base-lability prevented methylation of the C25-alcohol, preliminary ending a total synthesis of **3** and **4** and stimulating a mirrored approach (Chapter 6.2).

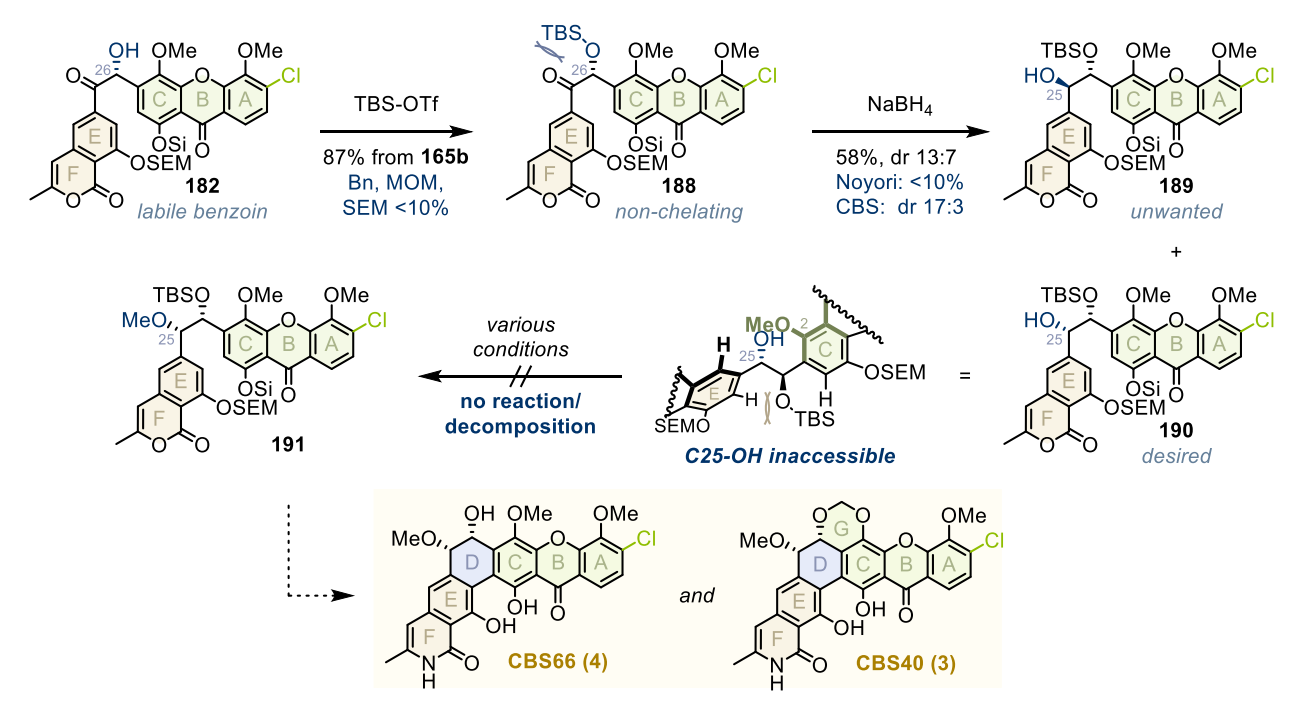


Figure 64. The central glycol emerged as sensitive, congested motive, preventing further elaboration.

6 From Synthesis to Pharmacology

6.1 Methodical Total Synthesis

Guided by mechanistic insights, Brassard's polar annulation strategy was systematically expanded towards congested, chlorine-bearing xanthones, but first a selective A-ring strategy was required (Figure 64). Throughout the studies, it became apparent that chlorination was intrinsically biased to the C9-position, and attempts to override this selectivity would result in low yield (Chapter 5.1-5.2). Consequently, oxidative remodeling of a chlorine-bearing starting material (Chapter 5.4) selectively yielded **143b** (79%), whereas conversion of non-chlorinated precursors performed five times worse (dark bars).

As anticipated from limited precedent, subsequent polar C-ring annulation proved particularly challenging. Bromoquinones quickly emerged as superior C-ring coupling partners compared to their iodo analogues, owing to the enhanced stability of both starting material and products (Chapter 5.1). This modification enabled access to C7-hydrogen-bearing xanthone **141a** (grey bars), but supply of chlorinated variants such as **141b** remained scarce (light bars). Detailed investigations revealed that a sterically biased, intramolecular hydrogen bond reduced acidity of the C5-phenol, limiting its reactivity (grey). Two solutions were identified: (1) an optimized surplus of mild base and base-labile quinone furnishes **141b** in excellent yield (75%) on small scale (Chapter 5.2), or (2) a small and strong base enabled large-scale synthesis (56%) with excellent atom economy (Chapter 5.4). Thus, depending on the desired scale – or dedication to perform multiple, smaller reactions – both protocols efficiently access chlorine-bearing **141b**.

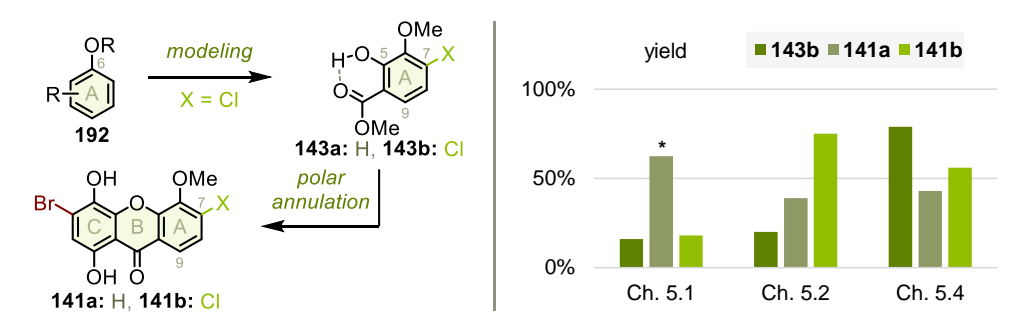


Figure 65. Systematically optimized xanthone synthesis. * inconsistent with later findings (Chapter 5.2).

These optimizations translate directly into an efficient synthesis of xanthone fragment **167** (Figure 66). Overall yields compare favorably with those of previously reported, partially undisclosed strategies (left chart). In particular, the small-scale yield of chloroxanthone **167b** (53%) demonstrates the effectiveness of the thoroughly optimized protocols (light bar).

Most notable is the brevity of the synthetic sequence (right chart). Only three key transformations are required – Dakin oxidation, directed *ortho*-metalation, polar annulation – and an extensive pre-functionalization of the C-ring is avoided (compare Chapter 3.2-3.3). As a result, chlorinated xanthone **167b** is accessible in just nine steps, and a class-leading four-step sequence leads to deschloro analogue **167a**.

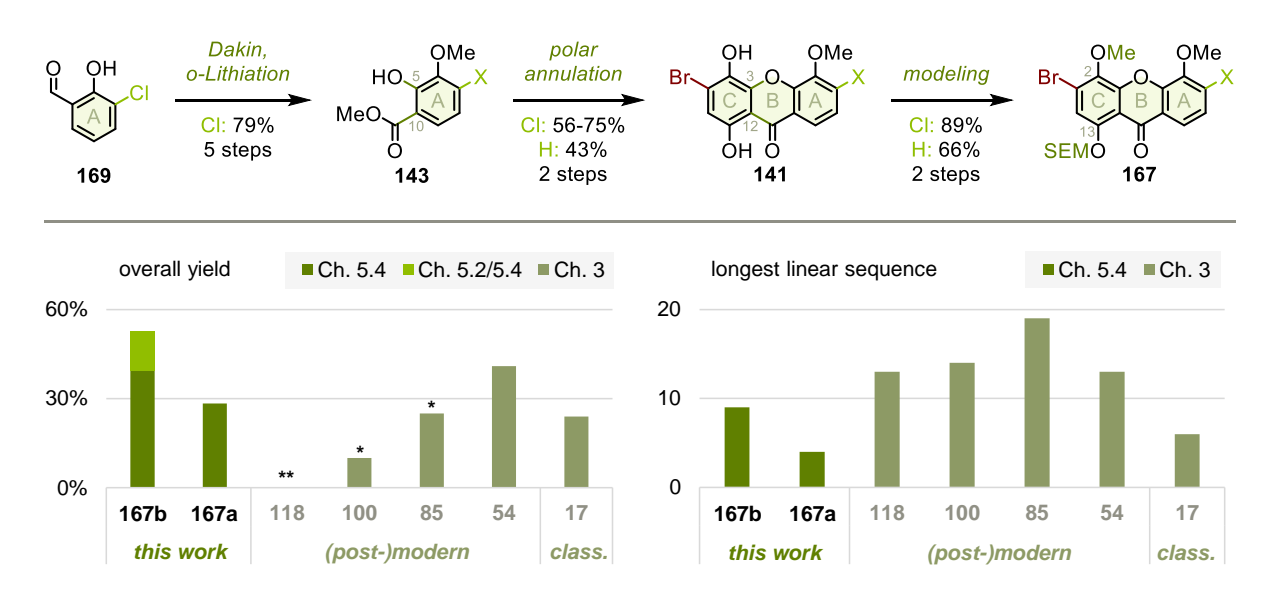


Figure 66. Thoroughly optimized sequences provide concise access to the congested xanthone fragment. (*)* (major) parts of fragment synthesis undocumented.

This trend continues in the synthesis of isocoumarin fragment **166c** (Figure 67). Particularly noteworthy is the excellent overall yield (70%), obtained in a single pass from bisphenol **36** (left chart). Key factors in this success were a site-selective Stille-Migita coupling, made possible by exploiting biased first-order kinetics, along with cryogenic isolation of sensitive silyl enol-ether **166c** (Chapter 5.4). The concise sequence length (right chart) originates from a strategically delayed aminolysis step. This decision not only circumvented laborious protective group chemistry, but also enabled the usage of reactive catalysts in subsequent transformations (compare Chapter 5.3).

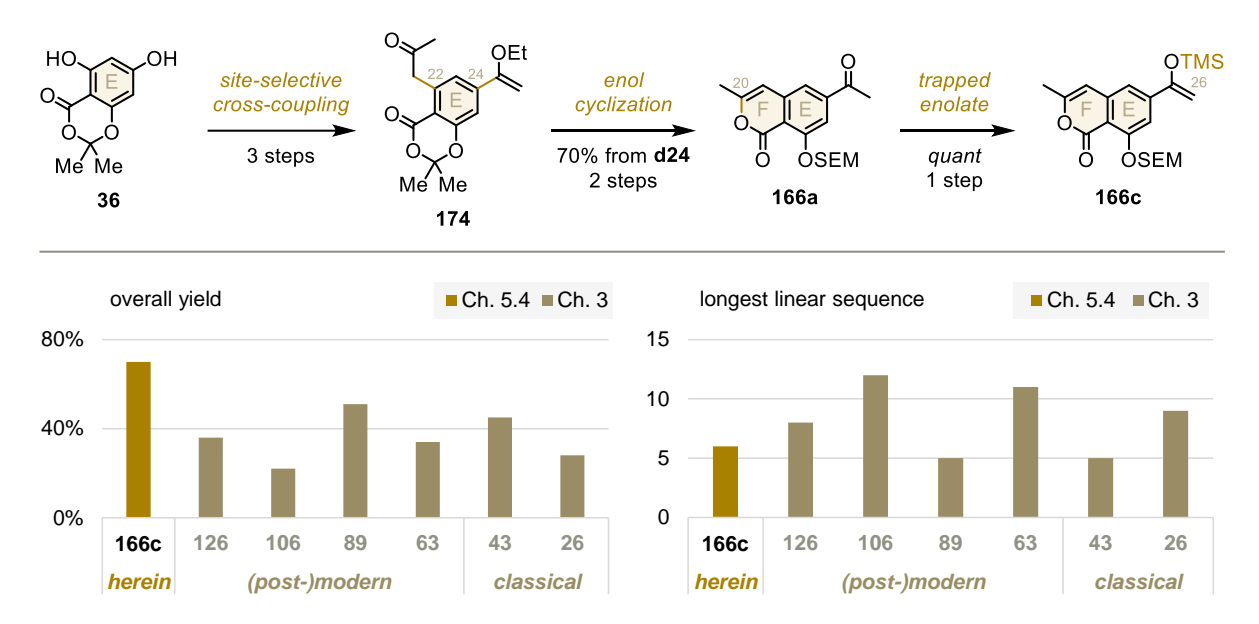


Figure 67. Site-selective cross-coupling facilitates high-yielding isocoumarin fragment synthesis.

An innovative, modular endgame complemented concise fragment syntheses (Figure 68). For the first time, the fresh-developed ligand type concept (Chapter 5.3) was applied to complex target synthesis (Chapter 5.4). This screening approach efficiently revealed promising conditions for a very demanding intermolecular, aromatic keto-arylation between advanced fragments **167** and **166c**, thus replacing exhaustive – and based on non-existent precedence also unsuccessful – brute-force screening with rational design. The resulting protocol proved general and afforded **165** in a single step with favorable yields (58-62%), outperforming several thoroughly optimized, multistep procedures based on traditional cross-coupling strategies (Chapter 3.2-3.3).

Moreover, Davis oxidation was serendipitously found to proceed with only catalytic quantities of base (Chapter 5.4). In fact, reduced base loading increased enantiopurity, suggesting that the intermediate hemiaminal is both sufficiently stable and catalytically competent. This finding broadened the substrate scope to include base-labile substrates such as **165**.

Finally, late-stage aminolysis selectively introduced the natural, unsubstituted C18-lactam as envisioned. Together with Noyori transfer hydrogenation and oxidative copper cyclization, these strategies culminated in the successful synthesis of CBS72 (5), CBS100 (6) and CBS87 (8).

Collectively, these total syntheses accessed previously unexplored chemical space, delivered solid to class-leading overall yields (left chart), and rivaled the step count of classical syntheses targeting structurally less complex polycyclic xanthones (right chart).

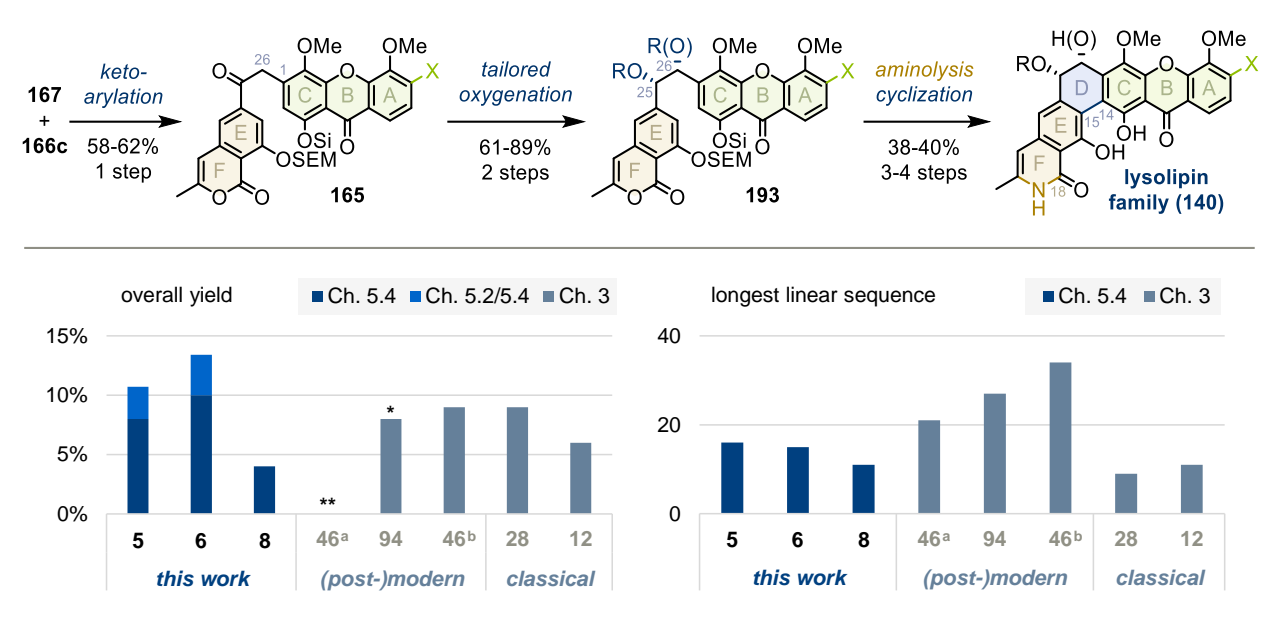


Figure 68. An innovative endgame culminates in class-leading total syntheses of lysolipin natural products. (*)* (major) parts of fragment synthesis undocumented. ^a Gao (2020), ^b Suzuki (2009).

Overall, these strategies resulted in unprecedented levels of ideality (Figure 69). Two out of every three reactions form a central bond, representing a two- to threefold improvement over existing approaches (Chapter 3.2-3.3). This outcome was made possible by diligent and systematic advances. While some methods may remain restricted to these substrates – for example rapid cryogenic chromatography requires large polarity differences between starting material and product for efficient separation – others hold the potential to reshape modern synthetic chemistry. Among these, the ligand-type screening approach stands out, as it requires only a handful of conditions to traverse large chemical spaces, a promise that holds even in complex target synthesis. Moreover, if proven general, catalytic Davis oxidation could unlock access to base-sensitive scaffolds, providing a valuable extension to asymmetric synthesis.

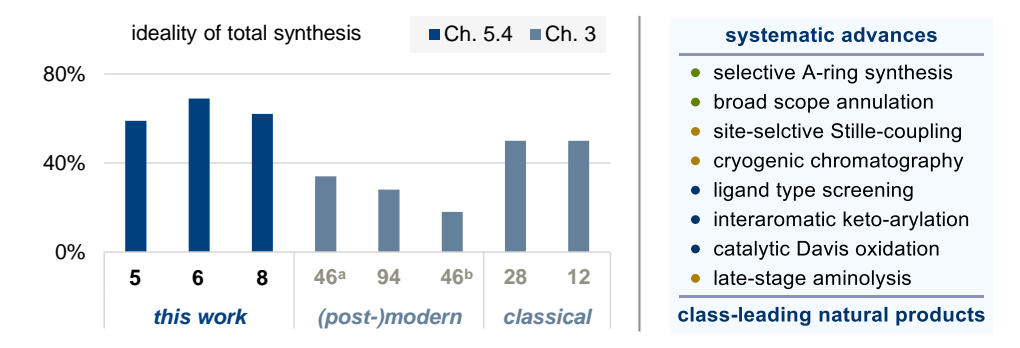


Figure 69. Unprecedented idealities originate from systematic advances. a Gao (2020), b Suzuki (2009).

6.2 Towards Uncharted Lysolipins

Despite methodical advances, emergence prohibited elaboration of **165** towards disparate substituted *cis*-glycol members (Chapter 5.4). In response, a mirrored synthetic sequence is proposed (Figure 70). Relocating the ketone donor to the xanthone fragments would furnish central desoxybenzoin **194**. Subsequent Davis oxidation could yield an unhindered C25-alcohol, which upon methylation could direct chelate-controlled reduction towards the desired C25-methylated *cis*-glycol **195**. Then, the established sequence of aminolysis, phenol deprotection, and copper-mediated D-ring cyclization could furnish CBS66 **(4)**. Importantly, acidic acetalization conditions are tolerated (compare Chapter 3.2), and liberate SEM-protected phenols without protecting them (see publication Chapter 5.4), suggesting that CBS40 **(3)** could be accessed by substituting the deprotection step with G-ring acetal formation. Furthermore, modifying the amine in the aminolysis step would enable the synthesis of C18-methyllactam members such as CBS60 **(2)**.

Together with the established sequences (see above), these strategies would provide access to fifteen of the twenty known lysolipin natural products (Chapter 2), thus enabling a systematic exploration of this privileged polycyclic xanthone family.

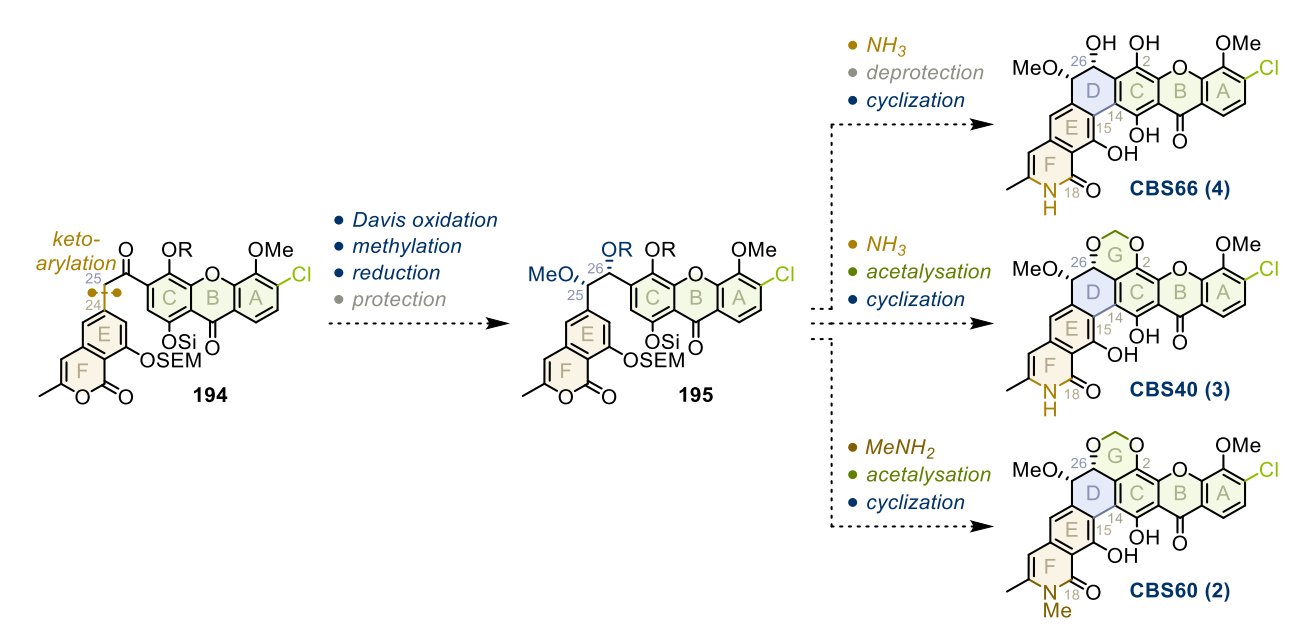


Figure 70. Proposed route to further lysolipin natural products.

6.3 Promising Drug Leads

In response to the poorly characterized pharmacological profile of lysolipin natural products (Chapter 2), the synthetic route was deliberately designed with modular exit vectors for later drug development (Figure 71). Whereas bioactive potency is broadly modulated by substituents on the central D-ring (blue), the F-ring (orange) and A-ring (green) provide tunable sites for target-specific interactions (Chapter 2 and 5.2).

Focusing on the F-ring, NMR studies revealed that the unsubstituted C18-lactam in CBS72 (5) undergoes tautomerization to its aromatic lactim form (Chapter 5.4). In line with a lipophilic pre-organization hypothesis, this transformation may be the cause of broad-spectrum activity, since methyl-substituted analogues such as **2**, which cannot tautomerize to a planar F-ring, display narrower but more efficient potencies, targeting specifically MRSA (Chapter 2). These findings suggest that late-stage introduction of primary amines (**197**) could bias the antibiotic profile towards these high-priority pathogens (Chapter 1). Furthermore, oxazolidine formation (Chapter 3.1-3.2) offers an interesting avenue for elaboration at the C19'-carboxylic acid (**198**), increasing scaffold diversity.

Cytotoxicity was primarily linked to the C7-substituent on the A-ring (Chapter 2 and 5.2). Hydrogen-bearing variants (199) exhibited no cytotoxic effects, indicating that selective dehalogenation may reduce off-target toxicity of lysolipin-inspired antibiotics. Conversely, phenyl groups at this site promoted antiproliferative activity, thus providing a strategic handle for the development of anticancer drugs through Suzuki-Miyaura coupling (200) (Chapter 5.3).

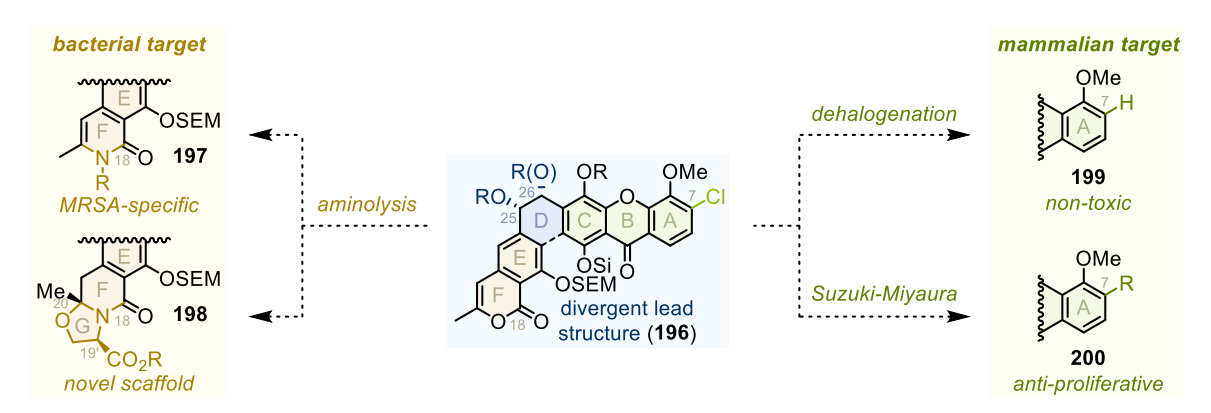


Figure 71. Exit vectors for target-specific lysolipin-inspired drugs.

6.4 Personal Conclusion

Living in the digital era, it is tempting to believe that algorithmic mining of the known chemical space will generate novel solutions from what has already been explored. But when faced with urgent and unsolved problems, this approach falls short, delivering neither innovation nor insight (Chapter 1). Worse still, this strategy risks forgetting science's core strength: it is not built on patterns, but on principles. Science is bound to the laws of nature.

By unravelling underlying mechanisms, science drives fundamental understanding, expands into uncharted territories, and ultimately discovers nature's answers to humanity's pressing needs, making research indispensable for development.

Above all, this thesis stands as a tribute to rational design: belief is religion, luck is gambling, yet science is knowledge.

7 References

- (1) Tacconelli, E.; Carrara, E.; Savoldi, A.; Harbarth, S.; Mendelson, M.; Monnet, D. L.; Pulcini, C.; Kahlmeter, G.; Kluytmans, J.; Carmeli, Y.; et al. Discovery, research, and development of new antibiotics: the WHO priority list of antibiotic-resistant bacteria and tuberculosis. Lancet Infect. Dis. 2018, 18, 318–327.
- (2) Douglas, J. J.; Campbell, A. D.; Buttar, D.; Fairley, G.; Johansson, M. J.; Mcintyre, A. C.; Metrano, A. J.; Morales, R. S.; Munday, R. H.; Nguyen, T. V. Q.; et al. The Implementation and Impact of Chemical High-Throughput Experimentation at AstraZeneca. ACS Catal. 2025, 1419, 5229–5256.
- (3) Mennen, S. M.; Alhambra, C.; Allen, C. L.; Barberis, M.; Berritt, S.; Brandt, T. A.; Campbell, A. D.; Castañón, J.; Cherney, A. H.; Christensen, M.; et al. The Evolution of High-Throughput Experimentation in Pharmaceutical Development and Perspectives on the Future. Org. Process Res. Dev. 2019, 23, 1213–1242.
- (4) Boström, J.; Brown, D. G.; Young, R. J.; Keserü, G. M. Expanding the medicinal chemistry synthetic toolbox. *Nat. Rev. Drug. Discov.* **2018**, *17*, 709–727.
- (5) Brown, D. G.; Boström, J. Analysis of Past and Present Synthetic Methodologies on Medicinal Chemistry: Where Have All the New Reactions Gone? *J. Med. Chem.* **2016**, *59*, 4443–4458.
- (6) Schneider, N.; Lowe, D. M.; Sayle, R. A.; Tarselli, M. A.; Landrum, G. A. Big Data from Pharmaceutical Patents: A Computational Analysis of Medicinal Chemists' Bread and Butter. *J. Med. Chem.* **2016**, *59*, 4385–4402.
- (7) Genheden, S.; Howell, G. P. An Analysis of Published Synthetic Routes, Route Targets, and Reaction Types (2000–2020). *Org. Process Res. Dev.* **2024**, *28*, 4225–4239.
- (8) Tommasi, R.; Brown, D. G.; Walkup, G. K.; Manchester, J. I.; Miller, A. A. ESKAPEing the labyrinth of antibacterial discovery. *Nat. Rev. Drug. Discov.* **2015**, *14*, 529–542.
- (9) Walsh, C. T.; Wencewicz, T. A. Prospects for new antibiotics: a molecule-centered perspective. *J. Antibiot.* **2014**, *67*, 7–22.
- (10) Lewis, K. The Science of Antibiotic Discovery. Cell 2020, 181, 29–45.
- (11) Pye, C. R.; Bertin, M. J.; Lokey, R. S.; Gerwick, W. H.; Linington, R. G. Retrospective analysis of natural products provides insights for future discovery trends. *Proc. Natl. Acad. Sci. U.S.A.* **2017**, *114*, 5601–5606.

- (12) Atanasov, A. G.; Zotchev, S. B.; Dirsch, V. M.; Supuran, C. T. Natural products in drug discovery: advances and opportunities. *Nat. Rev. Drug. Discov.* **2021**, *20*, 200–216.
- (13) Newman, D. J.; Cragg, G. M. Natural Products as Sources of New Drugs over the Nearly Four Decades from 01/1981 to 09/2019. *J. Nat. Prod.* **2020**, *83*, 770–803.
- (14) Blakemore, D. C.; Castro, L.; Churcher, I.; Rees, D. C.; Thomas, A. W.; Wilson, D. M.; Wood, A. Organic synthesis provides opportunities to transform drug discovery. *Nat. Chem.* 2018, 10, 383–394.
- (15) Peters, D. S.; Pitts, C. R.; McClymont, K. S.; Stratton, T. P.; Bi, C.; Baran, P. S. Ideality in Context: Motivations for Total Synthesis. *Acc. Chem. Res.* **2021**, *54*, 605–617.
- (16) Gaich, T.; Baran, P. S. Aiming for the ideal synthesis. *J. Org. Chem.* **2010**, *75*, 4657–4673.
- (17) Herzon, S. Emergent Properties of Natural Products. Synlett 2018, 29, 1823–1835.
- (18) Kong, L.; Deng, Z.; You, D. Chemistry and biosynthesis of bacterial polycyclic xanthone natural products. *Nat. Prod. Rep.* **2022**, *39*, 2057–2095.
- (19) Hornung, A.; Bertazzo, M.; Dziarnowski, A.; Schneider, K.; Welzel, K.; Wohlert, S.-E.; Holzenkämpfer, M.; Nicholson, G. J.; Bechthold, A.; Süssmuth, R. D.; et al. A genomic screening approach to the structure-guided identification of drug candidates from natural sources. *ChemBioChem* **2007**, *8*, 757–766.
- (20) Fischer, C.; Hornung, A.; Holzenkpämpfer, M.; Pelzer, S.; Priefert, H.; Renner, U.-D.; Vierling, S.; Wohlert, S.-E. Novel Lysolipin Derivatives. WO 2007/079715 A2, Dec 21, 2006.
- (21) Drautz, H.; Keller-Schierlein, W.; Zähner, H. Stoffwechselprodukte von Mikroorganismen 149. Mitteilung. Lysolipin I, ein neues Antibioticum aus Streptomyces violaceoniger. *Arch. Microbiol.* **1975**, *106*, 175–190.
- (22) Drautz, H.; Keller-Schierlein, W.; Zähner, H. Lysolipin I, ein neuer Hemmstoff der bakteriellen Zellwandsynthese. *Path. Microbiol.* **1975**, *42*, 236.
- (23) Robertsen, H.; Rohrer, S.; Kulik, A.; Wohlleben, W.; Mast, Y. Generation of lysolipin derivatives by genetic engineering. *Front. Chem. Biol.* **2024**, *3*, 1445095.
- (24) Dobler, M.; Keller-Schierlein, W. Metabolites of microorganisms. 162nd Communication.

 The crystal and molecular structure of lysolipin I. *Helv. Chim. Acta* **1977**, *60*, 178–185.
- (25) Lopez, P.; Hornung, A.; Welzel, K.; Unsin, C.; Wohlleben, W.; Weber, T.; Pelzer, S. Isolation of the lysolipin gene cluster of Streptomyces tendae Tü 4042. *Gene* **2010**, *461*, 5–14.
- (26) Qiao, Y. F.; Okazaki, T.; Ando, T.; Mizoue, K. Isolation and Characterization of a New Pyrano[4',3':6,7]naphtho[1,2-b]xanthene Antibiotic FD-594. *J. Antibiot.* **1998**, *51*, 282–287.

- (27) Eguchi, T.; Kondo, K.; Kakinuma, K.; Uekusa, H.; Ohashi, Y.; Mizoue, K.; Qiao, Y.-F. Unique Solvent-Dependent Atropisomerism of a Novel Cytotoxic Naphthoxanthene Antibiotic FD-594. *J. Org. Chem.* **1999**, *64*, 5371–5376.
- (28) Martins-Teixeira, M. B.; Carvalho, I. Antitumour Anthracyclines: Progress and Perspectives. *ChemMedChem* **2020**, *15*, 933–948.
- (29) Duthaler, R. O.; Mathies, P.; Petter, W.; Heuberger, C.; Scherrer, V. Experiments on the Total Synthesis of Lysolipin I. Part I. On Configuration and Conformation of 5-Substituted 1,2,3,4,4a,9,10,10a-Ocathydrophenanthrene-4,9-diones. *Helv. Chim. Acta* **1984**, *67*, 1217–1221.
- (30) Duthaler, R. O.; Wegmann, U. H.-U. Experiments on the total synthesis of Lysolipin I. Part II. Michael addition of 1,3-cyclohexanedione to quinone acetals. *Helv. Chim. Acta* **1984**, *67*, 1755–1766.
- (31) Duthaler, R. O.; Scherrer, V. Experiments on the total synthesis of Lysolipin I. Part III.

 Preparation and transformations of substituted 1,2,3,4-Tetrahydrodibenzofuran-1-ones.

 Helv. Chim. Acta 1984, 67, 1767–1775.
- (32) Kelly, T. R.; Jagoe, C. T.; Li, Q. Synthesis of (±)-Cervinomycins A1 and A2. *J. Am. Chem. Soc.* **1989**, *111*, 4522–4524.
- (33) Fischer, E.; Speier, A. Darstellung der Ester. Ber. Dtsch. Chem. Ges. 1895, 28, 3252–3258.
- (34) Hashimoto, N.; Aoyama, T.; Shioiri, T. New methods and reagents in organic synthesis. 14.

 A simple efficient preparation of methyl esters with trimethylsilyldiazomethane

 (TMSCHN2) and its application to gas chromatographic analysis of fatty acids. *Chem. Pharm. Bull.* **1981**, *29*, 1475–1478.
- (35) Simoneau, B.; Brassard, P. A new regiospecific synthesis of 1,4-dihydroxyxanthones. *J. Chem. Soc., Perkin Trans.* 1 **1984**, 1507.
- (36) Snieckus, V. Directed ortho metalation. Tertiary amide and O-carbamate directors in synthetic strategies for polysubstituted aromatics. *Chem. Rev.* **1990**, *90*, 879–933.
- (37) White, E. H. The Chemistry of the N-Alkyl-N-nitrosoamides. I. Methods of Preparation. *J. Am. Chem. Soc.* **1955**, *77*, 6008–6010.
- (38) White, E. H. The Chemistry of the N-Alkyl-N-nitrosoamides. II. A New Method for the Deamination of Aliphatic Amines. *J. Am. Chem. Soc.* **1955**, *77*, 6011–6014.
- (39) Mitsunobu, O. The Use of Diethyl Azodicarboxylate and Triphenylphosphine in Synthesis and Transformation of Natural Products. *Synthesis* **1981**, *1981*, 1–28.

- (40) Carlock, J. T.; Mack, M. P. A mild quamtitative method for the synthesis of a variety of heterocyclic systems. *Tetrahedron Lett.* **1978**, *19*, 5153–5156.
- (41) Mizoroki, T.; Mori, K.; Ozaki, A. Arylation of Olefin with Aryl Iodide Catalyzed by Palladium. *Bull. Chem. Soc. Jpn.* **1971**, *44*, 581.
- (42) Heck, R. F.; Nolley, J. P. Palladium-catalyzed vinylic hydrogen substitution reactions with aryl, benzyl, and styryl halides. *J. Org. Chem.* **1972**, *37*, 2320–2322.
- (43) Hosokawa, S.; Fumiyama, H.; Fukuda, H.; Fukuda, T.; Seki, M.; Tatsuta, K. The first total synthesis and structural determination of TMC-66. *Tetrahedron Lett.* **2007**, *48*, 7305–7308.
- (44) Tatsuta, K.; Hosokawa, S.; Fumiyama, H.; Fukuda, H.; Fukuda, T.; Seki, M. Total Synthesis of an Endothelin Converting Enzyme Inhibitor, TMC-66. *Heterocycles* **2008**, *76*, 699.
- (45) Maldonado-Domínguez, M.; Ruiz-Pérez, K.; González-Antonio, O.; Romero-Ávila, M.; Méndez-Stivalet, J.; Flores-Pérez, B. On the Brassard's rule of regioselectivity in Diels–Alder reactions between haloquinones and polar dienes. *RSC Adv.* **2016**, *6*, 75194–75201.
- (46) Savard, J.; Brassard, P. Regiospecific syntheses of quinones using vinylketene acetals derived from unsaturated esters. *Tetrahedron Lett.* **1979**, *20*, 4911–4914.
- (47) Sonogashira, K.; Tohda, Y.; Hagihara, N. A convenient synthesis of acetylenes: catalytic substitutions of acetylenic hydrogen with bromoalkenes, iodoarenes and bromopyridines. *Tetrahedron Lett.* **1975**, *16*, 4467–4470.
- (48) Liu, P.; Lanza, T. J.; Jewell, J. P.; Jones, C. P.; Hagmann, W. K.; Lin, L. S. A highly active catalyst system for the heteroarylation of acetone. *Tetrahedron Lett.* **2003**, *44*, 8869–8871.
- (49) Kosugi, M.; Hagiwara, I.; Sumiya, T.; Migita, T. Arylation and 1-Alkenylation on α-Position of Ketones via Tributyltin Enolates Catalyzed by Palladium Complex. *Bull. Chem. Soc. Jpn.* 1984, 57, 242–246.
- (50) Osborn, J. A.; Jardine, F. H.; Young, J. F.; Wilkinson, G. The preparation and properties of tris(triphenylphosphine)halogenorhodium(I) and some reactions thereof including catalytic homogeneous hydrogenation of olefins and acetylenes and their derivatives. *J. Chem. Soc., A* **1966**, 1711.
- (51) Duckett, S. B.; Newell, C. L.; Eisenberg, R. Observation of New Intermediates in Hydrogenation Catalyzed by Wilkinson's Catalyst, RhCl(PPh3)3, Using Parahydrogen-Induced Polarization. J. Am. Chem. Soc. 1994, 116, 10548–10556.

- (52) Nakajima, M.; Miyoshi, I.; Kanayama, K.; Hashimoto, S.; Noji, M.; Koga, K. Enantioselective Synthesis of Binaphthol Derivatives by Oxidative Coupling of Naphthol Derivatives Catalyzed by Chiral Diamine·Copper Complexes. *J. Org. Chem.* **1999**, *64*, 2264–2271.
- (53) Noji, M.; Nakajima, M.; Koga, K. A new catalytic system for aerobic oxidative coupling of 2-naphthol derivatives by the use of CuCl-amine complex: A practical synthesis of binaphthol derivatives. *Tetrahedron Lett.* **1994**, *35*, 7983–7984.
- (54) Röckl, J. L.; Pollok, D.; Franke, R.; Waldvogel, S. R. A Decade of Electrochemical Dehydrogenative C,C-Coupling of Aryls. *Acc. Chem. Res.* **2020**, *53*, 45–61.
- (55) Wu, J.; Kozlowski, M. C. Catalytic Oxidative Coupling of Phenols and Related Compounds. *ACS Catal.* **2022**, *12*, 6532–6549.
- (56) Masuo, R.; Ohmori, K.; Hintermann, L.; Yoshida, S.; Suzuki, K. First stereoselective total synthesis of FD-594 aglycon. *Angew. Chem. Int. Ed.* **2009**, *48*, 3462–3465.
- (57) Hintermann, L.; Suzuki, K. 2,5-Dihydroxyterephthalates, 2,5-Dichloro-1,4-benzoquinone-3,6-dicarbox-ylates, and Polymorphic 2,5-Dichloro-3,6-dihydroxyterephthalates. *Synthesis* **2008**, 2303–2306.
- (58) Frigerio, M.; Santagostino, M. A mild oxidizing reagent for alcohols and 1,2-diols: o-iodoxybenzoic acid (IBX) in DMSO. *Tetrahedron Lett.* **1994**, *35*, 8019–8022.
- (59) Hintermann, L.; Masuo, R.; Suzuki, K. Solvent-controlled leaving-group selectivity in aromatic nucleophilic substitution. *Org. Lett.* **2008**, *10*, 4859–4862.
- (60) Dorel, R.; Grugel, C. P.; Haydl, A. M. The Buchwald-Hartwig Amination After 25 Years. *Angew. Chem. Int. Ed.* **2019**, *58*, 17118–17129.
- (61) Ingoglia, B. T.; Wagen, C. C.; Buchwald, S. L. Biaryl Monophosphine Ligands in Palladium-Catalyzed C-N Coupling: An Updated User's Guide. *Tetrahedron* **2019**, *75*, 4199–4211.
- (62) Magano, J.; Dunetz, J. R. Large-scale applications of transition metal-catalyzed couplings for the synthesis of pharmaceuticals. *Chem. Rev.* **2011**, *111*, 2177–2250.
- (63) Sambiagio, C.; Marsden, S. P.; Blacker, A. J.; McGowan, P. C. Copper catalysed Ullmann type chemistry: from mechanistic aspects to modern development. *Chem. Soc. Rev.* **2014**, *43*, 3525–3550.
- (64) Miyake, H.; Tsumura, T.; Sasaki, M. Simple deprotection of acetal type protecting groups under neutral conditions. *Tetrahedron Lett.* **2004**, *45*, 7213–7215.

- (65) Kajigaeshi, S.; Kakinami, T.; Yamasaki, H.; Fujisaki, S.; Kondo, M.; Okamoto, T. Iodination of Phenols by Use of Benzyltrimethylammonium Dichloroiodate(1–). *Chem. Lett.* **1987**, *16*, 2109–2112.
- (66) Quintin, J.; Lewin, G. Regioselective 6-iodination of 5,7-dioxygenated flavones by benzyltrimethylammonium dichloroiodate. *Tetrahedron Lett.* **2004**, *45*, 3635–3638.
- (67) Bringmann, G.; Menche, D. Stereoselective total synthesis of axially chiral natural products via biaryl lactones. *Acc. Chem. Res.* **2001**, *34*, 615–624.
- (68) Tamiya, M.; Ohmori, K.; Kitamura, M.; Kato, H.; Arai, T.; Oorui, M.; Suzuki, K. General synthesis route to benanomicin-pradimicin antibiotics. *Chem. Eur. J.* **2007**, *13*, 9791–9823.
- (69) Mancuso, A. J.; Swern, D. Activated Dimethyl Sulfoxide: Useful Reagents for Synthesis. *Synthesis* **1981**, 165–185.
- (70) Ohmori, K.; Kitamura, M.; Suzuki, K. From Axial Chirality to Central Chiralities: Pinacol Cyclization of 2,2'-Biaryldicarbaldehyde to trans-9,10-Dihydrophenanthrene-9,10-diol. *Angew. Chem. Int. Ed.* **1999**, *38*, 1226–1229.
- (71) Wang, Y.; Wang, C.; Butler, J. R.; Ready, J. M. Dehydrogenative coupling to enable the enantioselective total synthesis of (-)-simaomicin α. *Angew. Chem. Int. Ed.* **2013**, *52*, 10796–10799.
- (72) SciFinder. https://scifinder-n.cas.org/ (accessed July 13, 2025).
- (73) Johnson, C. R.; Adams, J. P.; Braun, M. P.; Senanayake, C.; Wovkulich, P. M.; Uskoković, M.
 R. Direct α-iodination of cycloalkenones. *Tetrahedron Lett.* 1992, 33, 917–918.
- (74) Krafft, M.; Cran, J. A Convenient Protocol for the α -Iodination of α , β -Unsaturated Carbonyl Compounds with I 2 in an Aqueous Medium. *Synlett* **2005**, *2005*, 1263–1266.
- (75) Luche, J. L. Lanthanides in organic chemistry. 1. Selective 1,2 reductions of conjugated ketones. *J. Am. Chem. Soc.* **1978**, *100*, 2226–2227.
- (76) Dess, D. B.; Martin, J. C. Readily accessible 12-I-5 oxidant for the conversion of primary and secondary alcohols to aldehydes and ketones. *J. Org. Chem.* **1983**, *48*, 4155–4156.
- (77) Fujii, A.; Hashiguchi, S.; Uematsu, N.; Ikariya, T.; Noyori, R. Ruthenium(II)-Catalyzed Asymmetric Transfer Hydrogenation of Ketones Using a Formic Acid–Triethylamine Mixture. *J. Am. Chem. Soc.* **1996**, *118*, 2521–2522.
- (78) Krasovskiy, A.; Kopp, F.; Knochel, P. Soluble lanthanide salts (LnCl3.2LiCl) for the improved addition of organomagnesium reagents to carbonyl compounds. *Angew. Chem. Int. Ed.* 2006, 45, 497–500.

- (79) Ma, A.-J.; Ready, J. M. Synthetic Studies on the Kigamicins. Org. Lett. **2019**, 21, 1148–1151.
- (80) Barros, M. T.; Maycock, C. D.; Ventura, M. R. Enantioselective Total Synthesis of (+)-Eutypoxide B. *J. Org. Chem.* **1997**, *62*, 3984–3988.
- (81) Barros, M. T.; Maycock, C. D.; Ventura, M. R. The First Synthesis of (–)-Asperpentyn and Efficient Syntheses of (+)-Harveynone, (+)-Epiepoformin and (–)-Theobroxide. *Chem. Eur. J.* **2000**, *6*, 3991–3996.
- (82) Poon, K. W. C.; Dudley, G. B. Mix-and-heat benzylation of alcohols using a bench-stable pyridinium salt. *J. Org. Chem.* **2006**, *71*, 3923–3927.
- (83) Chan, K.-F.; Zhao, Y.; Chow, L. M.; Chan, T. H. Synthesis of (±)-5'-methoxyhydnocarpin-D, an inhibitor of the Staphylococcus aureus multidrug resistance pump. *Tetrahedron* **2005**, *61*, 4149–4156.
- (84) Riley, H. L.; Morley, J. F.; Friend, N. A. C. 255. Selenium dioxide, a new oxidising agent. Part I. Its reaction with aldehydes and ketones. *J. Chem. Soc.* **1932**, 1875.
- (85) Mallampudi, N. A.; Reddy, G. S.; Maity, S.; Mohapatra, D. K. Gold(I)-Catalyzed Cyclization for the Synthesis of 8-Hydroxy-3- substituted Isocoumarins: Total Synthesis of Exserolide F. *Org. Lett.* **2017**, *19*, 2074–2077.
- (86) Pfenninger, J.; Heuberger, C.; Graf, W. Steroids and sex hormones. Part 262. The radical induced stannane reduction of selenoesters and selenocarbonates: A new method for the degradation of carboxylic acids to nor-alkanes and for desoxygenation of alcohols to alkanes. *Helv. Chim. Acta* **1980**, *63*, 2328–2337.
- (87) Soheili, A.; Albaneze-Walker, J.; Murry, J. A.; Dormer, P. G.; Hughes, D. L. Efficient and general protocol for the copper-free sonogashira coupling of aryl bromides at room temperature. *Org. Lett.* **2003**, *5*, 4191–4194.
- (88) Netherton, M. R.; Fu, G. C. Air-stable trialkylphosphonium salts: simple, practical, and versatile replacements for air-sensitive trialkylphosphines. Applications in stoichiometric and catalytic processes. *Org. Lett.* **2001**, *3*, 4295–4298.
- (89) Marion, N.; Ramón, R. S.; Nolan, S. P. (NHC)Au(I)-catalyzed acid-free alkyne hydration at part-per-million catalyst loadings. *J. Am. Chem. Soc.* **2009**, *131*, 448–449.
- (90) Xie, T.; Zheng, C.; Chen, K.; He, H.; Gao, S. Asymmetric Total Synthesis of the Complex Polycyclic Xanthone FD-594. *Angew. Chem. Int. Ed.* **2020**, *59*, 4360–4364.
- (91) Mlynarski, S. N.; Schuster, C. H.; Morken, J. P. Asymmetric synthesis from terminal alkenes by cascades of diboration and cross-coupling. *Nature* **2014**, *505*, 386–390.

- (92) Heilbron, I.; Jones, E. R. H.; Sondheimer, F. 129. Researches on acetylenic compounds. Part XV. The oxidation of primary acetylenic carbinols and glycols. *J. Chem. Soc.* **1949**, 604.
- (93) Jang, W. J.; Lee, W. L.; Moon, J. H.; Lee, J. Y.; Yun, J. Copper-Catalyzed trans-Hydroboration of Terminal Aryl Alkynes: Stereodivergent Synthesis of Alkenylboron Compounds. *Org. Lett.* **2016**, *18*, 1390–1393.
- (94) Miyaura, N.; Suzuki, A. Stereoselective synthesis of arylated (E)-alkenes by the reaction of alk-1-enylboranes with aryl halides in the presence of palladium catalyst. *J. Chem. Soc., Chem. Commun.* **1979**, 866.
- (95) Kolb, H. C.; VanNieuwenhze, M. S.; Sharpless, K. B. Catalytic Asymmetric Dihydroxylation. *Chem. Rev.* **1994**, *94*, 2483–2547.
- (96) Omura, K. Rapid Conversion of Phenols to p-Benzoquinones under Acidic Conditions with Lead Dioxide. *Synthesis* **1998**, 1145–1148.
- (97) Meringdal, J. W.; Kilian, A.; Li, W. C.; Heinemann, M. J. B.; Rausch, M.; Schneider, T.; Menche, D. Modular Synthesis of Halogenated Xanthones by a Divergent Coupling Strategy. *J. Org. Chem.* **2022**, *87*, 9375–9383.
- (98) Kraus, G. A.; Liu, F. Synthesis of polyhydroxylated xanthones via acyl radical cyclizations. *Tetrahedron Lett.* **2012**, *53*, 111–114.
- (99) Azevedo, C.; Afonso, C.; Pinto, M. Routes to Xanthones: An Update on the Synthetic Approaches. *Curr. Org. Chem.* **2012**, *16*, 2818–2867.
- (100) Yang, Q.; Sheng, M.; Henkelis, J. J.; Tu, S.; Wiensch, E.; Zhang, H.; Zhang, Y.; Tucker, C.; Ejeh, D. E. Explosion Hazards of Sodium Hydride in Dimethyl Sulfoxide, N, N Dimethylformamide, and N, N -Dimethylacetamide. *Org. Process Res. Dev.* **2019**, *23*, 2210–2217.
- (101) Kilian, A. Beitrag zur Totalsynthese von Lysolipin I. Dissertation, Rheinische Friedrich-Wilhelms-Universität Bonn, Bonn, 2020.
- (102) Meringdal, J. W.; Bade, L.; Bendas, G.; Menche, D. Diversity Oriented Synthesis of Novel Xanthones Reveal Potent Doxorubicin-Inspired Analogs. *ChemMedChem* **2024**, *19*, e202400055.
- (103) World Health Organization. WHO Model List of Essential Medicines: 23rd list, 2023. https://www.who.int/publications/i/item/WHO-MHP-HPS-EML-2023.02 (accessed September 7, 2023).

- (104) Narezkina, A.; Narayan, H. K.; Zemljic-Harpf, A. E. Molecular mechanisms of anthracycline cardiovascular toxicity. *Clin. Sci.* **2021**, *135*, 1311–1332.
- (105) Kurniawan, Y. S.; Priyangga, K. T. A.; Jumina; Pranowo, H. D.; Sholikhah, E. N.; Zulkarnain, A. K.; Fatimi, H. A.; Julianus, J. An Update on the Anticancer Activity of Xanthone Derivatives: A Review. *Pharmaceuticals* **2021**, *14*, 1144–1183.
- (106) Gul, S.; Aslam, K.; Pirzada, Q.; Rauf, A.; Khalil, A. A.; Semwal, P.; Bawazeer, S.; Al-Awthan, Y. S.; Bahattab, O. S.; Al Duais, M. A.; et al. Xanthones: A Class of Heterocyclic Compounds with Anticancer Potential. *Curr. Top. Med. Chem.* **2022**, *22*, 1930–1949.
- (107) Tang, R.-J.; Milcent, T.; Crousse, B. Regioselective Halogenation of Arenes and Heterocycles in Hexafluoroisopropanol. *J. Org. Chem.* **2018**, *83*, 930–938.
- (108) Xiong, X.; Yeung, Y.-Y. Ammonium Salt-Catalyzed Highly Practical Ortho -Selective Monohalogenation and Phenylselenation of Phenols: Scope and Applications. ACS Catal. 2018, 8, 4033–4043.
- (109) Edwards, M. P.; Kump, R. A.; Kung, P. P.; Mcapline, I. J.; Ninkovic, S.; Rui, E. Y.; Sutton, S. C.; Tatlock, J. H.; Wythes, M. J.; Zehnder, L. R. Aryl and Heteroaryl Fused Lactams. US 2014/0179667 A1, Dec 18, 2013.
- (110) Dai, M.; Yuan, X.; Kang, J.; Zhu, Z.-J.; Yue, R.-C.; Yuan, H.; Chen, B.-Y.; Zhang, W.-D.; Liu, R.-H.; Sun, Q.-Y. Synthesis and biological evaluation of phenyl substituted polyoxygenated xanthone derivatives as anti-hepatoma agents. *Eur. J. Med. Chem.* **2013**, *69*, 159–166.
- (111) Taylor, C. J.; Pomberger, A.; Felton, K. C.; Grainger, R.; Barecka, M.; Chamberlain, T. W.; Bourne, R. A.; Johnson, C. N.; Lapkin, A. A. A Brief Introduction to Chemical Reaction Optimization. *Chem. Rev.* **2023**, *123*, 3089–3126.
- (112) Wall, B. J.; Koeritz, M. T.; Stanley, L. M.; VanVeller, B. A Practical Start-Up Guide for Synthetic Chemists to Implement Design of Experiments (DoE). *ACS Catal.* **2025**, *15*, 8885–8893.
- (113) Guthrie, J. P. Hydrolysis of esters of oxy acids: pKa values for strong acids; Brønsted relationship for attack of water at methyl; free energies of hydrolysis of esters of oxy acids; and a linear relationship between free energy of hydrolysis and pKa holding over a range of 20 pK units. *Can. J. Chem.* **1978**, *56*, 2342–2354.
- (114) Mandelkern, M.; Elias, J. G.; Eden, D.; Crothers, D. M. The dimensions of DNA in solution. *J. Mol. Biol.* **1981**, *152*, 153–161.

- (115) Meringdal, J. W.; Menche, D. Suzuki-Miyaura (hetero-)aryl cross-coupling: recent findings and recommendations. *Chem. Soc. Rev.* **2025**, *54*, 5746–5765.
- (116) D'Alterio, M. C.; Casals-Cruañas, È.; Tzouras, N. V.; Talarico, G.; Nolan, S. P.; Poater, A. Mechanistic Aspects of the Palladium-Catalyzed Suzuki-Miyaura Cross-Coupling Reaction. *Chem. Eur. J.* **2021**, *27*, 13481–13493.
- (117) Icons from thenounproject.com CC BY 3.0: "papers" (Greg Beck), "experiment" (Icon Studio), "Data Analysis" (erifqizeicon), "guide" (Ferdinand Partahi Jaya Tambunan).
- (118) Thomas, A. A.; Denmark, S. E. Pre-transmetalation intermediates in the Suzuki-Miyaura reaction revealed: The missing link. *Science* **2016**, *352*, 329–332.
- (119) Delaney, C. P.; Marron, D. P.; Shved, A. S.; Zare, R. N.; Waymouth, R. M.; Denmark, S. E. Potassium Trimethylsilanolate-Promoted, Anhydrous Suzuki-Miyaura Cross-Coupling Reaction Proceeds via the "Boronate Mechanism": Evidence for the Alternative Fork in the Trail. *J. Am. Chem. Soc.* **2022**, *144*, 4345–4364.
- (120) Payard, P.-A.; Perego, L. A.; Ciofini, I.; Grimaud, L. Taming Nickel-Catalyzed Suzuki-Miyaura Coupling: A Mechanistic Focus on Boron-to-Nickel Transmetalation. *ACS Catal.* **2018**, *8*, 4812–4823.
- (121) Thomas, A. A.; Wang, H.; Zahrt, A. F.; Denmark, S. E. Structural, Kinetic, and Computational Characterization of the Elusive Arylpalladium(II)boronate Complexes in the Suzuki-Miyaura Reaction. *J. Am. Chem. Soc.* **2017**, *139*, 3805–3821.
- (122) Borowski, J. E.; Newman-Stonebraker, S. H.; Doyle, A. G. Comparison of Monophosphine and Bisphosphine Precatalysts for Ni-Catalyzed Suzuki-Miyaura Cross-Coupling: Understanding the Role of the Ligation State in Catalysis. ACS Catal. 2023, 13, 7966–7977.
- (123) Shi, Y.; Derasp, J. S.; Maschmeyer, T.; Hein, J. E. Phase transfer catalysts shift the pathway to transmetalation in biphasic Suzuki-Miyaura cross-couplings. *Nat. Commun.* **2024**, *15*, 5436.
- (124) Shi, Y.; Derasp, J. S.; Guzman, S. M.; Patrick, B. O.; Hein, J. E. Halide Salts Alleviate TMSOK Inhibition in Suzuki-Miyaura Cross-Couplings. *ACS Catal.* **2024**, *14*, 12671–12680.
- (125) Newman-Stonebraker, S. H.; Smith, S. R.; Borowski, J. E.; Peters, E.; Gensch, T.; Johnson, H.
 C.; Sigman, M. S.; Doyle, A. G. Univariate classification of phosphine ligation state and reactivity in cross-coupling catalysis. *Science* 2021, 374, 301–308.

- (126) Newman-Stonebraker, S. H.; Wang, J. Y.; Jeffrey, P. D.; Doyle, A. G. Structure-Reactivity Relationships of Buchwald-Type Phosphines in Nickel-Catalyzed Cross-Couplings. *J. Am. Chem. Soc.* **2022**, *144*, 19635–19648.
- (127) West, M. J.; Watson, A. J. B. Ni vs. Pd in Suzuki-Miyaura sp2-sp2 cross-coupling: a head-to-head study in a comparable precatalyst/ligand system. *Org. Biomol. Chem.* **2019**, *17*, 5055–5059.
- (128) Cooper, A. K.; Burton, P. M.; Nelson, D. J. Nickel versus Palladium in Cross-Coupling Catalysis: On the Role of Substrate Coordination to Zerovalent Metal Complexes. *Synthesis* **2020**, *52*, 565–573.
- (129) Clavier, H.; Nolan, S. P. Percent buried volume for phosphine and N-heterocyclic carbene ligands: steric properties in organometallic chemistry. *Chem. Commun.* **2010**, *46*, 841–861.
- (130) Gensch, T.; Dos Passos Gomes, G.; Friederich, P.; Peters, E.; Gaudin, T.; Pollice, R.; Jorner, K.; Nigam, A.; Lindner-D'Addario, M.; Sigman, M. S.; et al. A Comprehensive Discovery Platform for Organophosphorus Ligands for Catalysis. *J. Am. Chem. Soc.* **2022**, *144*, 1205–1217.
- (131) Cox, P. A.; Leach, A. G.; Campbell, A. D.; Lloyd-Jones, G. C. Protodeboronation of Heteroaromatic, Vinyl, and Cyclopropyl Boronic Acids: pH-Rate Profiles, Autocatalysis, and Disproportionation. *J. Am. Chem. Soc.* **2016**, *138*, 9145–9157.
- (132) Cox, P. A.; Reid, M.; Leach, A. G.; Campbell, A. D.; King, E. J.; Lloyd-Jones, G. C. Base-Catalyzed Aryl-B(OH)2 Protodeboronation Revisited: From Concerted Proton Transfer to Liberation of a Transient Aryl Anion. *J. Am. Chem. Soc.* **2017**, *139*, 13156–13165.
- (133) Thomas, A. A.; Zahrt, A. F.; Delaney, C. P.; Denmark, S. E. Elucidating the Role of the Boronic Esters in the Suzuki-Miyaura Reaction: Structural, Kinetic, and Computational Investigations. *J. Am. Chem. Soc.* **2018**, *140*, 4401–4416.
- (134) Hayes, H. L. D.; Wei, R.; Assante, M.; Geogheghan, K. J.; Jin, N.; Tomasi, S.; Noonan, G.; Leach, A. G.; Lloyd-Jones, G. C. Protodeboronation of (Hetero)Arylboronic Esters: Direct versus Prehydrolytic Pathways and Self-/Auto-Catalysis. *J. Am. Chem. Soc.* **2021**, *143*, 14814–14826.
- (135) Oka, N.; Yamada, T.; Sajiki, H.; Akai, S.; Ikawa, T. Aryl Boronic Esters Are Stable on Silica Gel and Reactive under Suzuki-Miyaura Coupling Conditions. *Org. Lett.* **2022**, *24*, 3510–3514.
- (136) Molander, G. A.; Biolatto, B. Palladium-catalyzed Suzuki-Miyaura cross-coupling reactions of potassium aryl- and heteroaryltrifluoroborates. *J. Org. Chem.* **2003**, *68*, 4302–4314.

- (137) Ren, W.; Li, J.; Zou, D.; Wu, Y.; Wu, Y. Palladium-catalyzed Suzuki–Miyaura cross-coupling reaction of potassium 2-pyridyl trifluoroborate with aryl (heteroaryl) halides. *Tetrahedron* **2012**, *68*, 1351–1358.
- (138) Knapp, D. M.; Gillis, E. P.; Burke, M. D. A general solution for unstable boronic acids: slow-release cross-coupling from air-stable MIDA boronates. *J. Am. Chem. Soc.* **2009**, *131*, 6961–6963.
- (139) Dick, G. R.; Woerly, E. M.; Burke, M. D. A general solution for the 2-pyridyl problem. *Angew. Chem. Int. Ed.* **2012**, *51*, 2667–2672.
- (140) Yoshida, H.; Seki, M.; Kamio, S.; Tanaka, H.; Izumi, Y.; Li, J.; Osaka, I.; Abe, M.; Andoh, H.; Yajima, T.; et al. Direct Suzuki–Miyaura Coupling with Naphthalene-1,8-diaminato (dan)-Substituted Organoborons. *ACS Catal.* **2020**, *10*, 346–351.
- (141) Mutoh, Y.; Yamamoto, K.; Saito, S. Suzuki–Miyaura Cross-Coupling of 1,8-Diaminonaphthalene (dan)-Protected Arylboronic Acids. *ACS Catal.* **2020**, *10*, 352–357.
- (142) SciFinder. https://scifinder-n.cas.org/ (accessed June 21, 2024).
- (143) Fuentes-Rivera, J. J.; Zick, M. E.; Düfert, M. A.; Milner, P. J. Overcoming Halide Inhibition of Suzuki–Miyaura Couplings with Biaryl Monophosphine-Based Catalysts. *Org. Process Res. Dev.* **2019**, *23*, 1631–1637.
- (144) Delaney, C. P.; Kassel, V. M.; Denmark, S. E. Potassium Trimethylsilanolate Enables Rapid, Homogeneous Suzuki-Miyaura Cross-Coupling of Boronic Esters. *ACS Catal.* **2020**, *10*, 73–80.
- (145) Guo, X.; Dang, H.; Wisniewski, S. R.; Simmons, E. M. Nickel-Catalyzed Suzuki–Miyaura Cross-Coupling Facilitated by a Weak Amine Base with Water as a Cosolvent.

 Organometallics 2022, 41, 1269–1274.
- (146) Kassel, V. M.; Hanneman, C. M.; Delaney, C. P.; Denmark, S. E. Heteroaryl-Heteroaryl, Suzuki-Miyaura, Anhydrous Cross-Coupling Reactions Enabled by Trimethyl Borate. *J. Am. Chem. Soc.* **2021**, *143*, 13845–13853.
- (147) Notheis, M. J.; Sahiti, V.; Prangenberg, V.; Kruse, J. S.; Krbek, L. K. S. von. 2,8-Dihalogenated Diazocines: Versatile Reactants for Functionalized Photoswitches. *Synlett* **2025**, *36*, 1569–1573.
- (148) Notheis, M. J.; Schnakenburg, G.; Krbek, L. K. S. von. Light-Driven Ratchet Mechanism Accelerates Regioselective Metal-Cation Exchange in a Heterobimetallic Helicate. *Angew. Chem. Int. Ed.* **2025**, e202508952.

- (149) Guhlke, M.; Herbst, J.; Nguyen, T. G.; Schneider, A.; Dickschat, J. S.; Menche, D. Total Synthesis and Stereochemical Proposal of the Hexaene Framework of Bacillaene. *Org. Lett.* **2025**, *27*, 2317–2322.
- (150) Treiber, T.; Li, W.-S.; Bingel, M.; Müller, A.; Eckhardt, M.; Menche, D. Total Synthesis of Epicoccolides A and B by Oxidative Skeleton Rearrangement Leads to a Structural Revision and Questions the Proposed Biosynthesis. *Org. Lett.* **2025**, *27*, 6539–6544.
- (151) Meringdal, J. W.; Prangenberg, V.; Treiber, T.; Schneider, A. J.; Honsdorf, L.; Menche, D. Ligand Type Guided Keto-Arylation Enables Modular Total Synthesis of Polycyclic CBS Xanthones. *Angew. Chem. Int. Ed.* 2025, e202513532.
- (152) Johansson, C. C. C.; Colacot, T. J. Metal-catalyzed alpha-arylation of carbonyl and related molecules: novel trends in C-C bond formation by C-H bond functionalization. *Angew. Chem. Int. Ed.* **2010**, *49*, 676–707.
- (153) Marsh, G.; Stenutz, R.; Bergman, Å. Synthesis of Hydroxylated and Methoxylated Polybrominated Diphenyl Ethers Natural Products and Potential Polybrominated Diphenyl Ether Metabolites. *Eur. J. Org. Chem.* **2003**, 2566–2576.
- (154) Guo, W.; Li, J.; Fan, N.; Wu, W.; Zhou, P.; Xia, C. A Simple and Effective Method for Chemoselective Esterification of Phenolic Acids. *Synth. Commun.* **2005**, *35*, 145–152.
- (155) Lipshutz, B. H.; Pegram, J. J. β-(Trimethylsilyl)ethoxymethyl chloride. A new reagent for the protection of the hydroxyl group. *Tetrahedron Lett.* **1980**, *21*, 3343–3346.
- (156) Kosugi, M.; Sumiya, T.; Obara, Y.; Suzuki, M.; Sano, H.; Migita, T. (α-Ethoxyvinyl)tributyltin; An Efficient Reagent for the Nucleophilic Acetylation of Organic Halides via Palladium Catalysis. *Bull. Chem. Soc. Jpn.* **1987**, *60*, 767–768.
- (157) Aicart, M.; Mavoungou-Gomès, L. Conversion des furfurylalkyl et arylcetones en derives de l'isocoumarine et de l'isoquinoleine. *J. Heterocycl. Chem.* **1985**, *22*, 921–925.
- (158) Beletskaya, I. P.; Cheprakov, A. V. The heck reaction as a sharpening stone of palladium catalysis. *Chem. Rev.* **2000**, *100*, 3009–3066.
- (159) Watanabe, T.; Oga, K.; Matoba, H.; Nagatomo, M.; Inoue, M. Total Synthesis of Taxol Enabled by Intermolecular Radical Coupling and Pd-Catalyzed Cyclization. *J. Am. Chem. Soc.* **2023**, *145*, 25894–25902.
- (160) Gürtler, C.; Buchwald, S. L. A Phosphane-Free Catalyst System for the Heck Arylation of Disubstituted Alkenes: Application to the Synthesis of Trisubstituted Olefins. *Chem. Eur. J.* **1999**, *5*, 3107–3112.

- (161) Murray, P. M.; Bower, J. F.; Cox, D. K.; Galbraith, E. K.; Parker, J. S.; Sweeney, J. B. A Robust First-Pass Protocol for the Heck–Mizoroki Reaction. *Org. Process Res. Dev.* **2013**, *17*, 397–405.
- (162) Kuwajima, I.; Urabe, H. Regioselective arylation of silyl enol ethers of methyl ketones with aryl bromides. *J. Am. Chem. Soc.* **1982**, *104*, 6831–6833.
- (163) Mee, S. P. H.; Lee, V.; Baldwin, J. E. Stille coupling made easier-the synergic effect of copper(I) salts and the fluoride ion. *Angew. Chem. Int. Ed.* **2004**, *43*, 1132–1136.
- (164) Su, W.; Raders, S.; Verkade, J. G.; Liao, X.; Hartwig, J. F. Pd-catalyzed alpha-arylation of trimethylsilyl enol ethers with aryl bromides and chlorides: a synergistic effect of two metal fluorides as additives. *Angew. Chem. Int. Ed.* **2006**, *45*, 5852–5855.
- (165) Casado, A. L.; Espinet, P.; Gallego, A. M. Mechanism of the Stille Reaction. 2. Couplings of Aryl Triflates with Vinyltributyltin. Observation of Intermediates. A More Comprehensive Scheme. *J. Am. Chem. Soc.* **2000**, *122*, 11771–11782.
- (166) Littke, A. F.; Fu, G. C. A versatile catalyst for Heck reactions of aryl chlorides and aryl bromides under mild conditions. *J. Am. Chem. Soc.* **2001**, *123*, 6989–7000.
- (167) Hall, A. M. R.; Berry, D. B. G.; Crossley, J. N.; Codina, A.; Clegg, I.; Lowe, J. P.; Buchard, A.; Hintermair, U. Does the Configuration at the Metal Matter in Noyori-Ikariya Type Asymmetric Transfer Hydrogenation Catalysts? *ACS Catal.* **2021**, *11*, 13649–13659.
- (168) Corey, E. J.; Bakshi, R. K.; Shibata, S. Highly enantioselective borane reduction of ketones catalyzed by chiral oxazaborolidines. Mechanism and synthetic implications. *J. Am. Chem. Soc.* **1987**, *109*, 5551–5553.
- (169) Parveen, I.; Naughton, D. P.; Whish, W. J.; Threadgill, M. D. 2-nitroimidazol-5-ylmethyl as a potential bioreductively activated prodrug system: reductively triggered release of the PARP inhibitor 5-bromoisoquinolinone. *Bioorg. Med. Chem. Lett.* **1999**, *9*, 2031–2036.
- (170) Prantz, K.; Mulzer, J. Synthetic applications of the carbonyl generating Grob fragmentation. *Chem. Rev.* **2010**, *110*, 3741–3766.
- (171) Greene, A. E.; Le Drian, C.; Crabbe, P. An efficient total synthesis of (.+-.)-brefeldin-A. *J. Am. Chem. Soc.* **1980**, *102*, 7583–7584.
- (172) Davis, F. A.; Haque, M. S. Stereochemistry of the asymmetric oxidation of ketone enolates using (camphorylsulfonyl)oxaziridines. *J. Org. Chem.* **1986**, *51*, 4083–4085.

- (173) Davis, F. A.; Sheppard, A. C.; Chen, B. C.; Haque, M. S. Chemistry of oxaziridines. 14.

 Asymmetric oxidation of ketone enolates using enantiomerically pure

 (camphorylsulfonyl)oxaziridine. *J. Am. Chem. Soc.* **1990**, *112*, 6679–6690.
- (174) Ball, D. B. Diastereoselectivity in the Reduction of α-Hydroxyketones. An Experiment for the Chemistry Major Organic Laboratory. *J. Chem. Educ.* **2006**, *83*, 101.
- (175) Soni, R.; Hall, T. H.; Mitchell, B. P.; Owen, M. R.; Wills, M. Asymmetric Reduction of Electron-Rich Ketones with Tethered Ru(II)/TsDPEN Catalysts Using Formic Acid/Triethylamine or Aqueous Sodium Formate. *J. Org. Chem.* **2015**, *80*, 6784–6793.

8 Publications

- [1] Meringdal, J. W.; Kilian, A.; Li, W. C.; Heinemann, M. J. B.; Rausch, M.; Schneider, T.; Menche, D. Modular Synthesis of Halogenated Xanthones by a Divergent Coupling Strategy. J. Org. Chem. 2022, 87, 9375–9383.
 https://doi.org/10.1021/acs.joc.2c01157 (link)
- [2] Meringdal, J. W.; Bade, L.; Bendas, G.; Menche, D. Diversity Oriented Synthesis of Novel Xanthones Reveal Potent Doxorubicin-Inspired Analogs. *ChemMedChem* **2024**, *19*, e202400055.
 - https://doi.org/10.1002/cmdc.202400055 (link)
- [3] Meringdal, J. W.; Menche, D. Suzuki-Miyaura (hetero-)aryl cross-coupling: recent findings and recommendations. Chem. Soc. Rev. 2025, 54, 5746–5765.
 https://doi.org/10.1039/D4CS01108B (link)
- [4] Meringdal, J. W.; Prangenberg, V.; Treiber, T.; Schneider, A. J.; Honsdorf, L.; Menche, D. Ligand Type Guided Keto-Arylation Enables Modular Total Synthesis of Polycyclic CBS Xanthones. Angew. Chem. Int. Ed. 2025, e202513532. https://doi.org/10.1002/anie.202513532 (link)
- **Note** Due to copyright restrictions, the publications cannot be included in the digital version but are accessible via the provided links.